Fisheries and Oceans Canada | Pêches et Océans Canada
Ecosystems and Oceans Science | Sciences des écosystèmes et des océans

**Canadian Science Advisory Secretariat (CSAS)**

**Research Document 2019/046**

**Quebec Region**

# Physical Oceanographic Conditions in the Gulf of St. Lawrence during 2018

P.S. Galbraith[1], J. Chassé[2], C. Caverhill[3], P. Nicot[4], D. Gilbert[1], D. Lefaivre[1], C. Lafleur[1]

(1) Fisheries and Oceans Canada, Québec Region,
Maurice Lamontagne Institute,
P.O. Box 1000, Mont-Joli, Québec, G5H 3Z4

(2) Fisheries and Oceans Canada, Gulf Region,
Gulf Fisheries Centre,
P.O. Box 5030, Moncton, New Brunswick, E1C 9B6

(3) Fisheries and Oceans Canada, Maritimes Region,
Bedford Institute of Oceanography,
P.O. Box 1006, Dartmouth, Nova Scotia, B2Y 4A2

(4) Institut des sciences de la mer de Rimouski
Université du Québec à Rimouski,
310 allée des Ursulines, Rimouski, Québec, G5L 3A1

September 2019

Canada

**Foreword**

This series documents the scientific basis for the evaluation of aquatic resources and ecosystems in Canada. As such, it addresses the issues of the day in the time frames required and the documents it contains are not intended as definitive statements on the subjects addressed but rather as progress reports on ongoing investigations.

**Published by:**

Fisheries and Oceans Canada
Canadian Science Advisory Secretariat
200 Kent Street
Ottawa ON K1A 0E6

http://www.dfo-mpo.gc.ca/csas-sccs/
csas-sccs@dfo-mpo.gc.ca


ISSN 1919-5044

**Correct citation for this publication:**

Galbraith, P.S., Chassé, J., Caverhill, C., Nicot, P., Gilbert, D., Lefaivre, D. and Lafleur, C. 2019. Physical Oceanographic Conditions in the Gulf of St. Lawrence during 2018. DFO Can. Sci. Advis. Sec. Res. Doc. 2019/046. iv + 79 p.

***Aussi disponible en français :***

*Galbraith, P.S., Chassé, J., Caverhill, C., Nicot, P., Gilbert, D., Lefaivre, D. et Lafleur, C. 2019. Conditions océanographiques physiques dans le golfe du Saint-Laurent en 2018. Secr. can. de consult. sci. du MPO, Doc. de rech. 2019/046. iv + 83 p.*

## TABLE OF CONTENTS

## ABSTRACT

An overview of physical oceanographic conditions in the Gulf of St. Lawrence (GSL) in 2018 is presented as part of the Atlantic Zone Monitoring Program (AZMP). AZMP data as well as data from regional monitoring programs are analysed and presented in relation to long-term means. The annual average freshwater runoff of the St. Lawrence River measured at Québec City and its combination with rivers flowing into the Estuary (RIVSUM II) were both above normal. Sea-ice maximum volume was 9$^{th}$ lowest since 1969, but the winter mixed layer volume was near-normal. The August cold intermediate layer (CIL) showed warmer than normal minimum temperature (+1.6 SD) and less than normal volume of water colder than 1°C (-1.7 SD), and the seasonally averaged minimum temperature index was also warmer than normal. Near-surface water temperatures were at a record low in November, below normal in spring and fall and only above in August and September. The May to November average was near-normal, but the coldest since 2002. The timing of summer onset and post-season cooling of the surface layer were respectively later than normal (+0.8 weeks) and near normal. Deep water temperatures have been increasing overall in the Gulf, with inward advection from Cabot Strait. Gulf-wide average temperatures at 150 and 200 m are lower than the 2015 record highs but remain above normal at 3.0°C (+0.5°C, +1.0 SD) and 5.0°C (+0.6°C, +1.5 SD). New series record highs (since 1915) were set at 250 and 300 m, at 6.1°C (+0.8°C, +3.1 SD) and 6.4°C (+0.9°C, +5.8 SD) respectively. The bottom area covered by waters warmer than 6°C remained quite high in 2018 in Anticosti Channel and Esquiman Channel and Central Gulf, and increased sharply in and the northwest Gulf to reach a series record.

## INTRODUCTION

This document examines the physical oceanographic conditions and related atmospheric forcing in the Gulf of St. Lawrence in 2018 (Fig. 1). It complements similar reviews of the environmental conditions on the Newfoundland and Labrador Shelf and the Scotian Shelf and Gulf of Maine as part of the Department of Fisheries and Oceans' (DFO) Atlantic Zone Monitoring Program (AZMP; see Therriault et al. 1998 for background information on the program and Colbourne et al. 2017, and Hebert et al. 2018 for examples of past reviews in other AZMP regions). The last detailed report of physical oceanographic conditions in the Gulf of St. Lawrence was produced for the year 2017 (Galbraith et al. 2018). Specifically, it discusses air temperature, freshwater runoff, sea-ice volume, surface water temperature and salinity, winter water mass conditions (e.g., the near-freezing mixed layer volume, the volume of dense water that entered the Gulf through the Strait of Belle Isle), the summertime cold intermediate layer (CIL), and the temperature, salinity, and dissolved oxygen of the deeper layers. Some of the variables are spatially averaged over distinct regions of the Gulf (Fig. 2). The report uses data obtained from the AZMP, other DFO surveys, and other sources. Environmental variables are usually expressed as anomalies, i.e., deviations from their long-term mean. The long-term mean or normal conditions are calculated for the standard 1981–2010 reference period when possible. Furthermore, because these series have different units (°C, $m^3$, $m^2$, etc.), each anomaly time series is normalized by dividing by its standard deviation (SD), also calculated for the standard reference when possible. This allows a more direct comparison of the various series. Missing data are represented by grey cells in the tables, values within ±0.5 SD of the average as white cells, and conditions corresponding to warmer than normal (higher temperatures, reduced ice volumes, reduced cold-water volumes or areas) by more than 0.5 SD as red cells, with more intense reds corresponding to increasingly warmer conditions. Similarly, blue represents colder than normal conditions. Higher than normal freshwater inflow is shown as red, but does not necessarily correspond to warmer-than-normal conditions. Higher than normal stratification values are shown in blue because they are usually caused by lower upper layer salinity.

The summertime water column in the Gulf of St. Lawrence consists of three distinct layers: the surface layer, the cold intermediate layer (CIL), and the deeper water layer (Fig. 3). Surface temperatures typically reach maximum values in early to mid-August (Galbraith et al. 2012). Gradual cooling occurs thereafter, and wind forced mixing during the fall leads to a progressively deeper and cooler mixed layer, eventually encompassing the CIL. During winter, the surface layer thickens partly because of buoyancy losses (cooling and reduced runoff) and brine rejection associated with sea-ice formation, but mostly from wind-driven mixing prior to ice formation (Galbraith 2006). The surface winter layer extends to an average depth of 75 m, but may reach >150 m in places such as the Mécatina Trough where near freezing waters (-1.8 to 0ºC) from the Labrador shelf entering through the Strait of Belle Isle may extend from the surface to the bottom in depths >200 m) (Galbraith 2006). During spring, surface warming, sea-ice melt waters, and continental runoff produce a lower-salinity and higher-temperature surface layer. Underneath this surface layer, cold waters from the previous winter are partly isolated from the atmosphere and form the summer CIL. This layer will persist until the next winter, gradually warming up and deepening during summer (Gilbert and Pettigrew 1997; Cyr et al. 2011) and more rapidly during the fall as vertical mixing intensifies.

This report considers these three layers in turn, but first air temperature and the freshwater runoff are examined because they are significant drivers of the surface layer. The winter sea ice and winter oceanographic conditions are described; these force the summer CIL, which is presented next. The deeper waters, mostly isolated from exchanges with the surface, are presented last along with a summary of major oceanographic surveys.

## AIR TEMPERATURE

The air temperature data are the second generation of homogenized surface air temperature data, part of the Adjusted and Homogenized Canadian Climate Data (AHCCD), which accounts for shifts due to the relocation of stations, changes in observing practices and automation (Vincent et al. 2012). The monthly air temperature anomalies for several stations around the Gulf are shown in Fig. 4 for 2017 and 2018, as well as the average of all station anomalies. There are no air temperature data from Plum Point since mid-2016, so while the station data are included in the Gulf average climatology it is no longer part of the average anomalies.

Fig. 5 shows the annual, winter (December-March), and April-November mean air temperature anomalies averaged over all available stations shown in Fig. 4 since 1873. Record-high annual and winter temperatures occurred in 2010 and record-high April-November temperatures in 2012. Galbraith et al. (2012) found the average April-November air temperature over the Gulf from Environment Canada's National Climate Data and Information Archive (NCDIA) to be a good proxy for May-November sea-surface temperature over the Gulf (but excluding the estuary) and found within the former a warming trend of 0.9°C per century between 1873 and 2011; the same trend is found here over the selected ACCHD stations between 1873 and 2018 (Fig. 5). The NCDIA December-March air temperatures in the western Gulf were found to be highly correlated ($R^2$=0.67) with sea-ice properties, as well as with winter mixed layer volumes (Galbraith et al. 2010). Galbraith et al. (2013) found slightly higher correlations ($R^2$=0.72) with sea-ice using December-February ACCHD averages, possibly because March temperature are of less importance during low sea-ice cover since much of the sea-ice cover decrease has occurred much earlier in February.

It was the warmest July on record at Mont-Joli (+2.4°C, +2.3 SD), while Gaspé had its warmest July since 1931 (+2.9°C, +2.7 SD). In contrast, it was the coldest October on record at Baie Comeau (since 1965, -3.3°C, -2.9 SD), since 1925 in Bathurst (-2.7°C, -2.2 SD), since 1974 in Mont-Joli (-2.6°C, -2.1 SD) and coldest October overall since 1974 (-1.9°C, -1.8 SD). June was the coldest at Stephenville since 1943 (-2.9°C, -2.3 SD) and coldest overall since 1982 (-1.6°C, -1.6 SD). In between the cold spring and fall, the short summer was warmer than normal but we only have to go back to 2014-2015 to find warmer monthly temperatures for July and August. Averaged over all stations, the December-March air temperature average was above-normal (+1.2°C, +0.8 SD), the annual average was normal (-0.0°C, -0.1 SD), while the April-November average was the first below-normal anomaly since 2002 (-0.6°C, -1.0 SD).

## PRECIPITATION AND FRESHWATER RUNOFF

Freshwater runoff data for the St. Lawrence River are updated monthly (Fig. 6, lower curve) using the water level method from Bourgault and Koutitonsky (1999) and are available from the St. Lawrence Global Observatory. A hydrological watershed model was used to estimate the monthly runoff since 1948 for all other major rivers flowing into the Gulf of St. Lawrence, with discharge locations as shown in Fig. 7. The precipitation data (NCEP reanalysis, six hourly intervals) used as input in the model were obtained from the NOAA-CIRES Climate Diagnostics Center (Boulder, Colorado, USA; Kalnay et al. 1996). The data were interpolated to a ¼° resolution grid and the water routed to river mouths using a simple algorithm described here. When air temperatures were below freezing, the water was accumulated as snow in the watershed and later melted as a function of warming temperatures. Water regulation is modelled for three rivers that flow into the estuary (Saguenay, Manicouagan, Outardes) for which the annual runoff is redistributed following the climatology of the true regulated runoffs for 12 months thereafter. Runoffs were summed for each region shown and the climatology established for the 1981–2010 period. The waters that flow into the Estuary (region 1, Fig 7.)

were added to the St. Lawrence River runoff measured at Québec City to produce the RIVSUM II index, although no advection lags were introduced (Fig. 6, upper curve). In 2018, the spring freshet extended in time to include March. It was above normal for the period of March to May at +1.4 SD for the St. Lawrence River and +1.1 SD for the RIVSUM II index, but the latter was only caused by high St. Lawrence River runoff.

Monthly anomalies of the summed runoffs for 2017 and 2018 are shown in Fig. 8. The March St. Lawrence River runoff was second highest of the time series, after 1973. Rivers other than the St. Lawrence contribute about 5,000 $m^3 s^{-1}$ runoff to the Estuary, the equivalent of 40% of the St. Lawrence River, while the other tributaries distributed along the border of the GSL provide an additional 3,900 $m^3 s^{-1}$ in freshwater runoff to the system. River regulation has a strong impact on the relative contributions of sources. For example, in May 2015 the higher-than-average river runoff into the Estuary (an effect of the heavy precipitation in 2014 and river regulation) was almost as important as the below-normal St. Lawrence run-off (Galbraith et al. 2017). The 2018 hydrological simulation shows that rivers in regions 1 through 5 did not show the high March-May spring freshet of the St. Lawrence River, however the second highest December run-off occurred in the Northwest Gulf and Magdalen Shallows, after 1950 and equal to 2010. The long-term time series are shown, summed by large basins, in Fig. 9. Broad long-term patterns of runoff over the large basins were similar to that of the St. Lawrence River but interannual variability is low in the Northeast basin and Magdalen Shallows basin. The average run-off into the Estuary was below-normal at -1.5 SD. The annual average runoff of the St. Lawrence River measured at Québec City and RIVSUM II both show a general downward trend from the mid-1970s until 2001, an upwards trend between 2001 and 2011 and were at their highest level since 1974 in 2017 (Fig. 9). In 2018, the annual runoff was above-normal at 13,200 $m^3 s^{-1}$ (+1.4 SD) for the St. Lawrence River and 16,900 $m^3 s^{-1}$ (+0.7 SD) for the RIVSUM II index.

## SURFACE LAYER

The surface layer conditions of the Gulf are monitored by various complementary methods. The first is the shipboard thermosalinograph network (Galbraith et al. 2002), which consists of temperature-salinity sensors (SBE-21; Sea-Bird Electronics Inc., Bellevue, WA) that have been installed on various ships starting with the commercial ship Cicero of Oceanex Inc. in 1999 (retired in 2006) and on the Cabot from 2006 to fall 2013. The Oceanex Connaigra, was outfitted with a thermosalinograph in early 2015.

The second data source are 1 km resolution composites of Sea Surface Temperature (SST) generated using National Oceanic and Atmospheric Administration (NOAA) and European Organisation for the Exploitation of Meteorological Satellites (EUMETSAT) Advanced Very High Resolution Radiometer (AVHRR) satellite images available from the Maurice Lamontagne Institute sea surface temperature processing facility (details in Galbraith and Larouche 2011, and Galbraith et al. 2012). These data are available for the period of 1985-2013. From 2014 onwards, AVHRR composites of 1.5-km resolution provided by the Bedford Institute of Oceanography (BIO) Operational Remote Sensing group complete the data set. Monthly climatologies for the period of 1998-2012 common to both products were compared at the 1.5-km pixel level for cross-calibration. The BIO product is adjusted to the MLI product climatology as $SST_{IML} = 0.9794 \cdot SST_{BIO} - 0.13$ (-0.13°C adjustment at 0°C; -0.54°C at 20°C). This is in part explained by the fact that the MLI product used all available SST images while the BIO product uses only daytime passes, introducing a slight diurnal bias.

## SEA SURFACE TEMPERATURE

The May to November cycle of weekly averaged surface temperature over the Gulf of St. Lawrence is illustrated in Fig. 10. Galbraith et al. (2012) have shown that Gulf-averaged monthly air temperature and SST climatologies match up quite well with SST lagging air temperature by half a month. Maximum sea-surface temperatures are reached on average during the second week of August but that can vary by a few weeks from year to year. The maximum surface temperature averages to 15.6ºC over the Gulf during the second week of August (1985–2010), but there are spatial differences: temperatures on the Magdalen Shallows are the warmest in the Gulf, averaging 18.1ºC over that area, and the coolest are at the head of the St. Lawrence Estuary (7.0°C) and upwelling areas along the lower north shore.

Fig. 11 shows a mean annual cycle of water temperature at a depth of 8 m along the Montréal to St. John's shipping route based on thermosalinograph data collected from 2000 to 2018. The data were averaged for each day of the year at intervals of 0.1 degree of longitude to create a climatological composite along the ship track. The most striking climatological feature is the area at the head of the Laurentian Trough (69.5°W), where strong vertical mixing leads to cold summer water temperatures (around 5°C to 6°C and sometimes lower) and winter temperatures that are always above freezing (see also Fig. 10). The climatological cycle shows the progression to winter conditions, first reaching near-freezing temperatures in the Estuary and then progressing eastward with time, usually reaching Cabot Strait by the end of the winter (but no further).

Thermosalinograph data show that near-freezing surface layer conditions first appeared earlier than normal in winter (Fig. 11). Temperatures throughout the year were mostly below-normal to normal in the estuary and Gulf, except for August to mid-September, consistent with lagged air temperature anomalies (Fig. 4). November was particularly cold with anomalies exceeding 3°C from Central Gulf to Port aux Basques.

Monthly mean sea-surface temperatures from AVHRR imagery are presented as maps (Fig. 12), temperature anomaly maps (Fig. 13), spatial averages expressed as anomalies (Fig. 14) or as mean temperatures for the last two years (Fig. 15) as well as since 1985 (Figs. 16 and 17). Near-surface water temperatures were at series record lows (since 1985) in November in 4 Western regions as well as in June in Central Gulf and Cabot Strait. Averaged over the Gulf, they were at a record low in November (-1.3°C, -1.7 SD), below normal in spring (May and June) and fall (October and November) and only above normal in August and September. The May to November 2018 average was near-normal (-0.3°C, -0.5 SD), but was the coldest since 2002 when it averaged only 0.04°C warmer.

Sea-surface temperature monthly climatologies and time series were also extracted for more specific regions of the Gulf. The Magdalen Shallows, excluding Northumberland Strait, is divided into western and eastern areas as shown in Fig. 18. The monthly average SST for the Magdalen Shallows as a whole (region 8) is repeated in Fig. 19 along with averages for the western and eastern areas. Climatologies differ by roughly 0.5°C to 1°C between the western and eastern regions. Temperatures were at a series record high in August on the Eastern Shelf and at a series record low in November on the Western Shelf.

The number of weeks in the year that the mean weekly temperature is above 10°C for each pixel (Fig. 20) integrates summer surface temperature conditions into a single map displaying the length of the warm season. The average number of weeks with mean weekly temperature above 10°C are shown for each region as time series in Fig. 21. All regions had either below-normal or normal duration of warm season. On average over the Gulf, it was near normal in 2018.

Seasonal trends in relation to air temperature are examined by first displaying weekly averaged AVHRR SST in the GSL for all years between 1985 and 2018 (Fig. 22) with years on the x-axis and weeks of the year on the y-axis (See Galbraith and Larouche 2013 for a full description). Isotherms show the first and last occurrences of temperature averages of 12°C over the years, chosen to be representative of spring (and fall) transitions to (and from) typical summer temperatures. Although the selected temperature is arbitrary, the results that follow are not particularly sensitive to the exact temperature chosen because the surface mixed layer tends to warm and cool linearly in spring and fall (e.g. Fig. 10). A 10°C threshold is also used to demonstrate this. The Gulf had experienced earlier summer onset between 1985 and 2017 of -0.5 weeks per decade, but later-than-normal warming in 2018 by 1 week has rendered this trend no longer statistically significant. A progressively later fall cooling trend persists with the near-normal timing of fall cooling in 2018, although smaller in magnitude than reported last year (now 0.4 weeks per decade).

In spite of the reduced observed recent trends, the interannual variability in the time of year when the 12°C threshold is crossed is correlated with June-July average air temperature for the summer onset (1.1 week sooner per 1°C increase; $R^2$=0.60) and with September average air temperature for the fall (0.5 week later per 1°C increase; $R^2$=0.43). These air temperature averages, shown in Fig. 22, can be used as proxies prior to 1985 and for climate change predictions. The implication is that the duration of the Gulf of Lawrence warm season has increased and will increase by about 2 weeks for each 1°C of seasonal warming (e.g. associated with climate change).

## SEA ICE

Ice volume is estimated from three ice cover products obtained from the Canadian Ice Service (CIS), further processed into regular grid that are used in analyses. These are weekly Geographic Information System (GIS) charts covering the period 1969-2018 and daily charts covering the period 2009-2018. Both were gridded on a 0.01° latitude by 0.015° longitude grid (approximately 1 km resolution). The third CIS product consists of 5-km resolution gridded daily files covering the period 1998-2008. Some of the analyses described below were done using the weekly data exclusively, for long-term consistency, while for others daily data were used when available with results filtered using a 3-day running mean in order to smooth them, making them comparable to results calculated from weekly data.

Several products were computed to describe the sea-ice cover interannual variability: day of first and last occurrence and duration maps (Fig. 23) and regional averages (Fig. 24); distribution of ice thickness during the week of maximum volume (Fig. 25, upper panels) and maximum thickness reached at any week during the season (Fig. 25, lower panels); daily evolution of the estimated sea-ice volume in relation to the climatology and historical extremes (Fig. 26); estimated seasonal maximum ice volumes within the Gulf as well as on the Scotian Shelf (Fig. 27); time series of seasonal maximum ice volume, area (excluding thin new ice) and ice season duration in relation with December-to-March air temperature anomaly (Fig. 28).

There has been a declining trend in ice cover severity since 1990 with rebounds in 2003 and 2014 (Fig. 28). The correlation between annual maximum ice volume (including the cover present on the Scotian Shelf) and the December-February air temperature averaged over five Western Gulf stations (Sept-Îles, Mont-Joli, Gaspé, Charlottetown and Îles-de-la-Madeleine) accounted for 72% of the variance using the 1969–2012 time series (Galbraith et al. 2013). Fig. 28 shows a similar comparison using ice volume and the ACCHD December-to-March air temperature anomaly from Fig. 5 also yielding $R^2$ = 0.72. The correlation between air temperature and the ice parameters season duration and area are also very high ($R^2$ = 0.77-

0.78). Correlation coefficients are slightly higher when using January to February air temperatures, perhaps because March air temperatures have no effect on ice cover that has almost disappeared by then during very mild winters. Sensitivity of the ice cover to air temperature increase (e.g. through climate change) can be estimated using 1969-2018 co-variations between winter air temperature and sea-ice parameters, which indicate losses of 17 $km^3$, 31,000 $km^2$ and 14 days of sea-ice season for each 1°C increase in winter air temperature

Ice typically forms first in December in the St. Lawrence estuary and in shallow waters along New Brunswick, Prince Edward Island and the lower north shore and melts last in the northeast Gulf where the ice season duration tends to be longest apart from shallow bays elsewhere (Fig. 23a). Offshore sea ice is typically produced in the northern parts of the Gulf and drifts towards Îles-de-la-Madeleine and Cabot Strait during the ice season.

In 2018, the sea-ice cover formed earlier than normal in the Western portion and later than normal in Esquiman Channel (Fig. 23, Fig. 24). Its volume progressed normally until mid-January, then progressed about 1 SD below normal until the maximum was reached earlier than normal, before mid-February (Fig. 26). The seasonal maximum ice volume of only 35 $km^3$ ($9^{th}$ lowest at -1.1 SD) occurred the week of February $12^{th}$ (Fig. 25), $3^{rd}$ earliest of the time series; peak sea-ice volume is typically reached early during low sea-ice year (Fig. 26). The duration of 71 days was below-normal (-1.1 SD) as was the area (-0.6 SD) (Fig. 28). The short duration was mostly associated with early disappearance (last occurrence) of sea-ice, by up to 5 weeks in parts of Esquiman Channel (Fig. 23). These sea-ice conditions were consistent with above-normal winter air temperatures (+1.2°C, +0.8 SD). In the 9 year span since 2010, 7 of the 9 lowest maximum ice volumes of the time series have occurred (Fig. 28). Almost no ice was exported from the Gulf of St. Lawrence onto the Scotian Shelf in 2018 (Fig. 25, Fig. 27).

## WINTER WATER MASSES

A wintertime survey of the Gulf of St. Lawrence waters (typically 0–200 m) has been undertaken in early March since 1996, typically using a Canadian Coast Guard helicopter but from Canadian Coast Guard ships in 2016 and 2017. The survey, sampling methods, and results of the cold-water volume analysis in the Gulf and the estimate of the water volume advected into the Gulf via the Strait of Belle Isle over the winter are described in Galbraith (2006) and in Galbraith et al. (2006). Fig. 29 and Fig. 30 show gridded interpolations of near-surface temperature, temperature difference above freezing, salinity, cold layer thickness and bottom contacts, and thickness of the Labrador Shelf water intrusion for 2018 as well as climatological means.

The March surface mixed layer is usually very close (within 0.1°C) to the freezing point in most regions of the Gulf but thickness of the surface layer varies, leaving variability in the cold-water volume between mild and severe winters rather than in temperature. One exception was 2010 when, for the first time since the inception of the winter survey, the mixed layer was on average 1°C above freezing. During typical winters, surface waters in the temperature range of ~ 0°C to -1°C are only found from the northeast side of Cabot Strait spreading into the Gulf. Some of these warm waters have presumably entered the Gulf during winter and flowed northward along the west coast of Newfoundland, however it is also possible that local waters could have simply not cooled close to freezing. Conditions in March 2018 were warm in the triangle formed roughly by Gros Morne (NL), offshore of Heath Point on Anticosti and Port aux Basques (NL)（Fig. 29）, but the extent of waters warmer than 0°C was limited to two stations close to Port aux Basques. The lack of sea-ice in most of the Gulf during the survey was surprising given the extent of near-freezing waters.

Near-freezing waters with salinities of around 32 are responsible for the (local) formation of the CIL since that is roughly the salinity at the temperature minimum during summer. These are coded in green-blue in the salinity panel of Fig. 29 and are typically found to the north and east of Anticosti Island. Surface salinities were a bit lower than the climatology in this part of the Gulf during the winter of 2018.

Near-freezing waters with salinity >32.35 (colour-coded in violet) are considered to be too saline to have been formed from waters originating within the Gulf (Galbraith 2006) and are presumed to have been advected from the Labrador Shelf through the Strait of Belle Isle. These waters were not present at the surface of Mécatina Trough in March 2018 (Fig. 29). A T-S water mass criterion from Galbraith (2006) was used to identify intruding Labrador Shelf waters that have exhibited no evidence of mixing with warm and saline deep Gulf water. These waters only occupied a deep sub-surface layer in Mécatina Trough in March 2018 (top-right panel of Fig. 30). The recent history of Labrador Shelf water intrusions is shown in Fig. 31, where its volume is shown as well as the fraction it represents of all the cold-water volume in the Gulf. This volume was below-normal in March 2018 at 250 km³ (-1.1 SD), tying 2015 for the lowest value of the 1997-2018 time series, and representing only 2% (-1.2 SD) of the cold water (T< -1°C) in the Gulf.

The cold mixed layer depth typically reaches about 75 m in the Gulf and is usually delimited by the -1°C isotherm because the mixed layer is typically near-freezing and deeper waters are much warmer (Galbraith 2006). In March 2010 and 2011 much of the mixed layer was warmer than -1°C such that the criterion of T<0°C was also introduced (see middle panels of Fig. 30). The cold surface layer is the product of local formation as well as cold waters advected from the Labrador Shelf, and can consist either of a single water mass or of layers of increasing salinity with depth. This layer reaches the bottom in many regions of the Gulf, with interannual variability in whether the deepest parts of the Magdalen Shallow or of Mécatina Trough are reached (see bottom panels of Fig. 30). The thickness of the winter layer is usually greatest north and northeast of Anticosti Island, and the doming of the Anticosti Gyre isopycnals appears in the climatology as a thinner center part. In 2018, the typical thickness gradient towards the northeast was not as present, with higher thicknesses than usual found in Central Gulf and Cabot Strait.

Integrating the cold layer depth over the area of the Gulf (excluding the Estuary and the Strait of Belle Isle) yields a cold-water (< -1°C) volume of 12,600 km³ in 2018, near-normal at 0.3 SD above the 1996–2018 average. The interannual variability of winter volumes of water colder than 0 and 1°C are shown in Fig. 32. The mixed layer volume only increases to 13,800 km³ when water temperatures <0°C are considered which is 1.0 SD below the 1996–2018 average. This last volume of cold water corresponds to 41% of the total water volume of the Gulf (33,500 km³, excluding the Estuary).

## COLD INTERMEDIATE LAYER

### FORECAST FROM THE MARCH SURVEY

The summer CIL minimum temperature index (Gilbert and Pettigrew 1997) has been found to be highly correlated with the Gulf (excluding the estuary) volume of cold water (<-1°C) measured the previous March when much of the mixed layer is near-freezing (Galbraith 2006; updated relation in right panel of the present document Fig. 32). This is expected because the CIL is the remnant of the winter cold surface layer. A measurement of the volume of cold water present in March is therefore a valuable tool for forecasting the coming summer CIL conditions. The winter mixed layer in 2018 was near-freezing throughout most the Gulf, except

for an area centered on Port aux Basques extending toward Anticosti Island and mid-way up the western coast of Newfoundland. The overall thickness and volume of the layer colder than -1°C was near normal at +0.3 SD. The Cold Intermediate Layer for summer 2018 was therefore forecasted to be slightly colder than in 2017, with a Gilbert and Pettigrew (1997) index of around -0.28°C compared to -0.2°C in 2017 (Galbraith et al. 2018).

## AUGUST–SEPTEMBER CIL

The CIL minimum temperature, thickness and volume for T<0°C and <1°C were estimated using temperature profiles from all sources for August and September. Most data are from the multi-species surveys in September for the Magdalen Shallows and August for the rest of the Gulf. Using all available temperature profiles, spatial temperature interpolations of the Gulf were done for each 1-m depth increment, with the interpolated field bound between the minimum and maximum values observed within each of the different regions of the Gulf (Fig. 2) to avoid spurious extrapolations. The CIL thickness at each grid point is simply the sum of depth bins below the threshold temperature, and the CIL minimum temperature is only defined at grid points where temperature rises by at least 0.5°C at depths greater than that of the minimum, or if the grid point minimum temperature is below the CIL spatial average of the Gulf.

Fig. 33 shows the gridded interpolation of the CIL thickness <1°C and <0°C and the CIL minimum temperature for August–September 2018 as well their 1985-2010 climatology (1994-2010 for Mécatina Trough). The climatological period used here begins in 1985 instead of 1981 because there are too few data prior to 1985, when oceanographic data began to be sampled during multi-species surveys. The CIL thickness for T<0°C and T<1°C decreased compared to 2017, with conditions similar to 2000 and 2006 (not shown). Similar maps were produced for all years back to 1971 (although some years have no data in some regions), allowing the calculation of volumes for each region for each year as well as the climatologies shown on the left side of Fig. 33. The 2018 CIL water mass was thinner and warmer than the 1985-2010 climatologies, except in the Estuary and Mécatina Trough.

The time series of the regional August–September CIL volumes are shown in Fig. 34 (for <0°C and <1°C). Esquiman Channel and the Magdalen Shallows showed strong decreases in CIL volumes in 2018 compared to 2017, while the Estuary and northwest Gulf an increase. Fig. 35 shows the Gulf total volume of CIL water (<0°C and <1°C) and the average CIL core temperature from the August–September interpolated grids (e.g., Fig. 33). The CIL areal minimum temperature average and volume shown in Fig. 35 exclude data from Mécatina Trough which has very different water masses from the rest of the Gulf; it is influenced by inflow through the Strait of Belle Isle and is therefore not indicative of the climate in the rest of the Gulf. The CIL volumes as defined by T<0°C and <1°C decreased significantly (to -1.7 SD) compared to 2017 conditions (-0.6 SD), with very few areas of the Gulf occupied by any water colder than 0°C.

The time series of the CIL regional average minimum core temperatures are shown in Fig. 36. All regions, again except for the Estuary and northwest Gulf, show an increase in core temperature compared to 2017. The 2018 average temperature minimum (excluding Mecatina Trough, the Strait of Belle Isle and the Magdalen Shallows) was 0.3°C (+1.6 SD), an increase of 0.2°C from 2017, and is shown in Fig. 35 (bottom panel, green line). The average difference between this CIL index and the Gilbert and Pettigrew (1997) index (described below) is 0.27°C because of the warming between mid-June and the August survey. This index corresponds to a Gilbert and Pettigrew (1997) index of 0.0°C after rounding to the nearest decimal.

## NOVEMBER CIL CONDITIONS IN THE ST. LAWRENCE ESTUARY

The AZMP November survey usually provides a high-resolution conductivity-temperature-depth (CTD) sampling grid in the St. Lawrence estuary since 2006 although measurements are sparser in some years. This allows a higher resolution display of the CIL minimum temperature in the Estuary (Fig. 37). The data also show the temporal warming (Fig. 34) and thinning (Fig. 36) of the CIL since the August survey. Fig. 36 shows that the fairly rapid increase of the CIL minimum temperature occurring between August and November is fairly constant inter-annually in spite of the differences in August temperature. The station coverage in the Estuary in the fall of 2018 was sparse but results point to a thicker CIL than in the fall of 2017, with similar core temperatures (Fig. 37).

## SEASONAL MEAN CIL INDEX

The Gilbert and Pettigrew (1997) CIL index is defined as the mean of the CIL core temperatures observed between 1 May and 30 September of each year, adjusted to 15 July with a region-dependant warming rate. It was updated using all available temperature profiles measured within the Gulf between May and September inclusively since 1947 (black line of the bottom panel of Fig. 35). As expected, the CIL core temperature interpolated to 15 July is almost always colder than the estimate based on August and September data for which no temporal corrections were made. This is because the CIL is eroded over the summer and therefore its core warms over time.

This CIL index for summer 2018 was -0.05°C, above-normal at +0.9 SD. The 0.25°C increase from the summer 2017 CIL index is consistent with the decrease in CIL volume between August 2017 and 2018 discussed above and the increase of 0.2°C in the areal average of the minimum temperature in August. The warm winter conditions from 2010 to 2012 led to CIL indices that were still far below the record high observed in the 1960s and 1980s. The earlier CIL temperature minimums will need to be re-examined to confirm that they were calculated using data with sufficient vertical resolution to correctly resolve the core minimum temperature. It is also becoming increasingly clear that the winter mixed layer is not the only factor explaining summertime CIL conditions and that mechanisms having a multi-year cumulative effect are required to explain the interannual autocorrelations observed. For example, this may be linked to temperatures below CIL depth, which in warm years may create a higher temperature gradient that leads to higher heat fluxes and faster summertime CIL warming rates.

## SUMMARY OF CIL CONDITIONS

As a summary, Fig. 38 shows selected time series of winter and summertime CIL conditions (June and September bottom temperatures also related to the CIL are outlined below) and highlights the strong correlations between these various time series. Conditions related to the CIL were typically warmer-than-normal in 2018, somewhat surprisingly after near-normal winter surface mixed layer conditions.

## MAGDALEN SHALLOWS JUNE SURVEY

A long-standing assessment survey covering the Magdalen Shallows has taken place in June for mackerel assessments and was since merged with the June AZMP survey. This survey provides good coverage of the temperature conditions that are greatly influenced by the cold intermediate layer that reaches the bottom at roughly half of the surface area at this time of the year.

Near-surface waters warm quickly in June, mid-way between the winter minimum and the annual maximum in early August. This can introduce a bias if the survey dates are not the same each year. To account for this, the seasonal warming observed at the Shediac Valley AZMP monitoring station was evaluated. A linear regression was performed of temperature versus time for each meter of the water column for each year with monitoring data at Shediac Valley between May and July. Visual inspection showed that the depth-dependent warming rate was fairly constant for all years and an average was computed for every depth. Warming is maximal at the surface at 18°C per 100 days and, in spite of some uncertainties between 30 and 55 m, decreases almost proportionally with depth to reach 2°C per 100 days at 40 m, followed by a further linear decrease to reach 1°C per 100 days at 82 m (Galbraith and Grégoire 2015).

All available temperature profiles taken in June from a given year are binned at 1 m depth intervals (or interpolated if the resolution is too coarse) and then adjusted according to the sampling date to offset them to June 15$^{th}$ according to the depth-dependent warming rate extracted from Shediac Valley monitoring data. An interpolation scheme is used to estimate temperature at each 1 m depth layer on a 2 km resolution grid. Fig. 39 shows temperatures and anomalies at depths of 20, 30, 40 and 50 m. Fig. 40 shows averages over the grids at 10, 20, 30, 50 and 75 m for all years when interpolation was possible, as well as SST June averages since 1985, for both western and eastern regions of the Magdalen Shallows (Fig. 18). Temperatures were on average below normal at the surface down to 10 m, then normal to above-normal, particularly at 30 to 40 m on the Western Shelf (Fig. 39 and Fig. 40).

## BOTTOM WATER TEMPERATURES ON THE MAGDALEN SHALLOWS

Bottom temperature is also estimated at each point of the grids constructed from the June survey by looking up the interpolated temperature at the depth level corresponding to a bathymetry grid provided by the Canadian Hydrographic Service with some corrections applied (Dutil et al. 2012). The method is fully described in Tamdrari et al. (2012). A climatology was constructed by averaging all available temperature grids between 1981 and 2010 and anomaly grids were computed for each year. The June bottom temperature climatology as well as the 2018 reconstructed temperature and anomaly fields are shown in Fig. 41. The same method was applied using the available CTD data from August and September, thus including the multispecies surveys for the northern Gulf in August and for the Magdalen Shallows in September. These results are also shown in Fig. 41. While much of the deeper bottom water temperatures are climatologically still below 0°C in June, a remnant from the winter near-freezing mixed layer that reached the bottom, most of the area usually warms to below 1°C by August-September. Temperature anomalies in coastal shallow waters range from <-2.5°C to >+2.5°C, but anomalies tend to be of smaller magnitude in deeper waters.

Time series of the bottom area covered by water in various temperature intervals were estimated from the gridded data for the June surveys as well as for the September multispecies survey on the Magdalen Shallows (Fig. 42). The time series of areas of the Magdalen Shallows covered by water colder than 0, 1, 2, and 3°C in June and September are also shown in Fig. 38 as part of the CIL summary. In June 2018, none of the bottom of the Magdalen Shallows was covered by water with temperatures <-1°C, in contrast to somewhat colder conditions in June 2017. By September, almost none of the bottom was covered by water with temperatures <1°C on the south-eastern side of the Shallows; these are warmer than normal conditions (Fig. 38) that are nevertheless colder than during the recent 2010-2012 period. The area covered by water temperatures <0°C in June and <1°C in September had then reached a low (warm conditions) not seen since the early 1980s, but rebounded to near-normal in 2014 and 2015, and again in 2017. The areas were overall smaller than normal (warmer waters) in June 2018 (-0.7 SD) and in September (-1.3 SD). At higher threshold temperatures, areas with T< 2°C and <

3°C were below normal in June but normal by September 2018, reducing only slightly in area within that time span (Fig. 38).

## DEEP WATERS (>150 M)

The deeper water layer (>150 m) below the CIL originates at the entrance of the Laurentian Channel at the continental shelf and circulates towards the heads of Laurentian, Anticosti, and Esquiman channels without much exchange with the upper layers. The layer from 150 to 540 m is characterized by temperatures between 1 and >7°C and salinities between 32.5 and 35 (except for Mécatina Trough where near-freezing waters may fill the basin to 235 m in winter and usually persist throughout the summer). Interdecadal changes in temperature, salinity, and dissolved oxygen of the deep waters entering the Gulf at the continental shelf are related to the varying proportion of the source cold–fresh and high dissolved oxygen Labrador Current water and warm–salty and low dissolved oxygen slope water (McLellan 1957, Lauzier and Trites 1958, Gilbert et al. 2005). The deeper waters travel from the mouth of the Laurentian Channel to the Estuary in roughly three to four years (Gilbert 2004), decreasing in dissolved oxygen from in situ respiration and oxidation of organic material as they progress to the channel heads. The lowest levels of dissolved oxygen (around 20 percent saturation in recent years) are therefore found in the deep waters at the head of the Laurentian Channel in the Estuary.

### BOTTOM WATER TEMPERATURES IN AUGUST AND SEPTEMBER

The same method used to calculate bottom water temperature on the Magdalen Shallows was applied to the entire Gulf by combining all available CTD data from August and September, thus including the multispecies surveys for the northern Gulf in August and for the Magdalen Shallows in September into a single map (Fig. 43). All of the Gulf deep bottom water temperatures were above normal, with large areas of Central Gulf, Anticosti and Esquiman Channels, and northwest Gulf above 6°C.

As done for the Magdalen Shallows (Fig. 42), time series of the bottom area covered by water in various temperature intervals were also estimated for the other regions of the Gulf based on August-September temperature profile data (Figs. 44 and 45). The figures show compression of the bottom habitat area in the temperature range of 5–6°C in 1992, offset by larger colder 4–5°C habitat. In 2012, a return of >6°C temperatures to the sea floor began. By 2015, it had caused a large decrease of the 5–6°C habitat in Anticosti and Esquiman Channels, this time replaced by warmer 6–7°C habitat. The 6–7°C area then increased sharply in Central and northwest Gulf in 2017, and increased sharply again in northwest Gulf in 2018. Outside of the Magdalen Shallows and Mécatina Trough, there were almost no areas with bottom waters colder than 0°C in August 2018.

### DEEP TEMPERATURE MAXIMUM

The warm waters found at the bottom of the Laurentian Channel and elsewhere are associated with the deep temperature maximum evident in the temperature profiles in these areas (e.g. Fig. 3). The recent inter-annual progression to current conditions of the deep temperature maximum is shown on Fig. 46. Temperatures above 7°C have been recorded since 2012 in the Gulf near Cabot Strait. The Gulf-wide average and regional areal averages are shown in Fig. 47 for temperature and in Fig. 48 for salinity. The deep maximum temperature Gulf-wide average was at a series record high in 2018, at 6.38°C.

## TEMPERATURE AND SALINITY MONTHLY MEANS

Monthly temperature and salinity averages were constructed for various depths using a method used by Petrie et al. (1996) but using the geographical regions shown in Fig. 2. In this method, all available data obtained during the same month within a region and close to each depth bin are first averaged together for each year. Monthly averages from all available years from 1981 to 2010 and their standard deviations are then computed for climatologies. This two-fold averaging process reduces the bias that occurs when the numbers of profiles in any given year are different. These monthly averages were further averaged into regional yearly time series that are presented in Figs. 47 (temperature) and 48 (salinity) for 200 and 300 m. The 300 m observations suggest that temperature anomalies are advected up-channel from Cabot Strait to the northwestern Gulf in two to three years, consistent with the findings of Gilbert (2004), while variability at 200 m often appear or disappear everywhere at the same time, suggesting vertical changes. The regional averages are weighted into a Gulf-wide average in accordance to the surface area of each region at the specified depth. These Gulf-wide averages are shown for 150, 200 and 300 m in Figs. 47-49. Linear trends in temperature and salinity at 300 m of 2.3°C and 0.3 per century, respectively are shown on Fig. 49 (See also Galbraith et al. 2013 for other long term trends).

In 2018, the gulf-wide average salinities bounced back at all depths shallower than 300 m after a decrease in 2017 (Figs. 48 and 49), and increased slightly at 300 m to +1.1 SD. Gulf-wide average temperatures at 150 and 200 m are lower than the 2015 record highs but remain above normal at 3.0°C (+1.0 SD) and 5.0°C (+1.4 SD). New series record highs (since 1915) were set at 250 and 300 m, at 6.1°C (+3.0 SD) and 6.4°C (+5.7 SD) respectively. At 300 m, temperature increased to regional record highs in all deep regions of the Gulf: Estuary (5.6°C, +2.9 SD), Northwest Gulf (6.0°C, +4.4 SD), Central Gulf (6.5°C, +5.1 SD) and Cabot Strait (6.8C, +4.6 SD).

The warm anomalies present since 2010 at Cabot Strait have been progressing up the channel towards the Estuary since then, but waters that have followed into the gulf have also remained very warm and even increased in temperature such that the average overall temperature may continue to increase (Fig. 46). The potential for still warmer waters entering the Gulf exists, as evidenced by an average temperature of 9.2°C observed at the Laurentian Mouth at 200 m in 2016 (Fig. 47), a record since the series began in 1914, and a 2015 record high of 7.6°C at 300 m.

## SEASONAL AND REGIONAL AVERAGE TEMPERATURE STRUCTURE

In order to show the seasonal progression of the vertical temperature structure, regional averages are shown in Figs. 50 to 53 based on the profiles collected during the March helicopter survey, the June AZMP and mackerel surveys, the August multi-species survey (September survey for the Magdalen Shallows), and the October-November AZMP survey. All additional archived CTD data for those months were also used. The temperature scale was adjusted to highlight the CIL and deep-water features; the display of surface temperature variability is best suited to other tools such as remote sensing and thermographs. Average discrete depth layer conditions are summarized for the months of the 2017 and 2018 AZMP surveys in Fig. 54 for temperature and in Fig. 55 for salinity and 0-50 m stratification. For each survey the anomalies were computed relative to monthly temperature and salinity 1981-2010 climatologies calculated for each region, shown in grey as the mean value ± 0.5 SD in Figs. 50 to 53.

Caution is needed in interpreting the March profiles. Indeed, regional averaging of winter profiles does not work very well in the northeast Gulf (regions 3 and 4) because very different

water masses are present in the area such as the cold Labrador Shelf intrusion with saltier and warmer deeper waters of Anticosti Channel or Esquiman Channel. For example, the sudden temperature changes near the bottom of Mécatina Trough in 2018 resulted from the deepest cast used that contained colder deep waters. The highlights of March water temperatures shown in Fig. 50 include the previously discussed winter mixed layer, with near-normal thicknesses for T<-1°C and T<0°C, but very little waters with temperatures in between, as well as the higher winter layer thicknesses found in Central Gulf and Cabot Strait. The thermocline was much shallower than usual in the Northwest Gulf and Anticosti Channel and in in particular in the Estuary. Waters in the deepest parts of Mécatina Trough were on average warmer than normal because of the only partial renewal from a Labrador Shelf intrusion. Averages temperatures at 150 and 200 m actually fell between March and June, indicating a late renewal from the Labrador Shelf.

Temperatures in June, August and fall 2018 were characterized by CIL conditions with an unusual pattern of colder than normal in the estuary and warmer than normal in Anticosti Channel. From the 2017 and 2018 fall surveys, we note the high interannual variability of the CIL conditions in Anticosti Channel.

Deep-water temperatures were above normal in all regions along the Laurentian Channel, with most regions showing increases compared with 2017 conditions in waters deeper than 250 m depth. Temperatures at the depth of the temperature maximum (200 to >250 m) remained above normal in Esquiman Channel and Central Gulf, exceeding 6°C at depth, presumably advected in from the Cabot Strait recent record-high conditions.

## CURRENTS AND TRANSPORTS

Currents and transports are derived from a numerical model of the Gulf of St. Lawrence, Scotian Shelf, and Gulf of Maine. The model is prognostic, i.e., it allows for evolving temperature and salinity fields. It has a spatial resolution of 1/12° with 46 depth-levels in the vertical. The atmospheric forcing is taken from the Global Environmental Multiscale (GEM) model running at the Canadian Meteorological Center (CMC). Freshwater runoff is obtained from observed data and the hydrological model, as discussed in the freshwater runoff section. A simulation was run for 2006–2018 from which transports were calculated. The reader is reminded that the results outlined below are not measurements but simulations and improvements in the model may lead to changes in the transport values.

Figs. 56–58 show seasonal depth-averaged currents for 0–20 m, 20–100 m, and 100 m to the bottom for 2018. Currents are strongest in the surface mixed layer, generally 0–20 m, except in winter months when the 20–100 m and the 100m to bottom averages are almost as high (note the different scale for this depth). Currents are also strongest along the slopes of the deep channels. The Anticosti Gyre is always evident but strongest during winter months, when it even extends strongly into the bottom-average currents.

Monthly averaged transports across seven sections of the Gulf of St. Lawrence are shown in Fig. 59 for sections with some estuarine circulation, and in Fig. 60 for sections where only net transports are relevant. In Fig. 59, the net transport integrates both up and downstream circulation and, for example, corresponds to freshwater runoff at the Pointe-des-Monts section. The outflow transport integrates all currents heading toward the ocean, while the estuarine ratio corresponds to the outflow divided by the net transports. Note that the only section where estuarine circulation is dominant is at Pointe-des-Monts. The net transport at Honguedo is on average 15 times higher, consisting mostly of circulation around Anticosti Island first observed at the Jacques-Cartier section. Similarly, the net transport at Cabot Strait is mostly balanced by inflow from Belle Isle Strait such perhaps an estuarine ratio is perhaps a misleading description.

Transports through sections under the direct estuarine influence of the St. Lawrence River (e.g., Pointe-des-Monts) have a more direct response to change in freshwater runoff while others (e.g., Cabot Strait, Bradelle Bank) have a different response, presumably due to redistribution of circulation in the GSL under varying runoff. The estuarine circulation ratio is determined by the mixing intensities within the estuary and is greatly influenced by stratification. It is on average greatest during winter months and weakest during the spring freshet. In fact, it is sufficiently reduced in spring that the climatological outward transport at Pointe-des-Monts reaches its minimum value in June even though this month corresponds to the third highest net transport of the year, i.e. the estuary becomes sufficiently stratified that fresh water runoff tends to slip on top of the denser salty waters underneath. This occurred in 2017 when the exceptionally high April freshet led to decreased modeled estuarine circulation and decreased outward transport by entrainment at the Pointe-des-Monts section. However, the above-average run-off in March 2018 coincided with increased outward transport and estuarine ratio.

## HIGH FREQUENCY SAMPLING AZMP STATIONS

Sampling by the Maurice Lamontagne Institute began in 1991 at a station offshore of Rimouski (48° 40' N 68° 35' W, 320 m depth; Plourde et al. 2009), typically once a week during summer and less often during spring and fall and almost never in winter (Fig. 61). In 2013, following several analyses that identified good correlations and correspondences between the prior AZMP Anticosti Gyre and Gaspé Current stations with the Rimouski station, it was decided to drop sampling efforts at these logistically difficult stations and integrate the Rimouski station officially in the AZMP program and begin winter sampling there when opportunities arose. The AZMP station in the Shediac Valley (47° 46.8' N, 64° 01.8' W, 84 m depth) is sampled by the Bedford Institute of Oceanography, by DFO Gulf Region and by the Maurice Lamontagne Institute (Fig. 61). This station has been sampled irregularly since 1947, nearly every year since 1957, and more regularly during the summer months since 1999 when the AZMP program began. However, observations were mostly limited to temperature and salinity prior to 1999.

In 2018, Viking oceanographic buoys equipped with an automatic temperature and salinity profiler carried out 327 full-depth casts at Shediac Valley station between May 26 and November 1, and 384 casts to typically 200 m depth (and up to 320 m starting September 28 2018) at Rimouski station between April 19 and November 10.

Isotherms and isohalines as well as monthly averages of layer temperature and salinity, stratification, and CIL core temperature and thickness at <1°C are shown for 2016-2018 for the Rimouski station in Fig. 62 and for the Shediac Valley station in Fig. 63. The scorecard climatologies are calculated from 1991-2010 data for Rimouski station, and for 1981-2018 for Shediac Valley (The time span of the climatology is extended at Shediac Valley because of the sparseness of data prior to 1999). Buoy data are used for scorecard metrics for Rimouski station but not for the display of isotherms and isohalines.

At the Rimouski station, the gradual shift of cold-fresh deep anomalies present in 2010 to warmer-saltier waters advected from Cabot Strait lead to a shift to warm anomalies by May 2013 and a 300-m series record in temperature (5.77°C) observed in February 2018. The CIL was normal to colder and thicker than normal in 2018.

Conditions were variable at Shediac Valley station (Fig. 63), but included the second warmest surface monthly average temperature recorded at the station in August (18.7°C, +2.7°C, +2.9 SD).

Fig. 64 shows the interannual variability of some bulk layer averages from May to October for the two stations. Near-bottom temperature was at a record high at Rimouski station (5.60°C, +0.55°C, +2.0 SD).

## SUMMARY

Fig. 66 summarizes SST, summertime CIL and deep-water average temperatures. While May-November SST and August SST are well correlated ($R^2$ = 0.50 for the 1985-2018 AVHRR record), the August SST reached in 2012 and 2014 were very high anomalies compared the May-November averages, while in 2006 the reverse was found to be the case. Similarly, the high August SST anomaly observed in 2018 contrasts with the negative (but still near-normal) May-November anomaly.

Fig. 66 shows the fourth warmest August SST of the recent AVHRR record, the coldest May-November average SST since 2002, a small increase in the CIL temperature minimum and deep temperature at 150 m and 200 m, and an increase to a new series record high temperature at 300 m (6.4°C, +5.7 SD).

Another summary of the temperature state of the Gulf of St. Lawrence over a shorter time span (since 1971) allows the inclusion of more data sets, and three sets of four time series are chosen to represent surface, intermediate and deep conditions (Fig. 67). The SST summer and fall timing are from Fig. 22 (12°C threshold) with air temperature proxies used prior to 1985. Sea-ice is grouped as an intermediate feature since all are associated with winter formation. Fig. 67 shows the sums of these three sets of anomalies representing the state of different parts of the system and is reproduced on Fig. 68 with each time series contribution shown as stacked bars (Petrie et al. 2007). These composite indices measure the overall state of the climate system with positive values representing warm conditions and negative representing cold conditions. The plot also indicates the degree of correlation between the various measures of the environment. In 2018, the surface index was near-normal at +0.3 SD, the intermediate index was warmer than normal at +1.1 SD and the deep index increased slightly to +3.0 SD, its third highest value record after the 2015 record high and 2016 value.

## KEY FINDINGS

- The annual average runoff from the St. Lawrence River measured at Québec City and RIVSUM II were above-normal at 13,200 $m^3s$-1 (+1.4 SD) and 16,900 $m^3s$-1 (+0.7 SD) respectively. The St. Lawrence River spring freshet extended early to include March, and the March-May average was above-normal (+1.4 SD).
- Sea ice maximum volume was 9th lowest since 1969 at 35 $km^3$ (-1.1 SD). In the 9 year span since 2010, 7 of the 9 lowest maximum ice volumes of the time series have occurred.
- The winter surface mixed cold layer (<- 1°C) volume of 12,600 $km^3$ was near normal (+0.3 SD against 1996–2018 climatology). The Labrador Shelf water intrusion volume into Mécatina Trough of 250 $km^3$ tied with 2015 for the lowest observation (1997-2018), representing only 2% of the cold water in the Gulf.
- The August cold intermediate layer (CIL) was warmer (+1.6 SD) and thinner (-1.7 SD for volume colder than 1°C) than normal, warmer than conditions of 2017. The Gilbert and Pettigrew minimum temperature index, which includes data over a longer season, was above normal (-0.05°C, +0.9 SD). This slightly different result in terms of anomaly is caused by the different years included in the climatology; the temperatures are consistent with each other when adjusted for warning between mid-July and mid-August (difference of 0.1°C).

- The timing of summer onset and post-season cooling of the surface layer were respectively later than normal (+0.6 SD, +0.8 weeks) and near normal (+0.2 SD, +0.2 weeks).
- Near-surface water temperatures were at a record low in November (since 1985, -1.3°C, -1.7 SD), below normal in spring (May and June) and fall (October and November) and only above in August and September. The May to November 2018 average was near-normal (-0.3°C, -0.5 SD), but the coldest since 2002.
- Deep water temperatures have been increasing overall in the Gulf, with inward advection from Cabot Strait. Gulf-wide average temperatures at 150 and 200 m are lower than the 2015 record highs but remain above normal at 3.0°C (+1.0 SD) and 5.0°C (+1.4 SD). New series record highs (since 1915) were set at 250 and 300 m, at 6.1°C (+3.0 SD) and 6.4°C (+5.7 SD) respectively. At 300 m, temperature increased to regional record highs in all deep regions of the Gulf: Estuary (5.6°C, +2.9 SD), Northwest Gulf (6.0°C, +4.4 SD), Central Gulf (6.5°C, +5.1 SD) and Cabot Strait (6.8C, +4.6 SD).
- Bottom area covered by waters warmer than 6°C remained quite high in 2018 in Anticosti Channel, Esquiman Channel and Central Gulf, and increased sharply in and the northwest Gulf to reach a series record.

## OUTLOOK FOR 2019

Air temperatures were well below normal over the Gulf in October and November 2018, near-normal in December and January and slightly below normal in February 2019. This was the setting for the March 2019 survey, which provides an outlook for CIL conditions expected for the remainder of 2019. Fig. 65 shows the surface mixed layer temperature, salinity, and thickness (at T<-1°C and T<0°C), as well as the thickness and extent of the cold and saline layer that has intruded into the Gulf from the Labrador shelf. All of the winter mixed layer was cold (below -1°C), out to Port aux Basques, which is a rare event. The volume of the surface mixed layer colder than -1°C was at a 24-year series record high of 15,200 $km^3$, 45% of all waters of the Gulf. The Cold Intermediate Layer for summer 2019 is therefore forecasted to be much colder than in 2018, with a Gilbert and Pettigrew (1997) index of around -0.64°C compared to -0.05°C in 2018.

Concerning deep waters, recall that record high temperatures have been recorded in Cabot Strait since 2012, and that overall the Gulf waters at 300 m were in 2017 at a 100+ year record high. Although the March helicopter survey only rarely samples deeper than 210 m, temperatures higher than 7°C were measured at three stations in the area of Cabot Strait, reached 7.6°C inside the Gulf. This signifies the continuation of warmer than normal conditions at depth.

## ACKNOWLEDGEMENTS

We are grateful to the people responsible for CTD data acquisition during the surveys used in this report:

- Rimouski station monitoring: Roger Pigeon, Félix St-Pierre, Michel Rousseau, Rémi Desmarais, Anthony Ouellet, Nicolas Coulombe, Louis Gagné and Guillaume Mercier.
- Shediac Valley monitoring station: Roger Pigeon, Michel Rousseau, Kevin Pauley, Tom Hurlbut
- March survey: Peter Galbraith, Anthony Ouellet, Michel Dubé, Eddy Perron and the Transport Canada group in Ottawa for the design and build of the new oceanographic winch.

- June AZMP transects: Caroline Lafleur, Félix St-Pierre, Rémi Desmarais, Nicolas Coulombe, Marie-Lyne Dubé, Marjolaine Blais, David Leblanc, Anthony Ouellet, Jean-Denis Thibeault, the officers and crew of the Coriolis II.
- August Multi-species survey: Rémi Desmarais, Anthony Ouellet, Nicolas Coulombe, Jean-Denis Thibeault; the officers and crew of the CCGS Teleost.
- October-November AZMP survey: David Leblanc, Félix St-Pierre, Sonia Michaud, Isabelle St-Pierre, Louis Gagné, Marjolaine Blais, Nicolas Coulombe, Laure Devine, Marie-Noëlle Bourassa; the officers and crew of the CCGS Hudson.
- September Multi-species survey: Luc Savoie for providing the CTD data.
- Northumberland Strait survey: Mark Hanson and Joël Chassé.
- Data management: Laure Devine, Caroline Lafleur, Marie-Noëlle Bourassa, Isabelle St-Pierre, Brian Boivin.

CTD maintenance: Roger Pigeon, Félix St-Pierre, Michel Rousseau.

Data from the following sources are also gratefully acknowledged:

- Air temperature: Environment Canada.
- Sea-ice: Canadian Ice Service, Environment Canada. Processing of GIS files by Paul Nicot.
- Runoff at Québec City: Denis Lefaivre.
- Runoff from hydrological modelling: Joël Chassé and Diane Lavoie.
- Historical AVHRR SST remote sensing (IML): Pierre Larouche, Bernard Pettigrew.
- AVHRR SST remote sensing (BIO): Carla Caverhill.

All figures were made using the free software Gri (Kelley and Galbraith 2000).

We are grateful to David Hebert and Frédéric Cyr for reviewing the manuscript and providing insightful comments.

## REFERENCES CITED

Benoît, H.P., Savenkoff, C., Ouellet, P., Galbraith, P.S., Chassé, J. and Fréchet, A. 2012. Impacts of fishing and climate-driven changes in exploited marine populations and communities with implications for management, in State-of-the-Ocean Report for the Gulf of St. Lawrence Integrated Management (GOSLIM) Area, H. P. Benoît, J. A. Gagné, C. Savenkoff, P. Ouellet and M.-N. Bourassa, Eds. Can. Manuscr. Rep. Fish. Aquat. Sci. 2986: viii + 73 pp.

Bourgault, D. and Koutitonsky, V.G. 1999. Real-time monitoring of the freshwater discharge at the head of the St. Lawrence Estuary. Atmos. Ocean, 37 (2): 203–220.

Colbourne, E., Holden, J., Snook, S., Han, G., Lewis, S., Senciall, D., Bailey, W., Higdon, J., and Chen, N. 2017. Physical oceanographic conditions on the Newfoundland and Labrador Shelf during 2016. DFO Can. Sci. Advis. Sec. Res. Doc. 2017/079. v + 50 p.

Cyr, F., Bourgault, D. and Galbraith, P.S. 2011. Interior versus boundary mixing of a cold intermediate layer. J. Gephys. Res. (Oceans), 116, C12029, doi:10.1029/2011JC007359.

Dutil, J.-D., Proulx, S., Galbraith, P.S., Chassé, J., Lambert, N. and Laurian, C. 2012. Coastal and epipelagic habitats of the estuary and Gulf of St. Lawrence. Can. Tech. Rep. Fish. Aquat. Sci. 3009: ix + 87 p.

Galbraith, P.S. 2006. Winter water masses in the Gulf of St. Lawrence. J. Geophys. Res., 111, C06022, doi:10.1029/2005JC003159.

Galbraith, P.S. and Grégoire, F. 2015. Habitat thermique du maquereau bleu; profondeur de l'isotherme de 8 °C dans le sud du golfe du Saint-Laurent entre 1960 et 2014. Secr. can. de consult. sci. du MPO. Doc. de rech. 2014/116. v + 13 p.

Galbraith, P.S. and Larouche, P. 2011. Sea-surface temperature in Hudson Bay and Hudson Strait in relation to air temperature and ice cover breakup, 1985-2009. J. Mar. Systems, 87, 66-78.

Galbraith, P.S. and Larouche, P. 2013. Trends and variability in eastern Canada sea-surface temperatures. Ch. 1 (p. 1-18) In: Aspects of climate change in the Northwest Atlantic off Canada [Loder, J.W., G. Han, P.S. Galbraith, J. Chassé and A. van der Baaren (Eds.)]. Can. Tech. Rep. Fish. Aquat. Sci. 3045: x + 190 p.

Galbraith, P.S., Saucier, F.J., Michaud, N., Lefaivre, D., Corriveau, R., Roy, F., Pigeon, R. and Cantin, S. 2002. Shipborne monitoring of near-surface temperature and salinity in the Estuary and Gulf of St. Lawrence. Atlantic Zone Monitoring Program Bulletin, Dept. of Fisheries and Oceans Canada. No. 2: 26–30.

Galbraith, P.S., Desmarais, R., Pigeon, R. and Cantin, S. 2006. Ten years of monitoring winter water masses in the Gulf of St . Lawrence by helicopter. Atlantic Zone Monitoring Program Bulletin, Dept. of Fisheries and Oceans Canada. No. 5: 32–35.

Galbraith, P.S., Larouche, P., Gilbert, D., Chassé, J. and Petrie, B. 2010. Trends in sea-surface and CIL temperatures in the Gulf of St. Lawrence in relation to air temperature. Atlantic Zone Monitoring Program Bulletin, 9: 20-23.

Galbraith P.S., Larouche, P., Chassé, J. and Petrie, B. 2012. Sea-surface temperature in relation to air temperature in the Gulf of St. Lawrence: interdecadal variability and long term trends. Deep Sea Res. II, V77–80, 10–20.

Galbraith. P.S., Hebert, D., Colbourne, E. and Pettipas, R. 2013. Trends and variability in eastern Canada sub-surface ocean temperatures and implications for sea ice. Ch.5 In: Aspects of climate change in the Northwest Atlantic off Canada [Loder, J.W., G. Han, P.S. Galbraith, J. Chassé and A. van der Baaren (Eds.)]. Can. Tech. Rep. Fish. Aquat. Sci. 3045: x + 192 p.

Galbraith, P.S., Chassé, J., Caverhill, C., Nicot, P., Gilbert, D., Pettigrew, B., Lefaivre, D., Brickman, D., Devine, L., and Lafleur, C. 2017. Physical Oceanographic Conditions in the Gulf of St. Lawrence in 2016. DFO Can. Sci. Advis. Sec. Res. Doc. 2017/044. v + 91 p.

Galbraith, P.S., Chassé, J., Caverhill, C., Nicot, P., Gilbert, D., Lefaivre, D. and Lafleur, C. 2018. Physical Oceanographic Conditions in the Gulf of St. Lawrence during 2017. DFO Can. Sci. Advis. Sec. Res. Doc. 2018/050. v + 79 p.

Gilbert, D. 2004. Propagation of temperature signals from the northwest Atlantic continental shelf edge into the Laurentian Channel. ICES CM, 2004/N:7, 12 pp.

Gilbert, D. and Pettigrew, B. 1997. Interannual variability (1948-1994) of the CIL core temperature in the Gulf of St. Lawrence. Can. J. Fish. Aquat. Sci., 54 (Suppl. 1): 57–67.

Gilbert, D., Sundby, B., Gobeil, C., Mucci, A. and Tremblay, G.-H. 2005. A seventy-two-year record of diminishing deep-water oxygen in the St. Lawrence estuary: The northwest Atlantic connection. Limnol. Oceanogr., 50(5): 1654–1666.

Hammill, M.O. and Galbraith, P.S. 2012. Changes in seasonal sea-ice cover and its effect on marine mammals, in State-of-the-Ocean Report for the Gulf of St. Lawrence Integrated Management (GOSLIM) Area, H. P. Benoît, J. A. Gagné, C. Savenkoff, P. Ouellet and M.-N. Bourassa, Eds. Can. Manuscr. Rep. Fish. Aquat. Sci. 2986: viii + 73 pp.

Hebert, D., Pettipas, R., Brickman, D., and Dever, M. 2018. Meteorological, Sea Ice and Physical Oceanographic Conditions on the Scotian Shelf and in the Gulf of Maine during 2016. DFO Can. Sci. Advis. Sec. Res. Doc. 2018/016. v + 53 p..

Kalnay, E., Kanamitsu, M., Kistler, R., Collins, W., Deaven, D., Gandin, L., Iredell, M., Saha, S., White, G., Woollen, J., Zhu, Y., Chelliah, M., Ebisuzaki, W., Higgins, W., Janowiak, J., Mo, K., Ropelewski, C., Wang, J., Leetmaa, A., Reynolds, R., Jenne, R. and Josephé, D. 1996. The NCEP/NCAR 40-year reanalysis project. Bull. Am. Meteorol. Soc. 77, 437–470.

Kelley, D.E. and Galbraith, P.S. 2000. Gri: A language for scientific illustration, Linux J., 75, 92 101.

Lauzier, L.M. and Trites, R.W. 1958. The deep waters of the Laurentian Channel. J. Fish. Res. Board Can. 15: 1247–1257.

McLellan, H.J. 1957. On the distinctness and origin of the slope water off the Scotian Shelf and its easterly flow south of the Grand Banks. J. Fish. Res. Board. Can. 14: 213–239.

Petrie, B., Drinkwater, K., Sandström, A., Pettipas, R., Gregory, D., Gilbert, D. and Sekhon, P. 1996. Temperature, salinity and sigma-t atlas for the Gulf of St. Lawrence. Can. Tech. Rep. Hydrogr. Ocean Sci., 178: v + 256 pp.

Petrie, B., Pettipas, R.G. and Petrie, W.M. 2007. An overview of meteorological, sea ice and sea surface temperature conditions off eastern Canada during 2006. DFO Can. Sci. Advis. Sec. Res. Doc. 2007/022.

Plourde, S., Joly, P., St-Amand, L. and Starr, M. 2009. La station de monitorage de Rimouski : plus de 400 visites et 18 ans de monitorage et de recherche. Atlantic Zone Monitoring Program Bulletin, Dept. of Fisheries and Oceans Canada. No. 8: 51-55.

Tamdrari, H., Castonguay, M., Brêthes, J.-C., Galbraith, P.S. and Duplisea, D.E. 2012. The dispersal pattern and behaviour of cod in the northern Gulf of St. Lawrence: results from tagging experiments, Can. J. Fish. Aquat. Sci. 69: 112-121.

Therriault, J.-C., Petrie, B., Pépin, P., Gagnon, J., Gregory, D., Helbig, J., Herman, A., Lefaivre, D., Mitchell, M., Pelchat, B., Runge, J. and Sameoto, D. 1998. Proposal for a Northwest Atlantic zonal monitoring program. Can. Tech. Rep. Hydrogr. Ocean Sci., 194: vii + 57 pp.

Vincent, L. A., Wang, X. L., Milewska, E. J., Wan, H., Yang, F. and Swail, V. 2012. A second generation of homogenized Canadian monthly surface air temperature for climate trend

## FIGURES

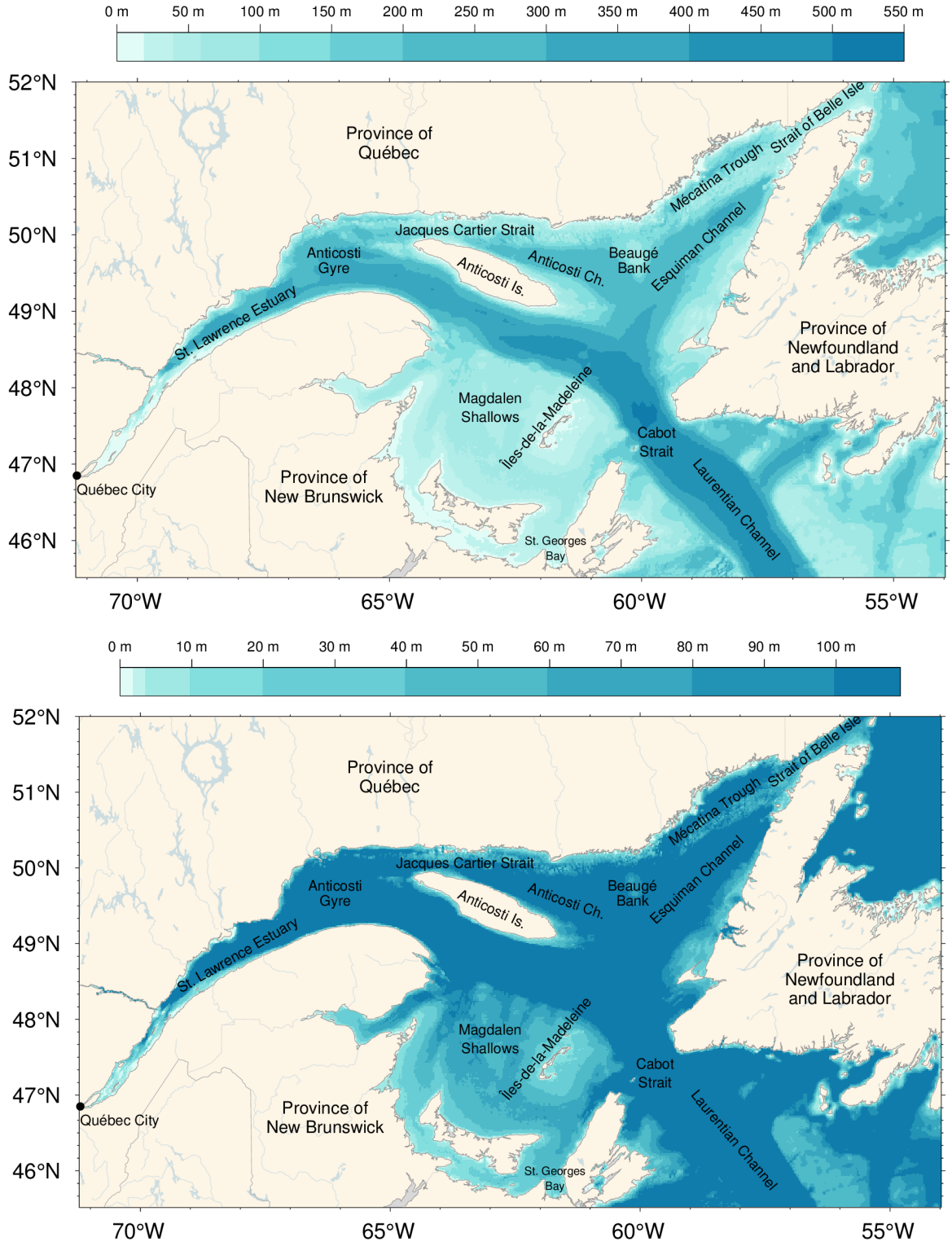


*Fig. 1. The Gulf of St. Lawrence. Locations discussed in the text are indicated. Bathymetry datasets used are from the Canadian Hydrographic Service to the west of 56°47' W (with some corrections applied to the baie des Chaleurs and Magdalen Shallows) and TOPEX data to the east. Bottom panel shows detail for 0-100 m bathymetry.*

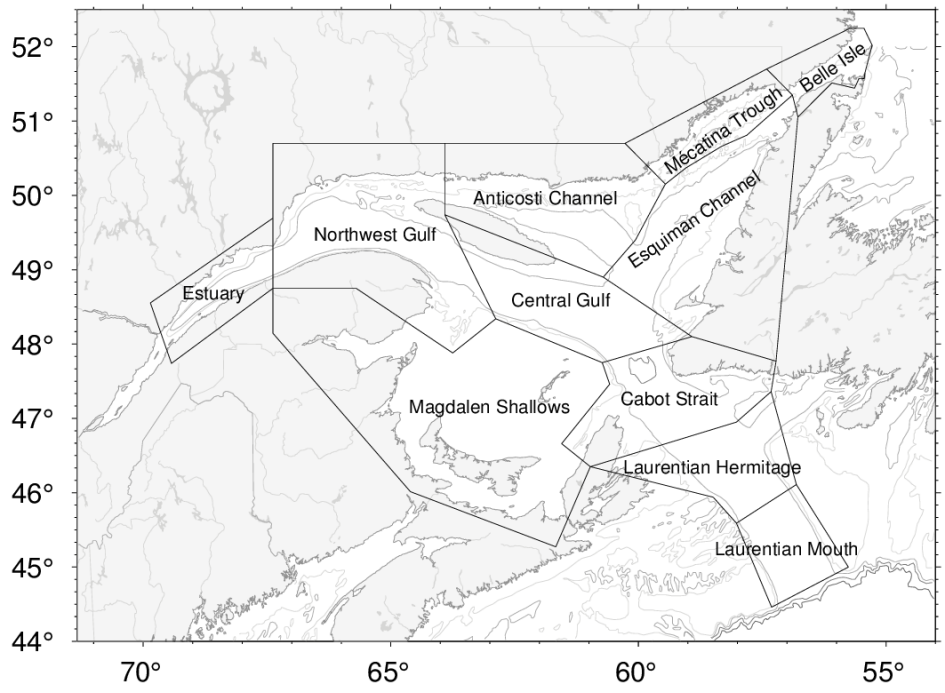


*Fig. 2. Gulf of St. Lawrence divided into oceanographic regions.*

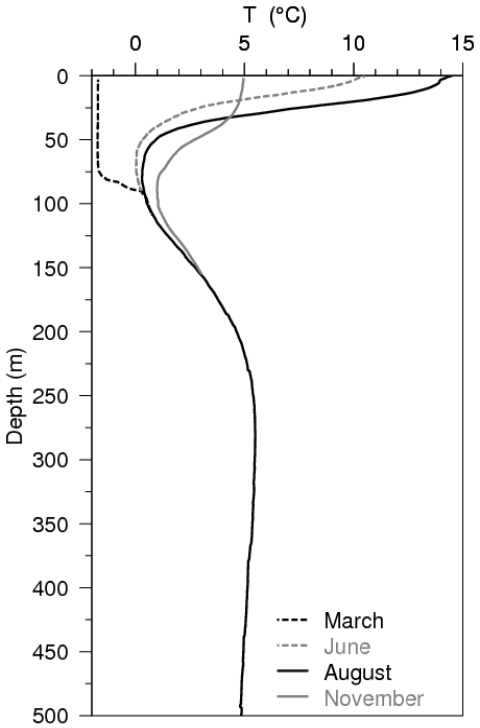


*Fig. 3. Typical seasonal progression of the depth profile of temperature observed in the Gulf of St. Lawrence. Profiles are averages of observations in August, June and November 2007 in the northern Gulf. The dashed line at left shows a single winter temperature profile (March 2008), with near freezing temperatures in the top 75 m. The cold intermediate layer (CIL) is defined as the part of the water column that is colder than 1°C, although some authors use a different temperature threshold. Figure from Galbraith et al. (2012).*

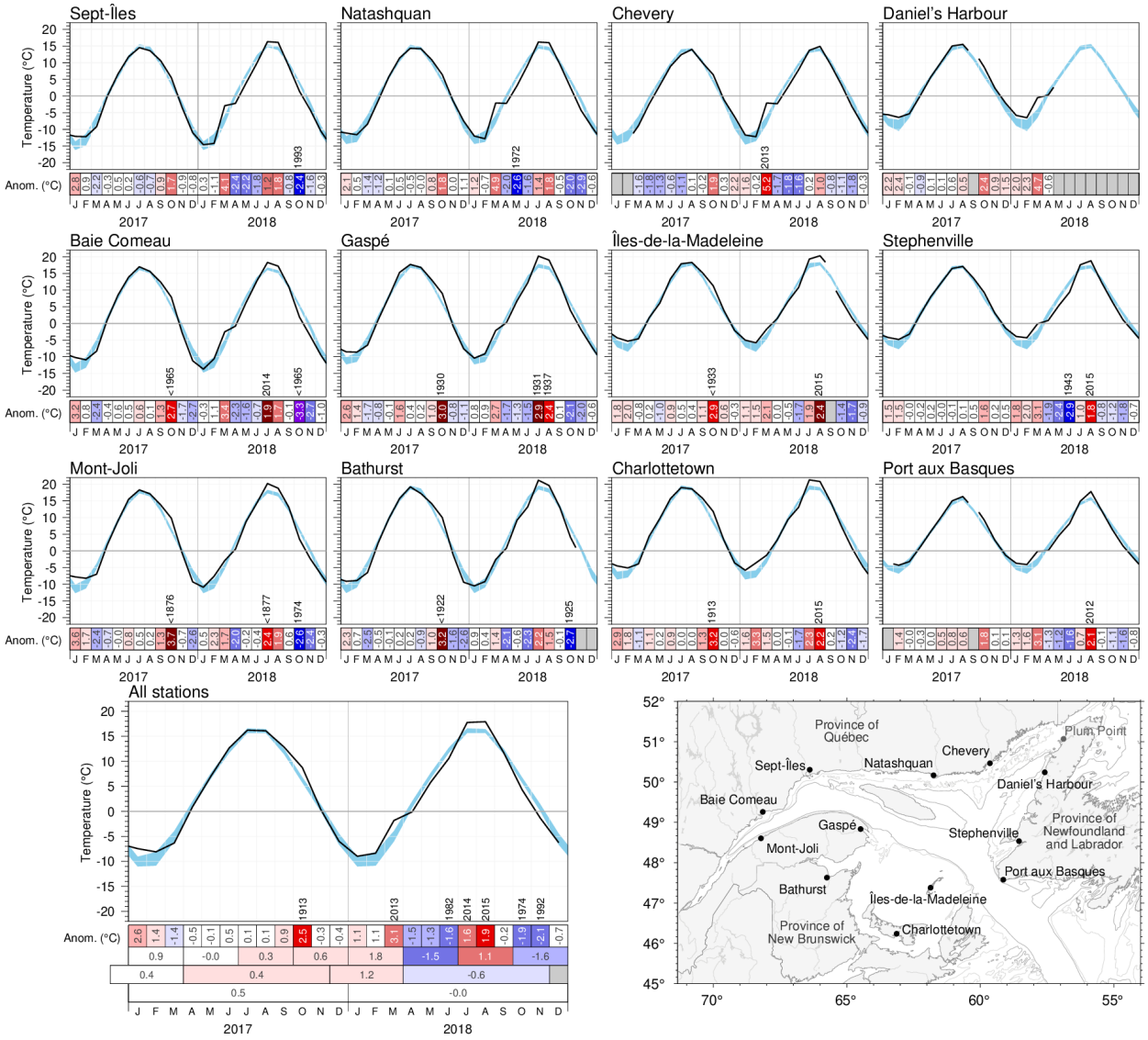


*Fig. 4. Monthly air temperatures and anomalies for 2017 and 2018 at selected stations around the Gulf as well as the average for all stations. The blue area represents the 1981–2010 climatological monthly mean ± 0.5 SD. Months with 4 or more days of missing data are omitted. The bottom scorecards are colour-coded according to the monthly normalized anomalies based on the 1981–2010 climatologies for each month, but the numbers are the monthly anomalies in ºC. For anomalies greater than 2 SD from normal, the prior year with a greater anomaly is indicated. Seasonal, December-March, April-November and annual anomalies are included for the all-station average.*

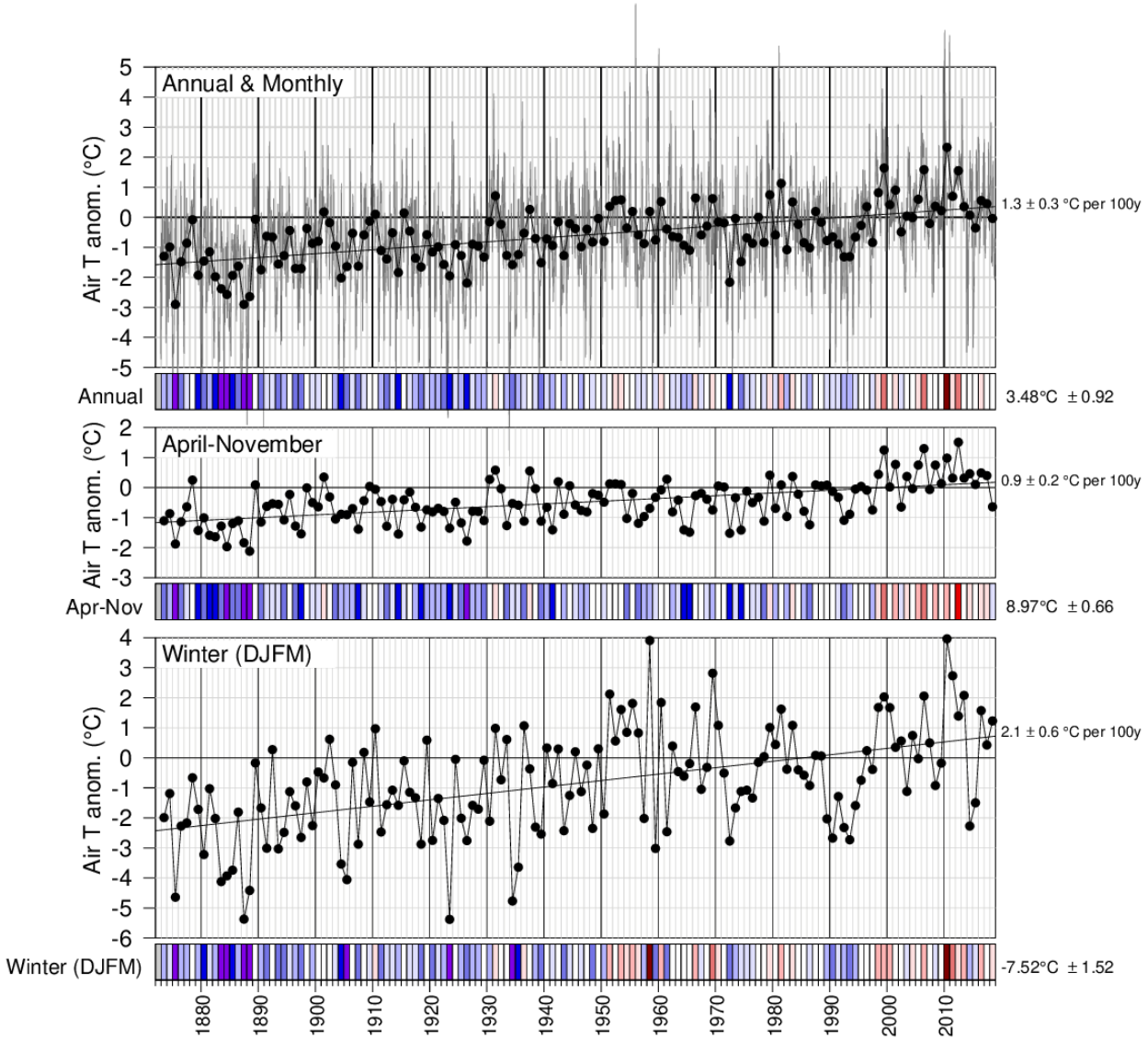


*Fig. 5. Annual, April-November December-March mean air temperature anomalies averaged for the selected stations around the Gulf from Fig. 4. The bottom scorecards are colour-coded according to the normalized anomalies based on the 1981–2010 climatology. Trends plus and minus their 95% confidence intervals are shown. April-November air temperature anomalies tend to be highly-correlated with May-November sea-surface temperature anomalies (Galbraith et al. 2012; Galbraith and Larouche 2013) whereas winter air temperature anomalies correlate highly with sea-ice cover parameters and winter mixed-layer volume (Galbraith et al. 2010; Galbraith et al. 2013)*

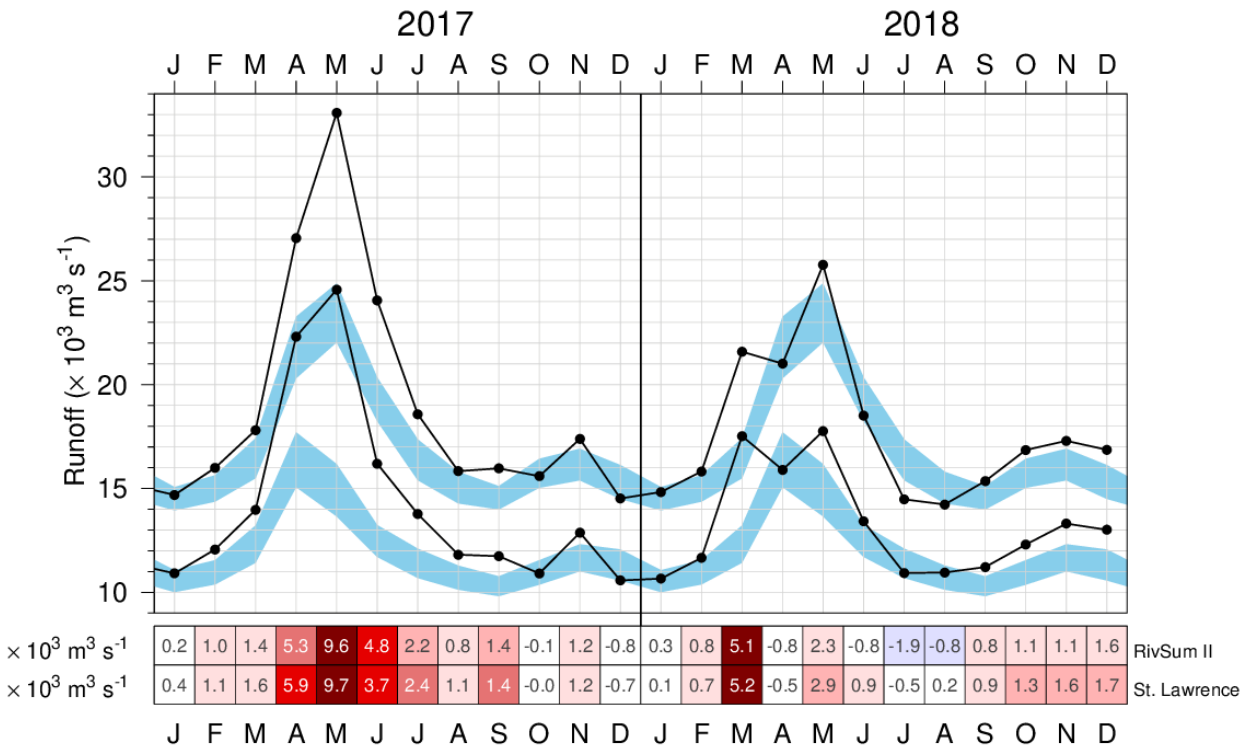


*Fig. 6. Monthly mean freshwater flow of the St. Lawrence River at Québec City (lower curve) and its sum with rivers flowing into the St. Lawrence Estuary (RIVSUM II, upper curve). The 1981–2010 climatological mean (± 0.5 SD) is shown (blue shading). The scorecards are colour-coded according to the monthly anomalies normalized for each month of the year, but the numbers are the actual monthly anomalies in $10^3$ $m^3s^{-1}$.*

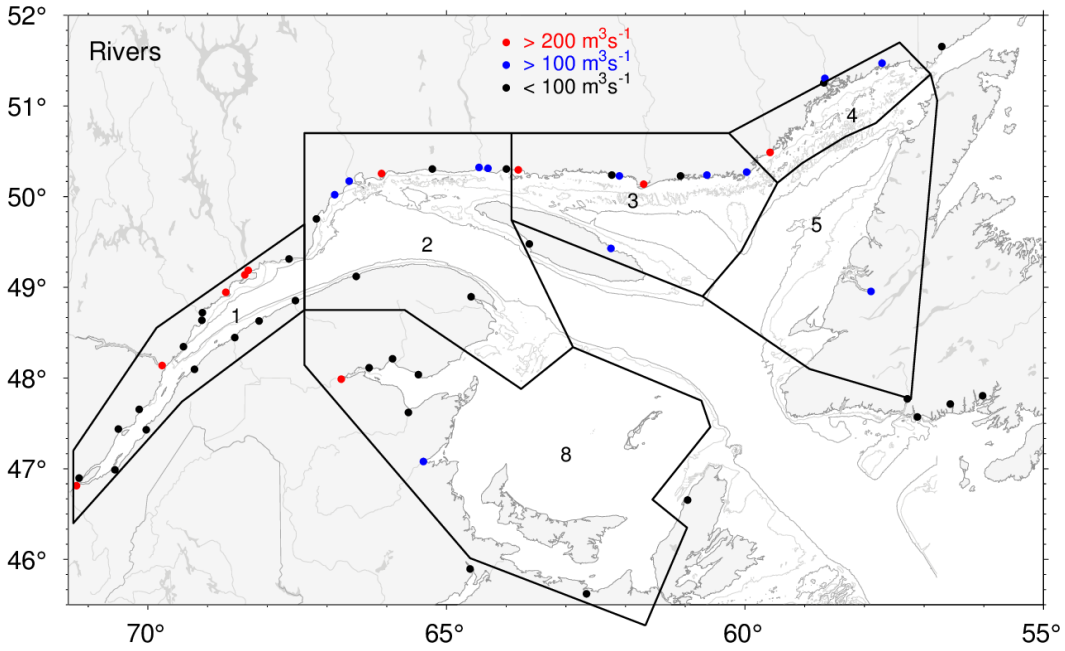


*Fig. 7. River discharge locations for the regional sums of runoffs listed in Fig. 8. Red and blue dots indicate rivers that have climatological mean runoff greater than 200 $m^3s^{-1}$ and between 100 and 200 $m^3s^{-1}$, respectively.*

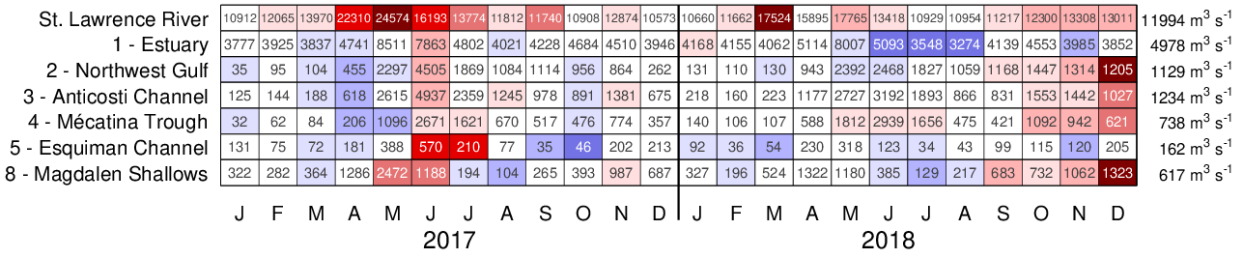


*Fig. 8. Monthly anomalies of the St. Lawrence River runoff and sums of all other major rivers draining into separate Gulf regions for 2017 and 2018. The scorecards are colour-coded according to the monthly normalized anomalies based on the 1981–2010 climatologies for each month, but the numbers are the monthly average runoffs in $m^3\ s^{-1}$. Numbers on the right side are annual climatological means. Runoff regulation is simulated for three rivers that flow into the Estuary (Saguenay, Manicouagan, Outardes).*

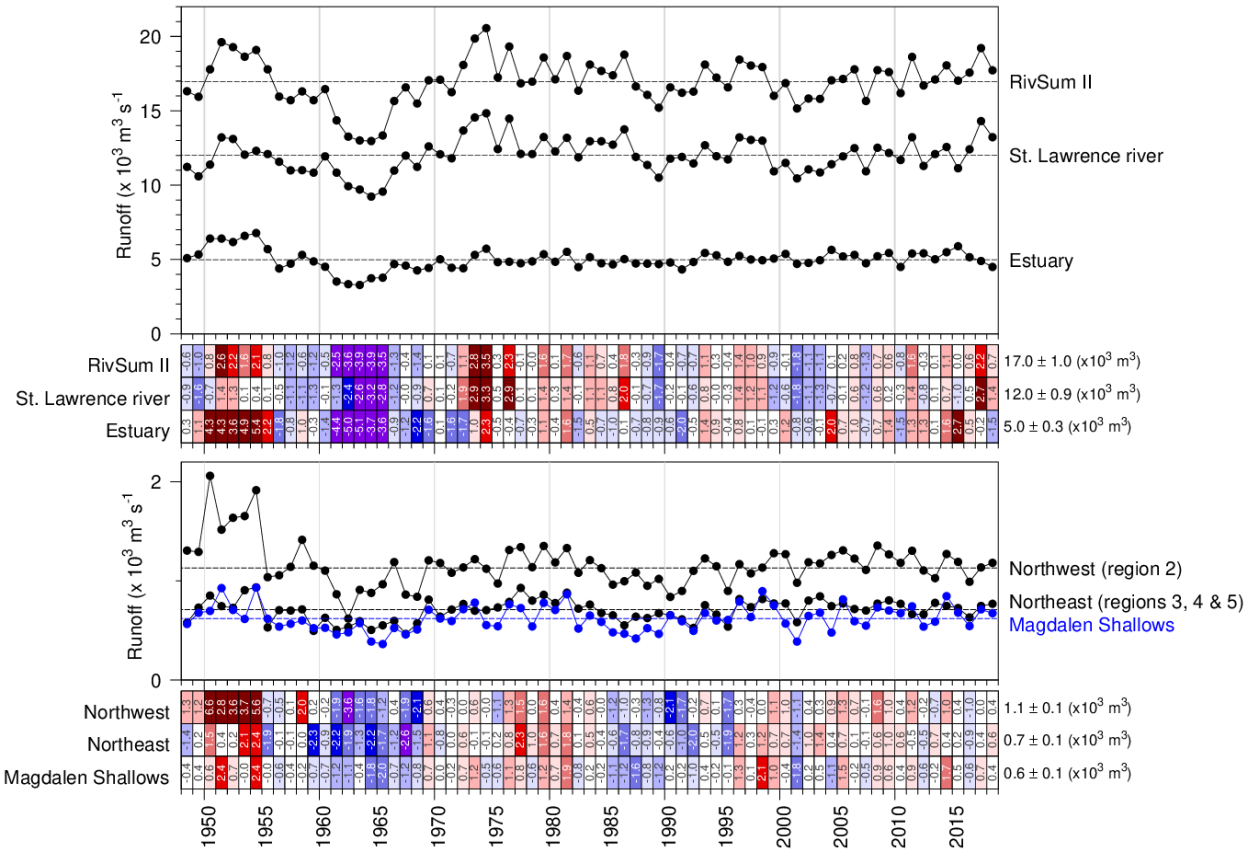


*Fig. 9. Annual mean freshwater flow of the St. Lawrence River at Québec City and of the sum of all rivers flowing into regions of the Estuary and Gulf (RivSum II) (top panel) and into 3 other oceanographic regions of the Gulf (bottom panel). The 1981–2010 climatological mean is shown as horizontal lines and indicated on the right side of the scorecards. Numbers in scorecards are normalized anomalies.*

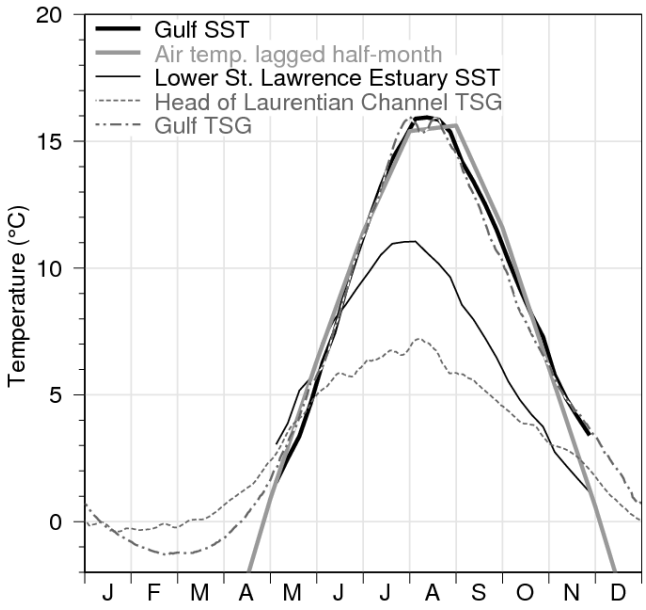


*Fig. 10. Sea-surface temperature climatological seasonal cycle in the Gulf of St. Lawrence. AVHRR temperature weekly averages for 1985 to 2010 are shown from May to November (ice-free months) for the Gulf (thick black line) and the cooler Lower St. Lawrence Estuary (thin black line), defined as the area west of the Pointe-des-Monts section and east of approx 69°30'W. Thermosalinograph data averages for 2000 to 2010 are shown for the head of the Laurentian Channel (at 69°30'W, grey dashed line) and for the average over the Gulf waters along the main shipping route between the Pointe-des-Monts and Cabot Strait sections (gray dash-dotted line). Monthly air temperature averaged over eight stations in the Gulf of St. Lawrence are shown offset by 2 weeks into the future (thick grey line; winter months not shown). Figure from Galbraith et al. (2012).*

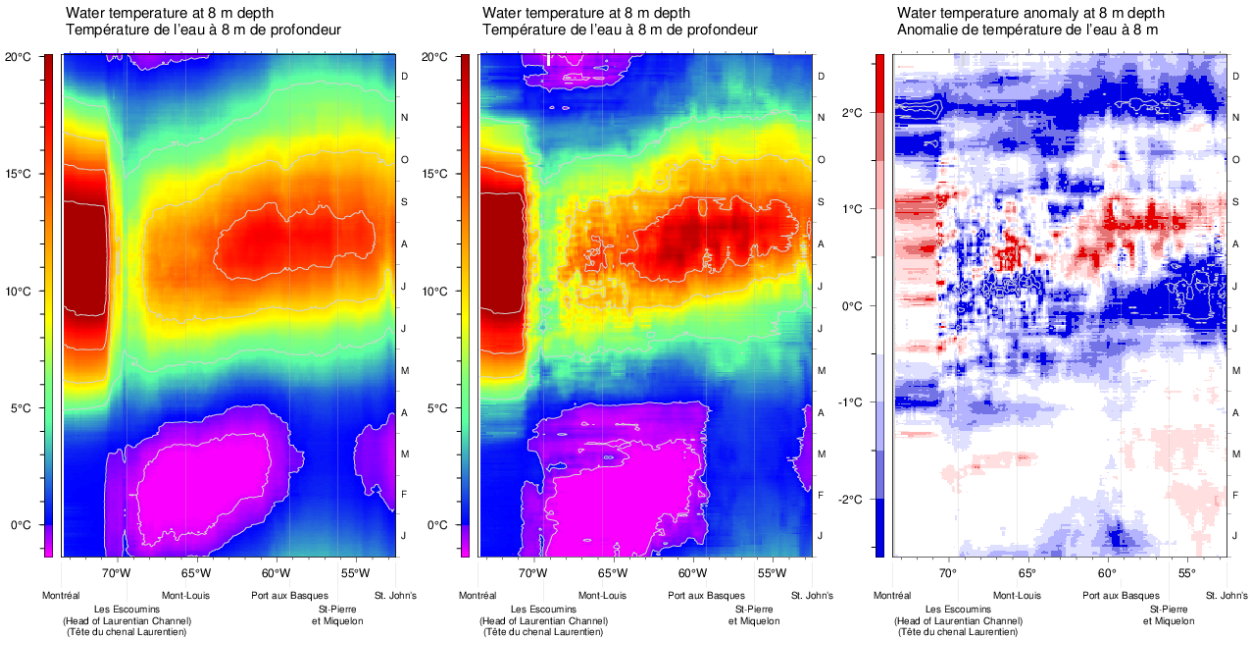


*Fig. 11. Hovmöller diagram of thermosalinograph data at 8 m depth along the Montréal to St. John's shipping route: composite mean annual cycle of the water temperature for the 2000–2018 period (left panel),composite annual cycle of the water temperature for 2018 (middle panel), and water temperature anomaly for 2018 relative to the 2000–2018 composite (right panel).*

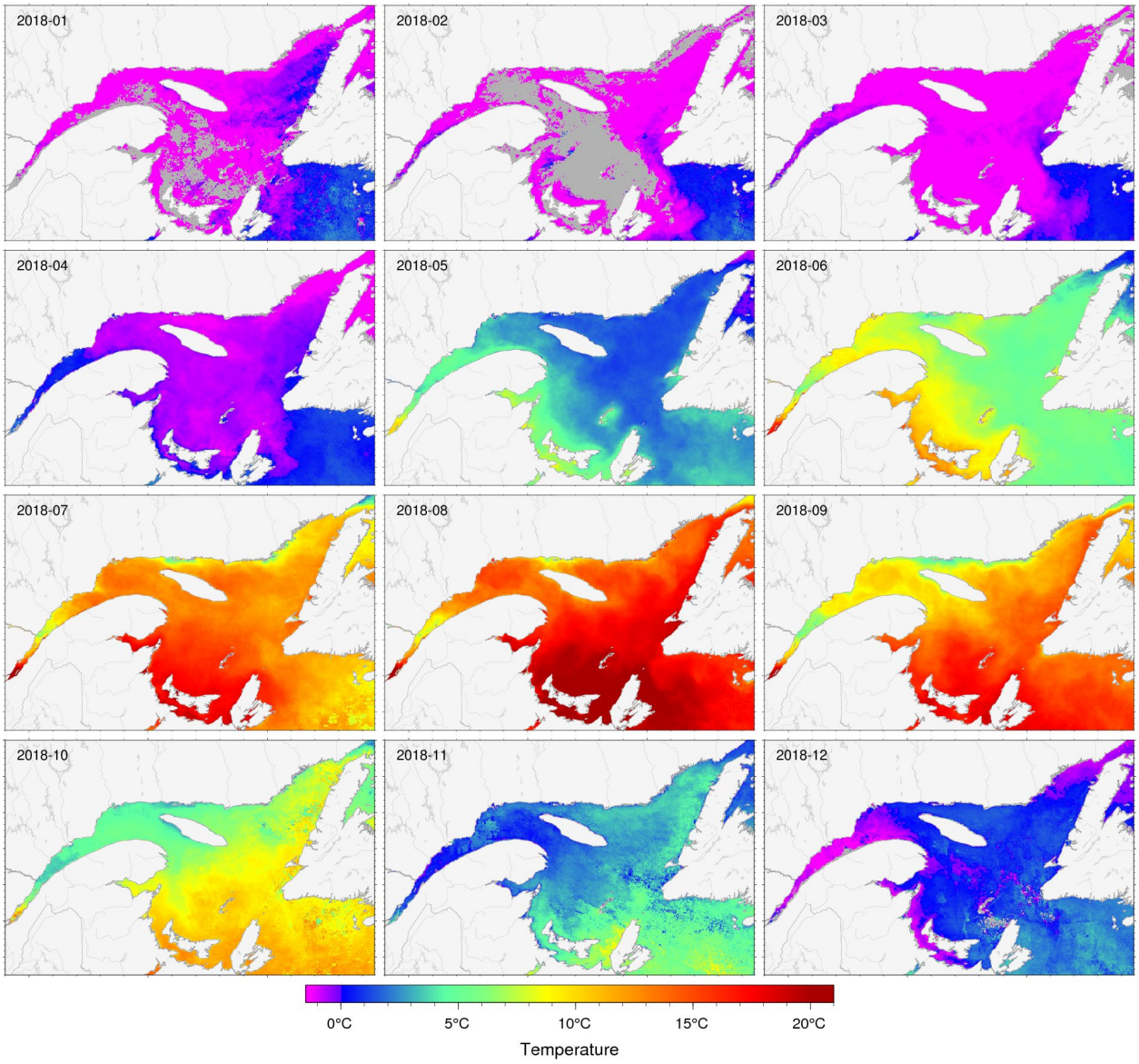


*Fig. 12. Sea-surface temperature monthly averages for 2018 as observed with AVHRR remote sensing. Grey areas have no data for the period due to ice cover or clouds.*

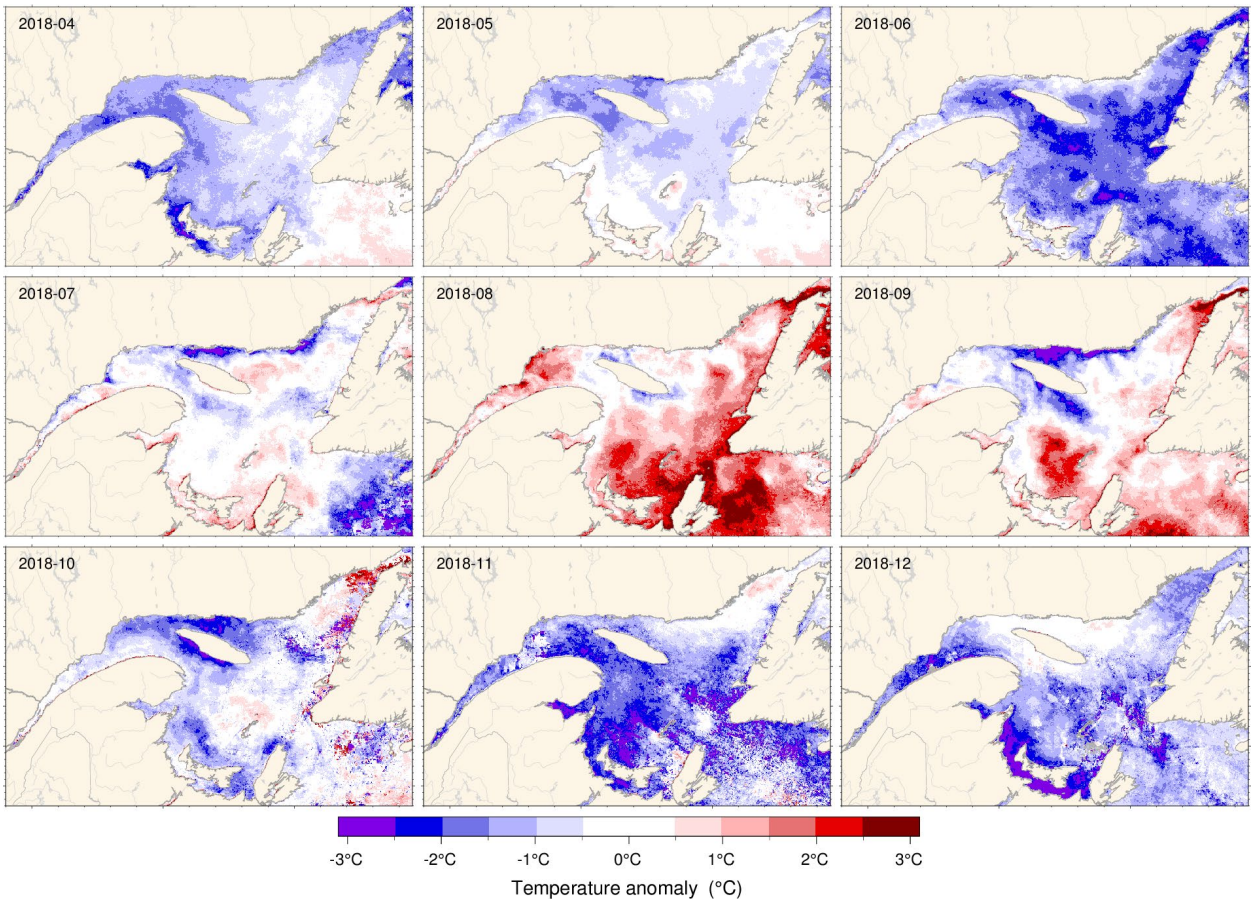


*Fig. 13. Sea-surface temperature monthly anomalies for April-December 2018 based on monthly climatologies calculated for the 1985–2010 period observed with AVHRR remote sensing.*

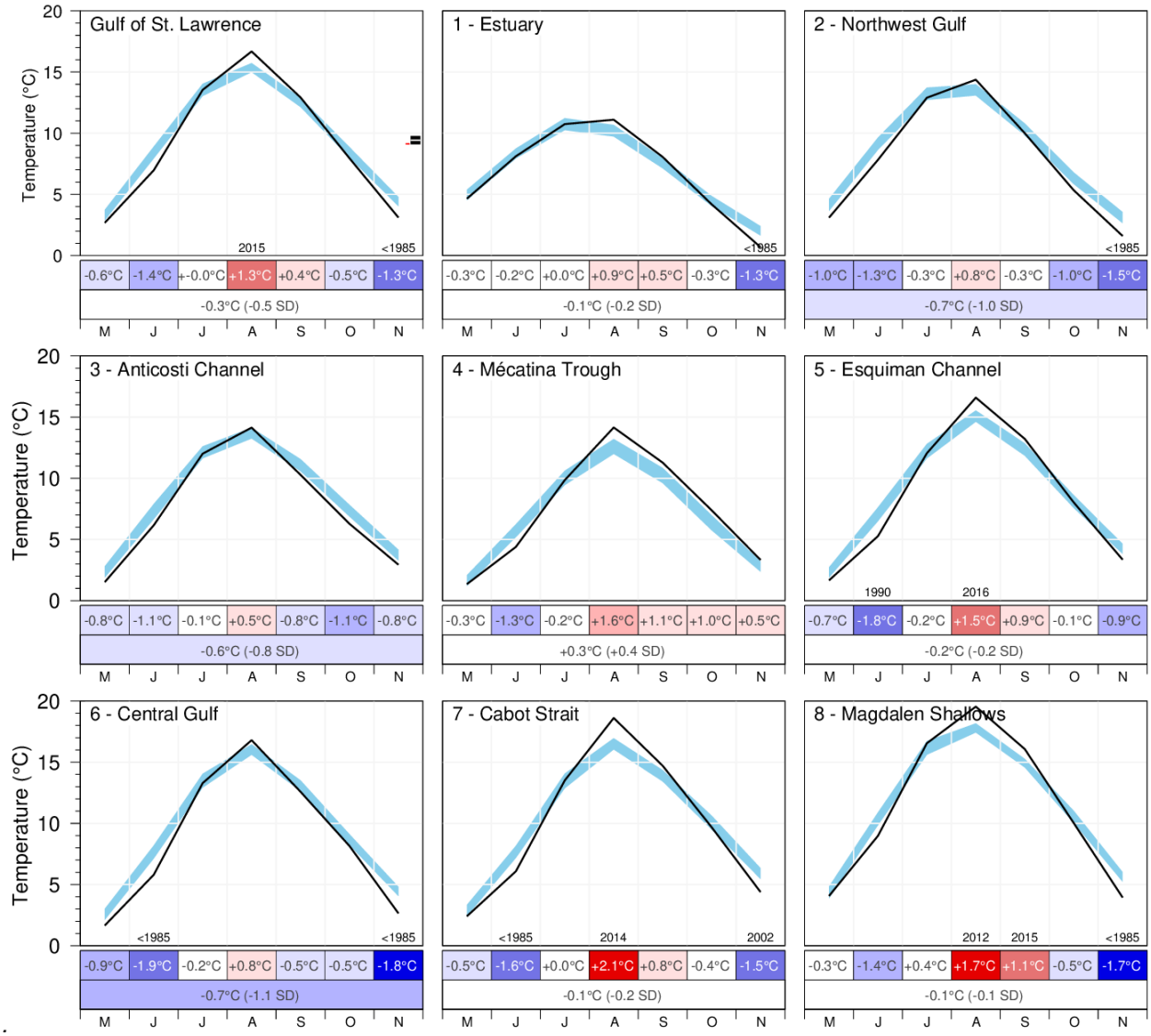


*Fig. 14. AVHRR SST May to November monthly averages over the Gulf and over the eight regions of the Gulf. The blue area represents the 1981–2010 climatological monthly mean ± 0.5 SD. The scorecards are colour-coded according to the normalized anomalies based on the 1985–2010 climatologies for each month or for the May-November period (bottom row), but the numbers are the monthly average temperature anomalies.*

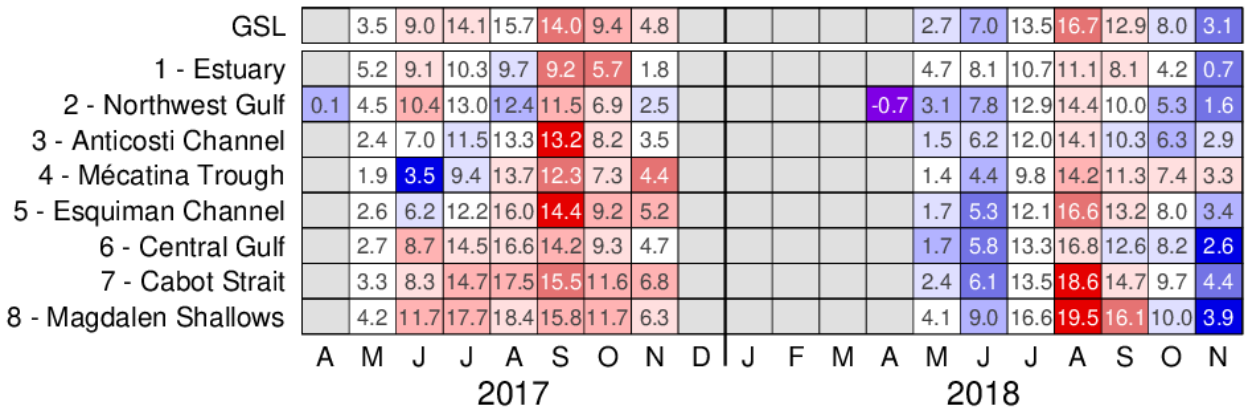


*Fig. 15. AVHRR SST May to November monthly anomalies averaged over the Gulf and the eight regions of the Gulf for 2017 and 2018 (April results are also shown for the Northwest Gulf). The scorecards are colour-coded according to the monthly normalized anomalies based on the 1985–2010 climatologies for each month, but the numbers are the monthly average temperatures.*

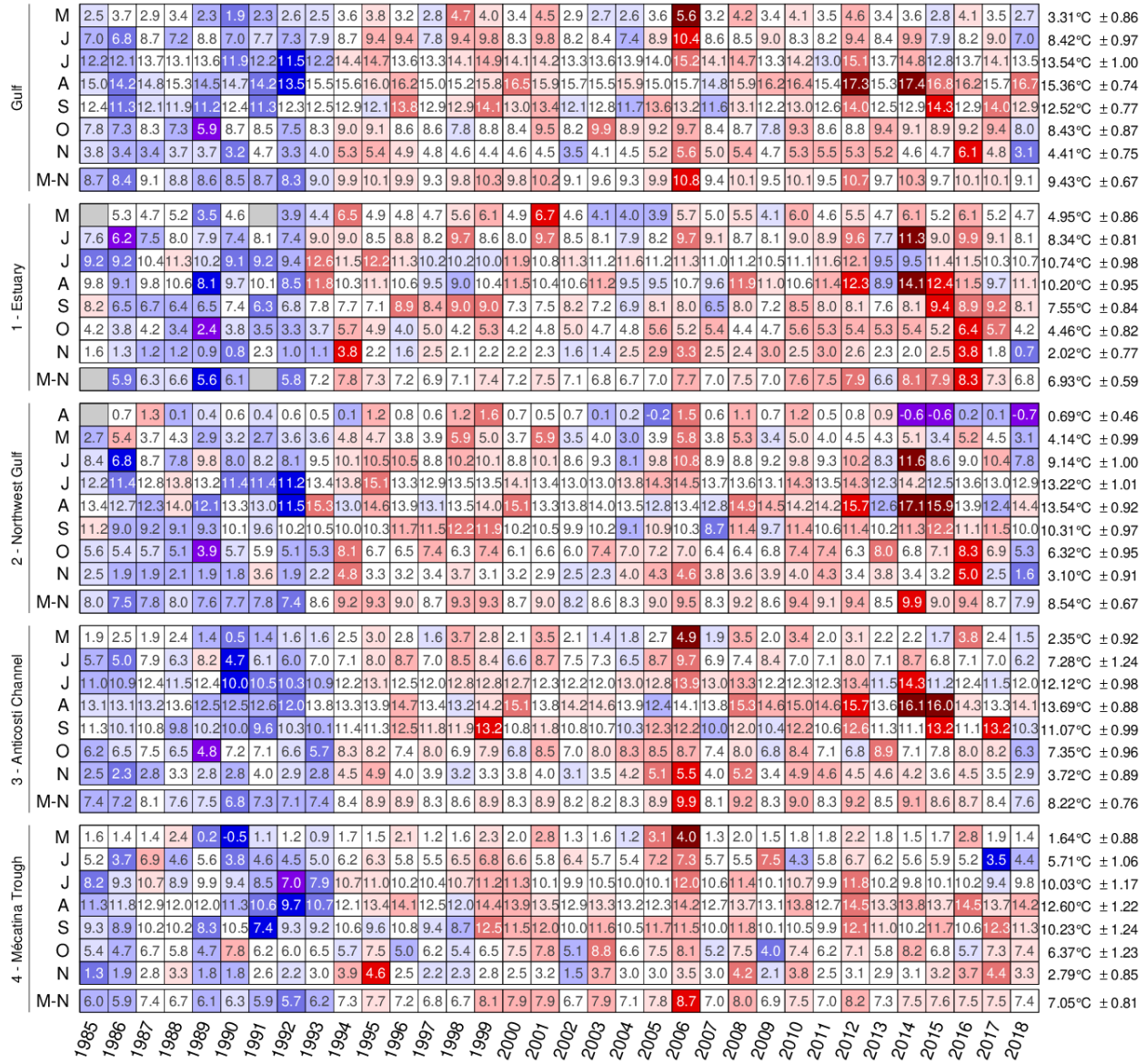


*Fig. 16. AVHRR SST May to November monthly anomalies averaged over the Gulf of St. Lawrence and over the first four regions of the Gulf. The scorecards are colour-coded according to the monthly normalized anomalies based on the 1985–2010 climatologies for each month, but the numbers are the monthly average temperatures in ºC. The 1985-2010 mean and standard deviation are indicated for each month on the right side of the table. April anomalies are included for the Northeast Gulf because those regions are typically ice-free by then. The May to November average is also included.*

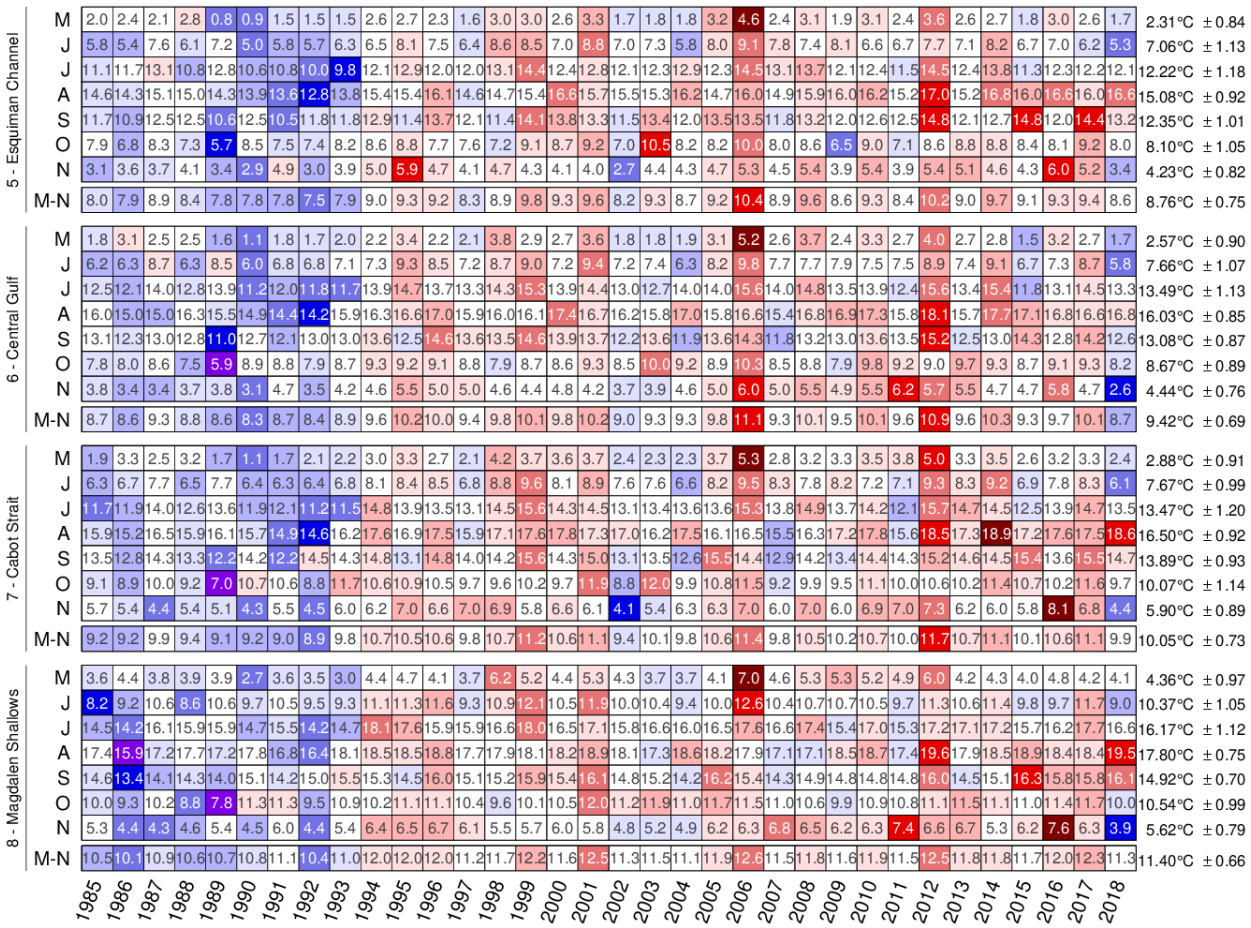


*Fig. 17. AVHRR SST May to November monthly anomalies averaged over the remaining four regions of the Gulf. The scorecards are colour-coded according to the monthly normalized anomalies based on the 1985–2010 climatologies for each month, but the numbers are the monthly average temperatures in ºC. The 1985-2010 mean and standard deviation are indicated for each month on the right side of the table. The May to November average is also included.*

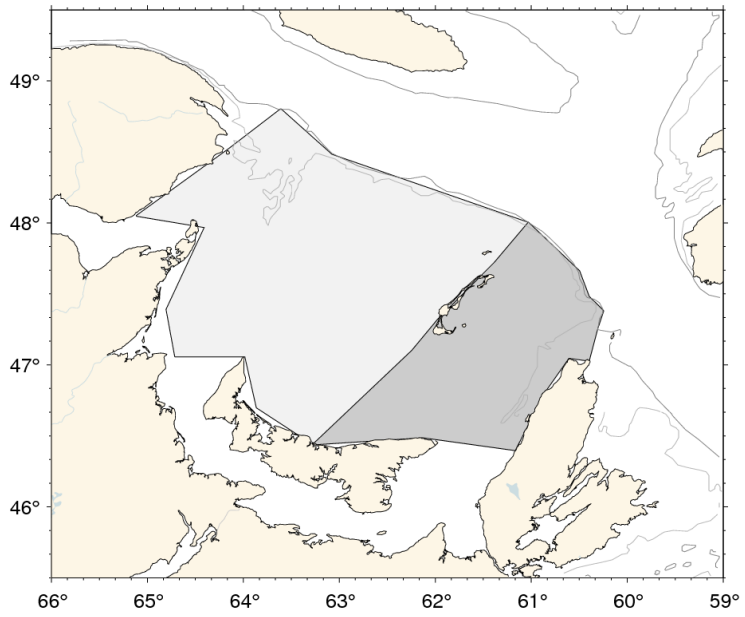


*Fig. 18. Areas defined as the western and eastern Magdalen Shallows.*

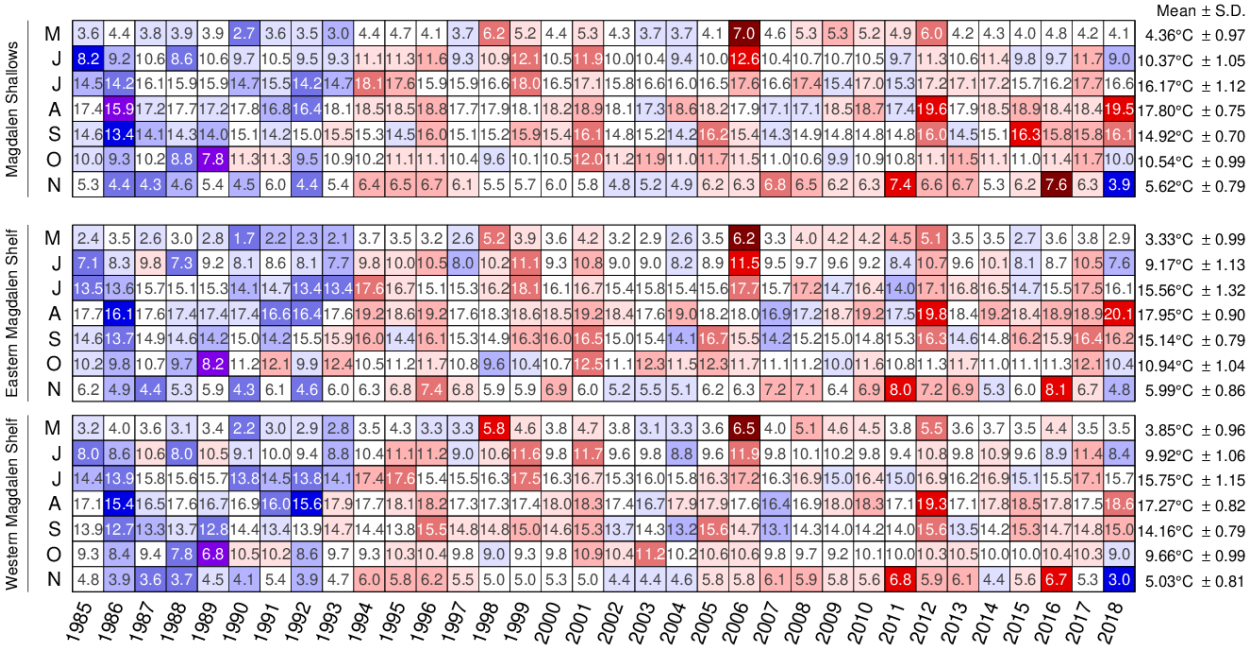


*Fig. 19. AVHRR SST May to November monthly anomalies averaged over the Magdalen Shallows (region 8 of the Gulf) and the eastern and western subregions of the Magdalen Shallows (Fig. 18). The scorecards are colour-coded according to the monthly normalized anomalies based on the 1985–2010 climatologies for each month, but the numbers are the monthly average temperatures in ºC. The 1985-2010 mean and standard deviation are indicated for each month on the right side of the table.*

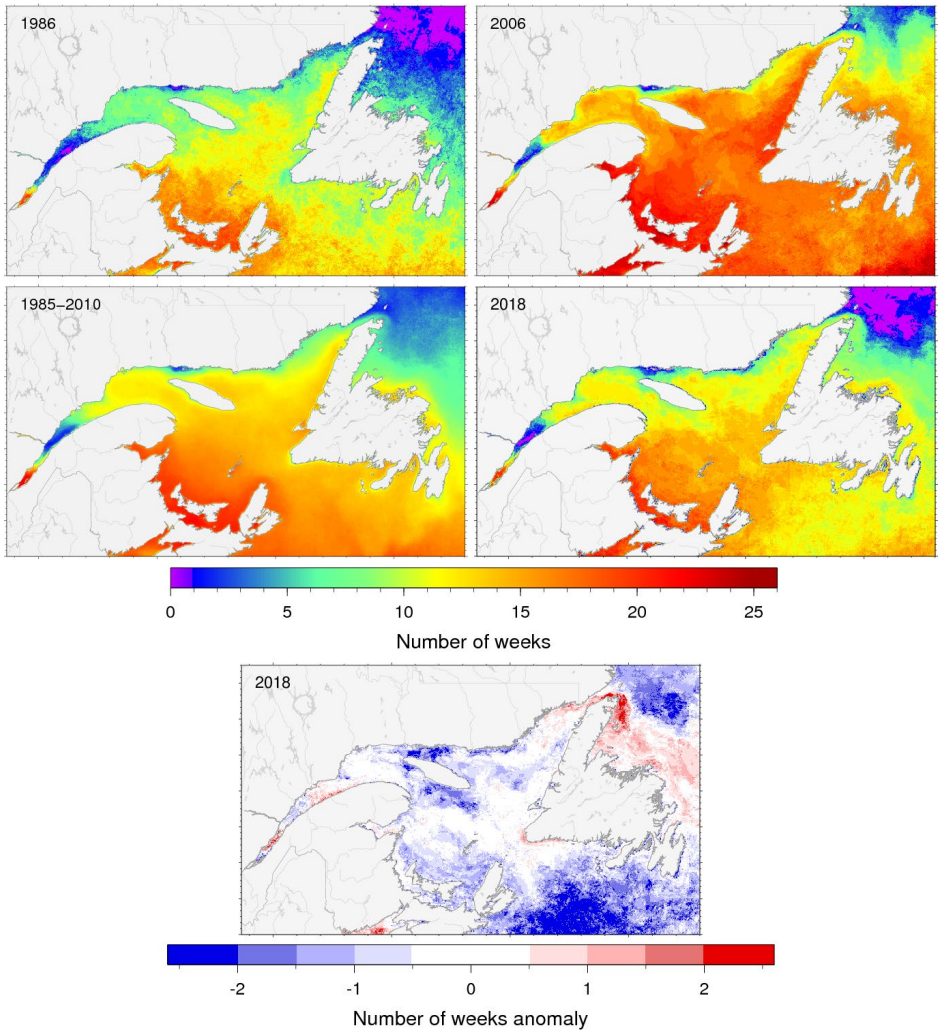


*Fig. 20. Yearly number of weeks with mean weekly surface temperature >10°C. (Top) Years with the minimum (1986, top left) and maximum (2006, top right) number of weeks are shown along with the 1985–2010 climatological average (lower left) and the chart for 2018. (Bottom) Anomaly for 2018 relative to 1985-2010 climatology, expressed in numbers of weeks.*

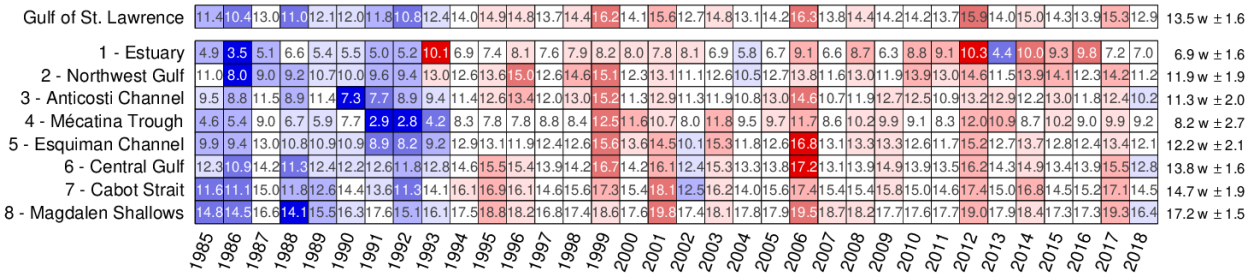


*Fig. 21. Yearly number of weeks with mean weekly surface temperature >10°C, averaged for the entire Gulf and each region of the Gulf. The scorecards are colour-coded according to the normalized anomalies based on the 1985–2010 time series, but the numbers are the average number of weeks above 10°C for each year.*

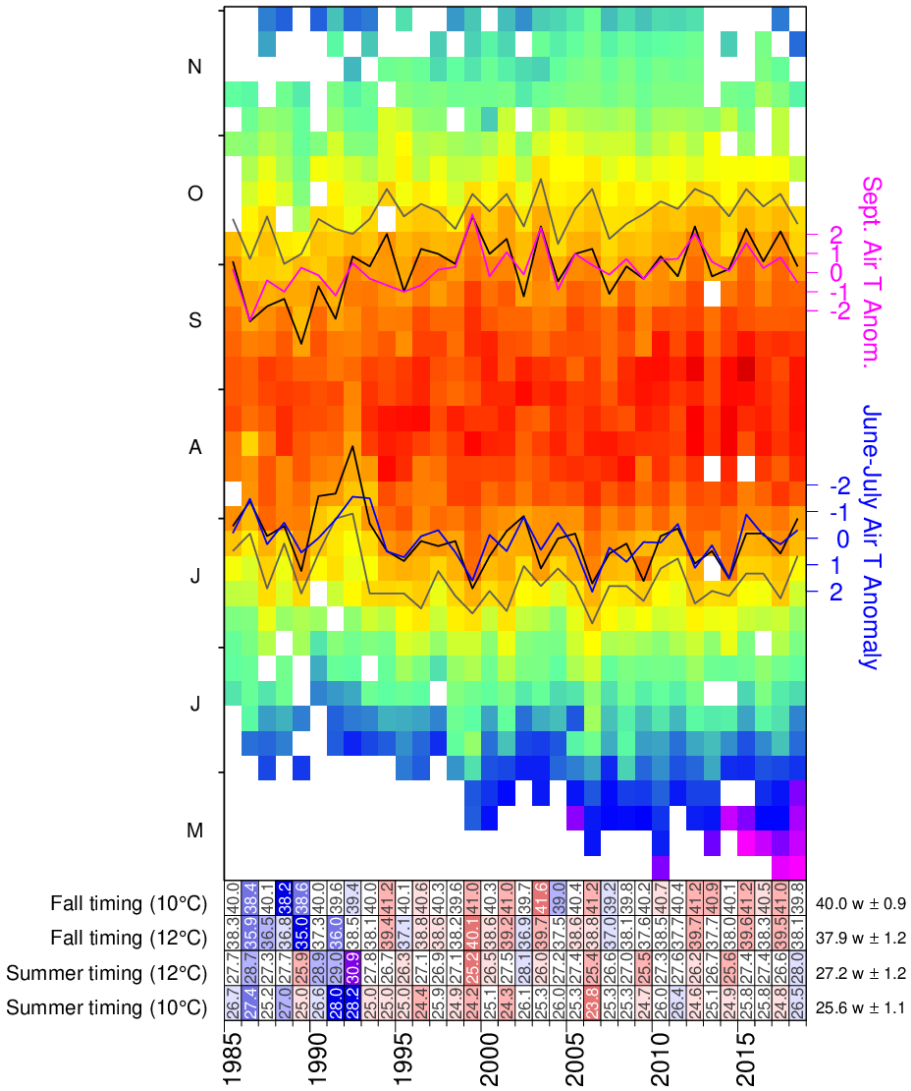


*Fig. 22. Weekly average SST (1985-2018) matrix for the Gulf of St. Lawrence. Black lines show first and last occurrence of the 12°C isotherm and proxies based on June-July (blue line) and September (magenta) average air temperature are also shown (axes on right). Gray lines show first and last occurrence of the 10°C isotherm. The scorecards are colour-coded according to the normalized anomalies based on the 1985–2010 time series, but the numbers are week numbers when the threshold was crossed. Updated from Galbraith and Larouche 2013.*

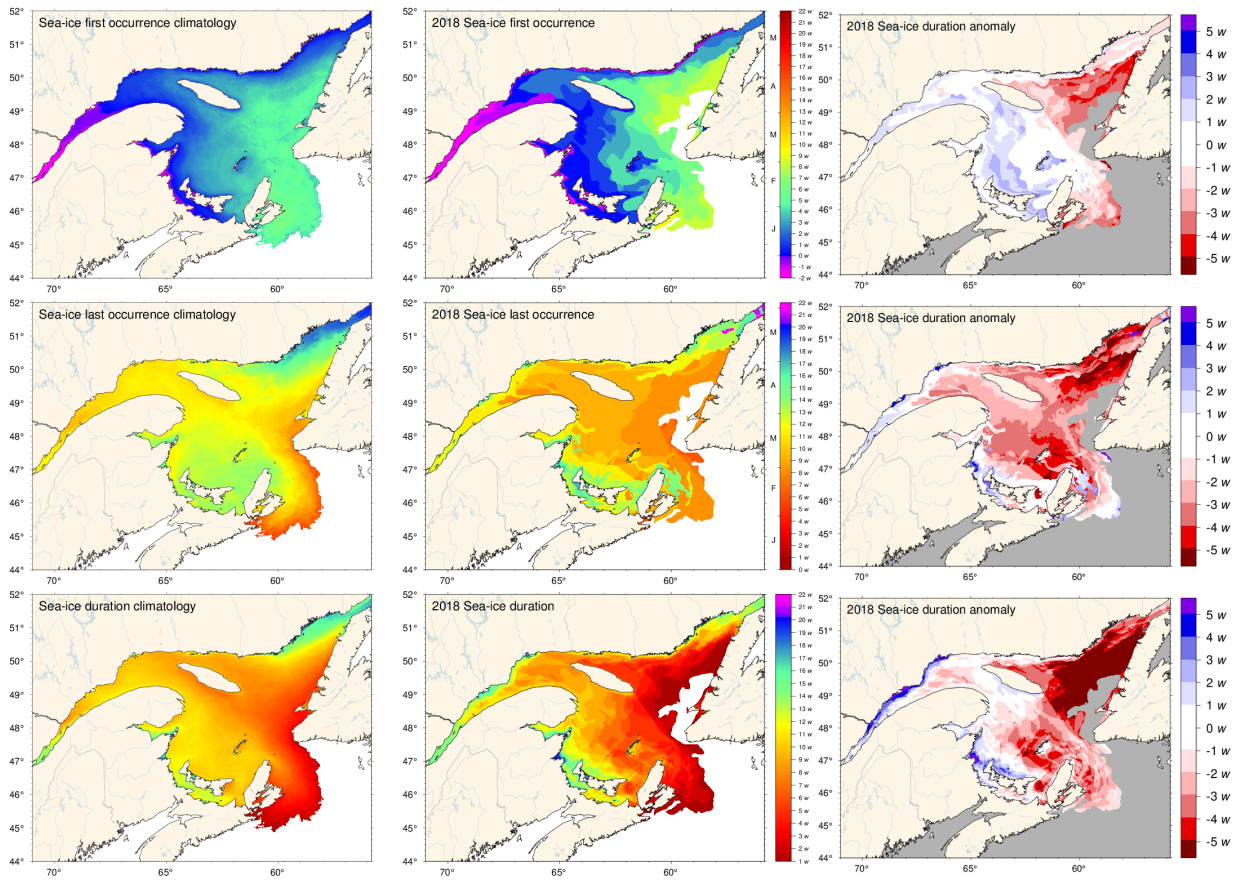


*Fig. 23. First and last occurrence of ice and ice season duration based on weekly data. The 1981-2010 climatologies are shown (left) as well as the 2018 values (middle) and anomalies (right). First and last occurrence is defined here as the first and last weekly chart in which any amount of ice is recorded for each pixel and are illustrated as day-of-year. Ice duration sums the number of weeks with ice cover for each pixel. Climatologies are shown for pixels that had at least 15 years out of the 30 with occurrence of sea-ice, and therefore also show the area with 50% likelihood of having some sea-ice at any time during any given year.*

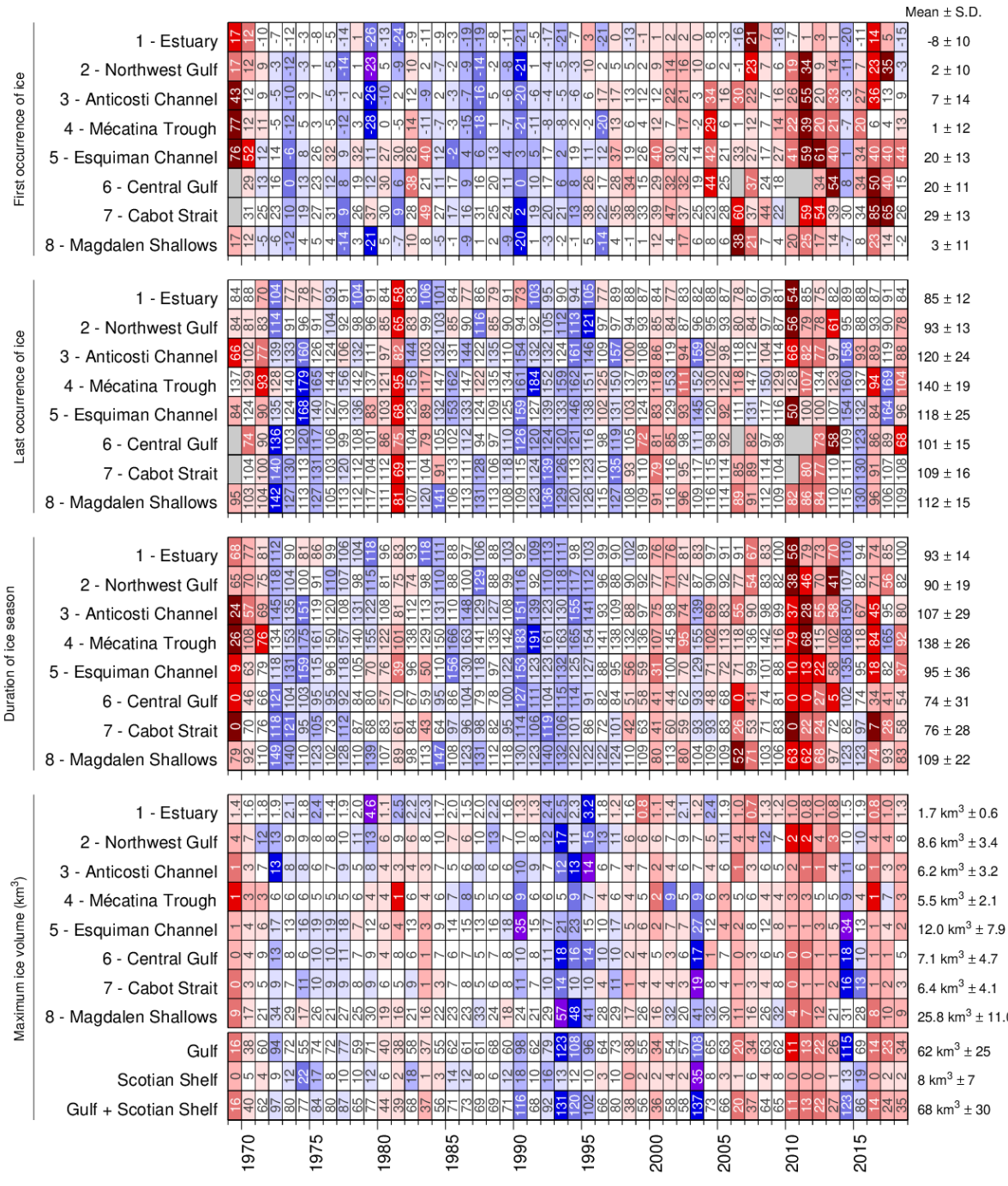


*Fig. 24. First and last day of ice occurrence, ice duration and maximum seasonal ice volume by region. The time when ice was first and last seen in days from the beginning of each year is indicated for each region, and the colour code expresses the anomaly based on the 1981–2010 climatology, with blue (cold) representing earlier first occurrence and later last occurrence. The threshold is 5% of the largest ice volume ever recorded in the region. Numbers in the table are the actual day of the year or volume, but the colour coding is according to normalized anomalies based on the climatology of each region. Duration is the numbers of days that the threshold was exceeded. All results based on weekly data.*

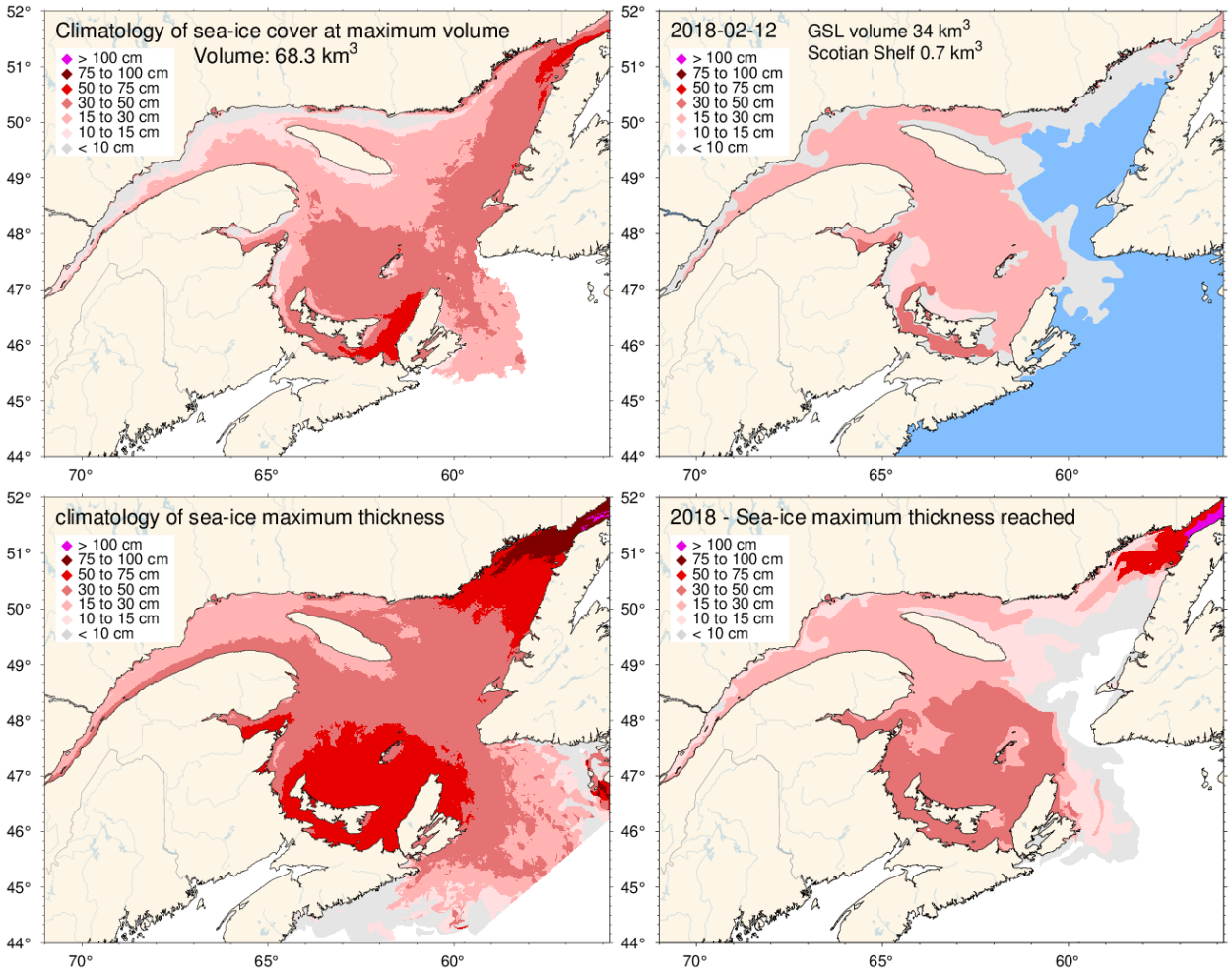


*Fig. 25. Ice thickness map for 2018 for the week of the year with the maximum annual volume including the portion covering the Scotian Shelf (upper right panel) and similarly for the 1981-2010 climatology of the weekly maximum (upper left panel). Note that these maps reflect the ice thickness distribution on that week, and not the maximum observed at any given location during the year. That information is shown by the lower panels, showing the 1981-2010 climatology and 2018 distribution of the thickest ice recorded during the season at any location.*

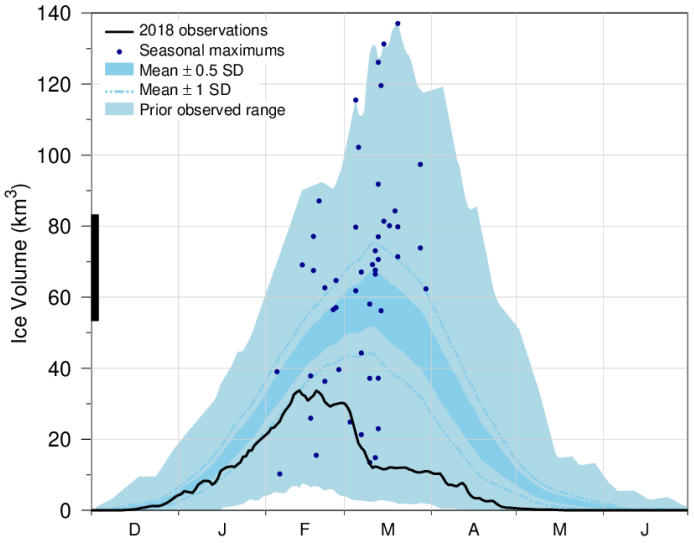


*Fig. 26. Time series of the 2017-2018 daily mean ice volume for the Gulf of St. Lawrence and Scotian Shelf (black line), the 1981-2010 climatological mean volume plus and minus 0.5 and 1 SD (dark blue area and dashed line), the minimum and maximum span of 1969-2018 observations (light blue) and the date and volumes of 1969-2018 seasonal maximums (blue dots). The black thick line on the left indicates the mean volume plus and minus 0.5 SD of the annual maximum ice volume, which is higher than the peak of the mean daily ice volume distribution.*

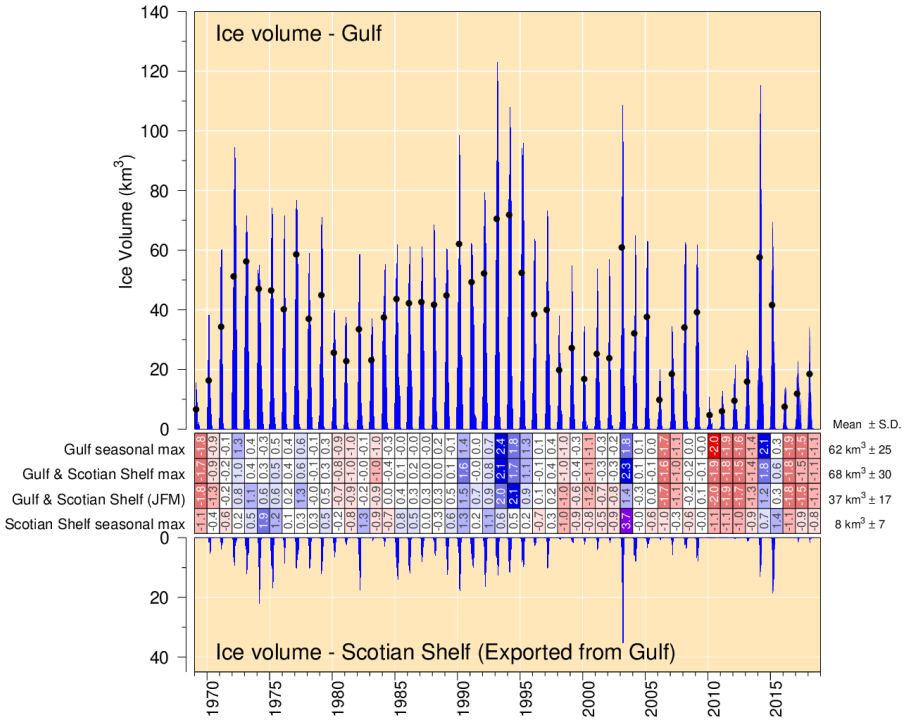


*Fig. 27. Estimated weekly maximum ice volume in the Gulf of St. Lawrence (upper panel) and on the Scotian Shelf seaward of Cabot Strait defined by its narrowest crossing (lower panel). Dots show January-March averages of combined Gulf and Scotian Shelf volumes. Scorecards show numbered normalized anomalies for the Gulf, combined Gulf and Shelf, combined Gulf and Shelf January to March average, and Shelf-only annual maximum volumes from weekly ice data. The mean and standard deviation are indicated on the right side using the 1981–2010 climatology.*

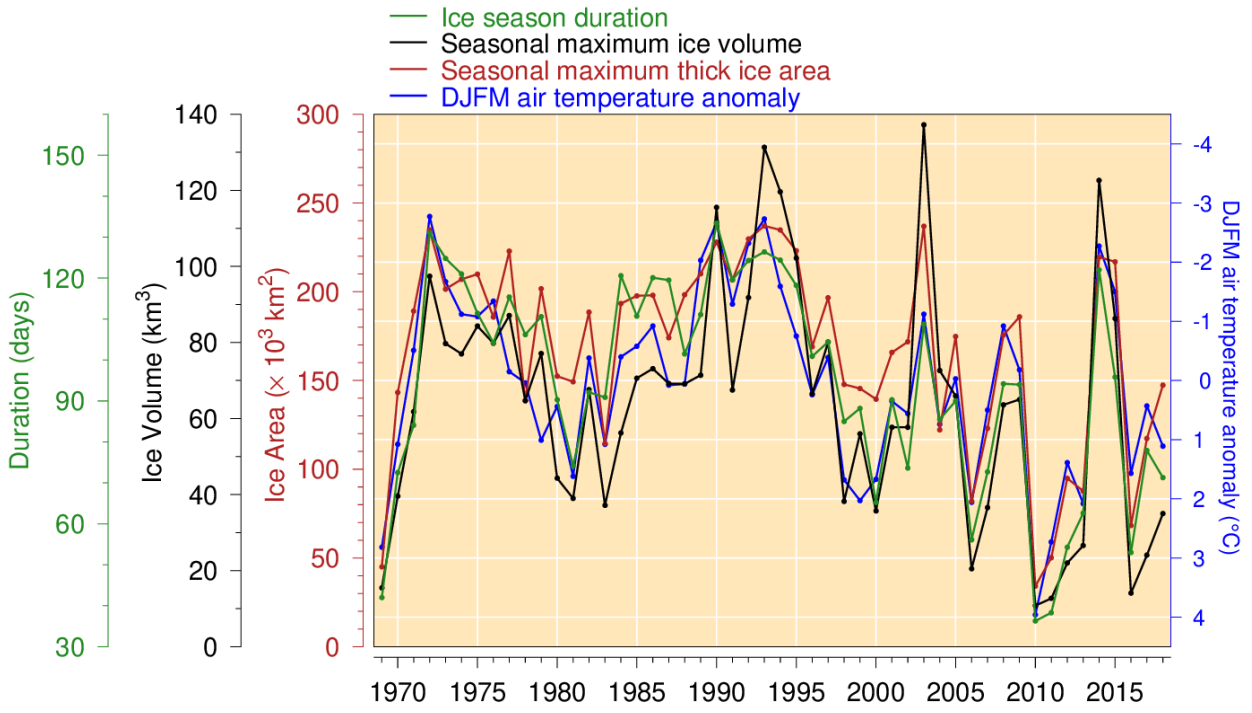


*Fig. 28. Seasonal maximum ice volume and area including the portion on the Scotian Shelf (excluding ice less than 15 cm thick), ice season duration and December-to-March air temperature anomaly (Figure adapted from Hammill and Galbraith 2012, but here not excluding small floes and adding February and March data to the air temperature anomalies). All sea-ice products are based on weekly data. Linear relations indicate losses of 17 km$^3$, 31,000 km$^2$ and 14 days of sea-ice season for each 1°C increase in winter air temperature ($R^2$ of 0.72, 0.78 and 0.77 respectively).*

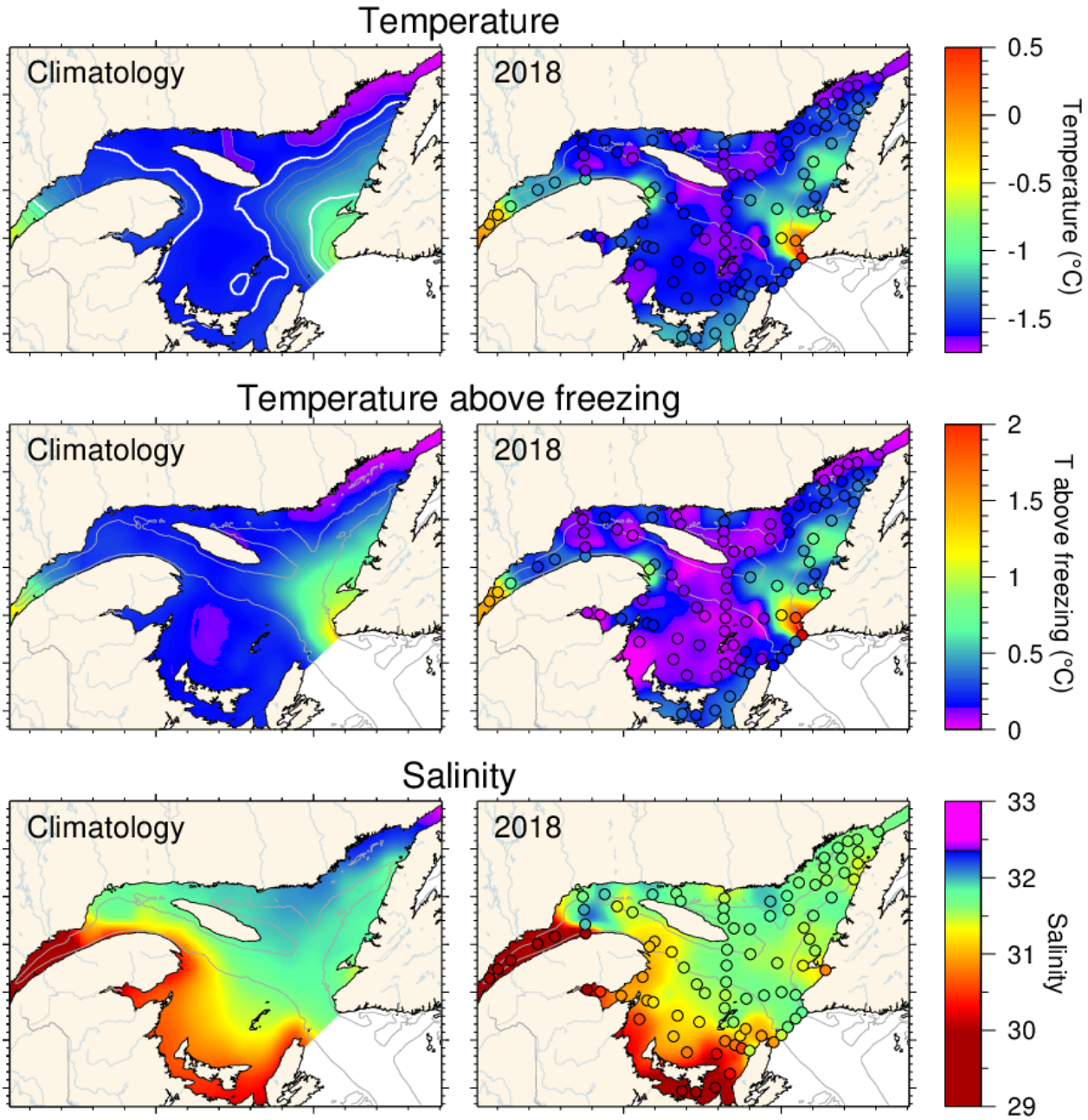


*Fig. 29. Winter surface layer characteristics from the March 2018 survey compared with climatological means: surface water temperature (upper panel), temperature difference between surface water temperature and the freezing point (middle panel), and salinity (lower panel). Symbols are coloured according to the value observed at the station, using the same colour palette as the interpolated image. A good match is seen between the interpolation and the station observations where the station colours blend into the background. Black symbols indicate missing or bad data. The climatologies are based on 1996-2018 for salinity but exclude 2010 as an outlier for temperature and temperature above freezing.*

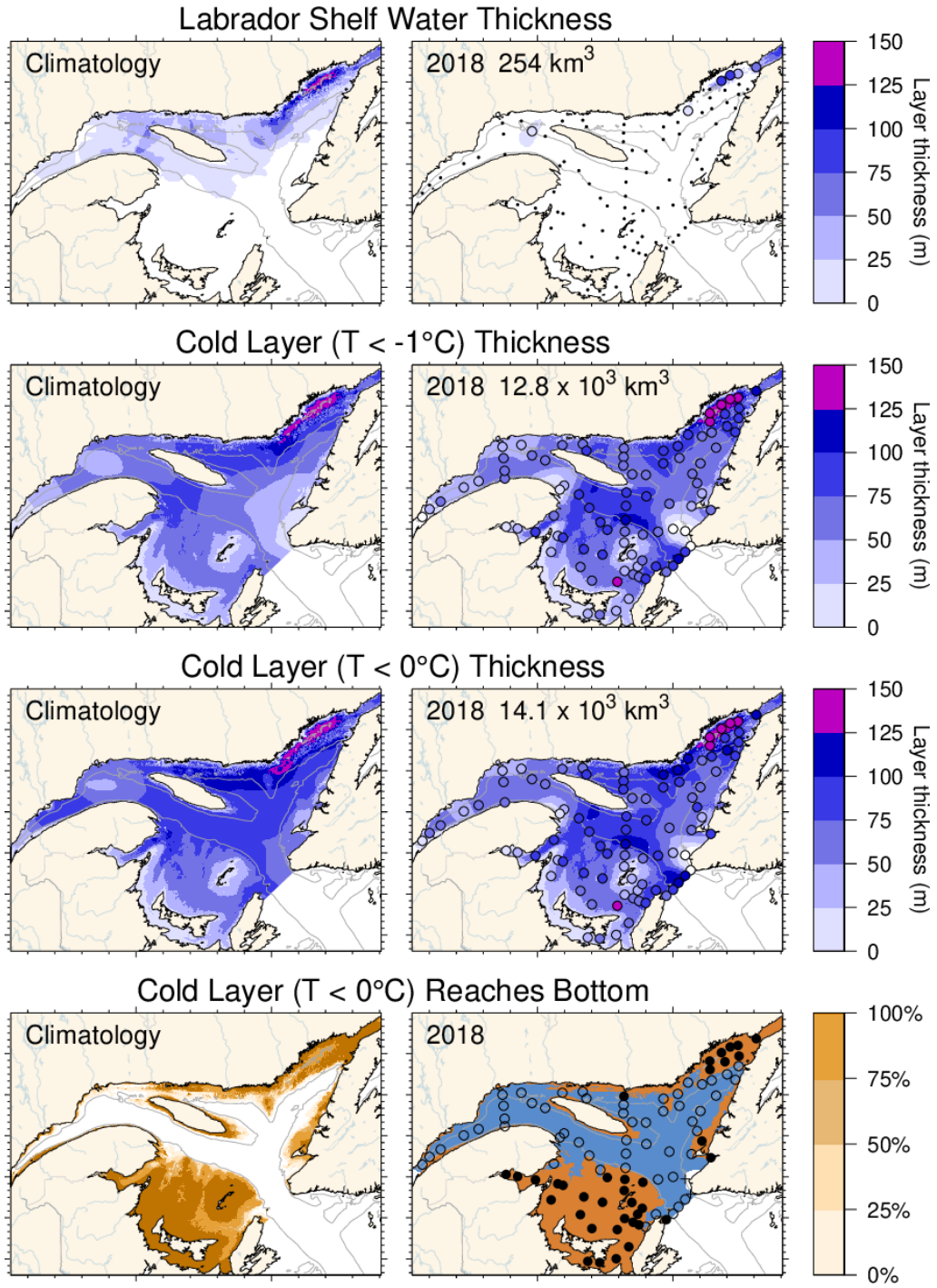


*Fig. 30. Winter surface layer characteristics from the March 2018 survey compared with climatological means: estimates of the thickness of the Labrador Shelf water intrusion (upper panels), cold layer (T<-1°C, T<0°C) thickness (middle panels), and maps indicating where the cold layer (T<0°C) reaches the bottom (in brown; lower panels). Station symbols are coloured according to the observed values as in Fig. 29. For the lower panels, the stations where the cold layer reached the bottom are indicated with filled circles while open circles represent stations where the layer did not reach the bottom. Integrated volumes are indicated for the first six panels (including an approximation for the Estuary but excluding the Strait of Belle Isle). The climatologies are based on 1997-2018 for the Labrador Shelf water intrusion, 1996-2018 for the cold layer (T<0°C) but excludes 2010 for T<-1°C.*

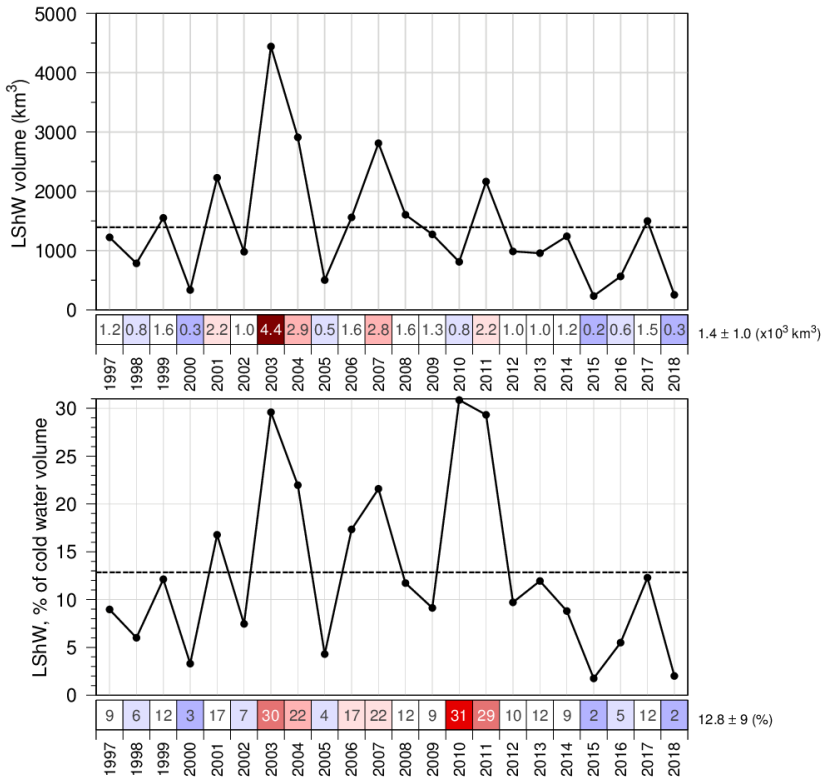


*Fig. 31. Estimated volume of cold and saline Labrador Shelf water that flowed into the Gulf over the winter through the Strait of Belle Isle. The bottom panel shows the volume as a percentage of total cold-water volume (<-1ºC). The numbers in the boxes are actual values colour-coded according to their 1997-2018 climatology anomaly. Coverage of Mecatina Trough was insufficient in 1996 to provide an estimated volume.*

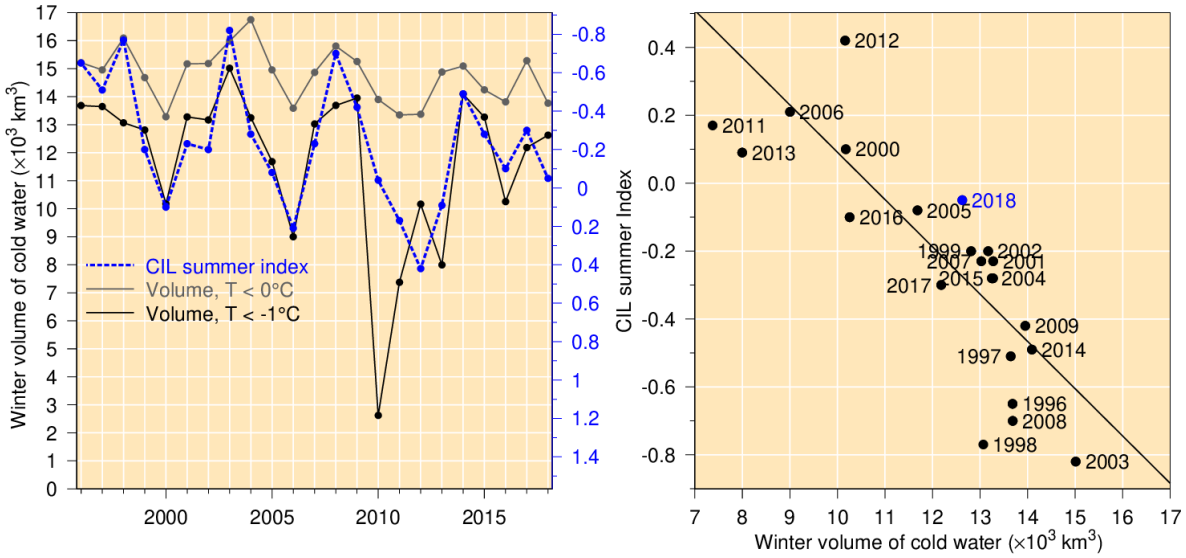


*Fig. 32. Left panel: winter surface cold (T<-1°C and T<0°C) layer volume (excluding the Estuary and the Strait of Belle Isle) time series (black and grey lines) and summer CIL index (blue dashed line). Right panel: Relation between summer CIL index and winter cold-water volume with T<-1°C (regression for 1996-2017 data pairs, excluding 1998 [see Galbraith 2006] as well as the 2010 and 2011 mild winters). Note that the CIL scale in the left panel is reversed.*

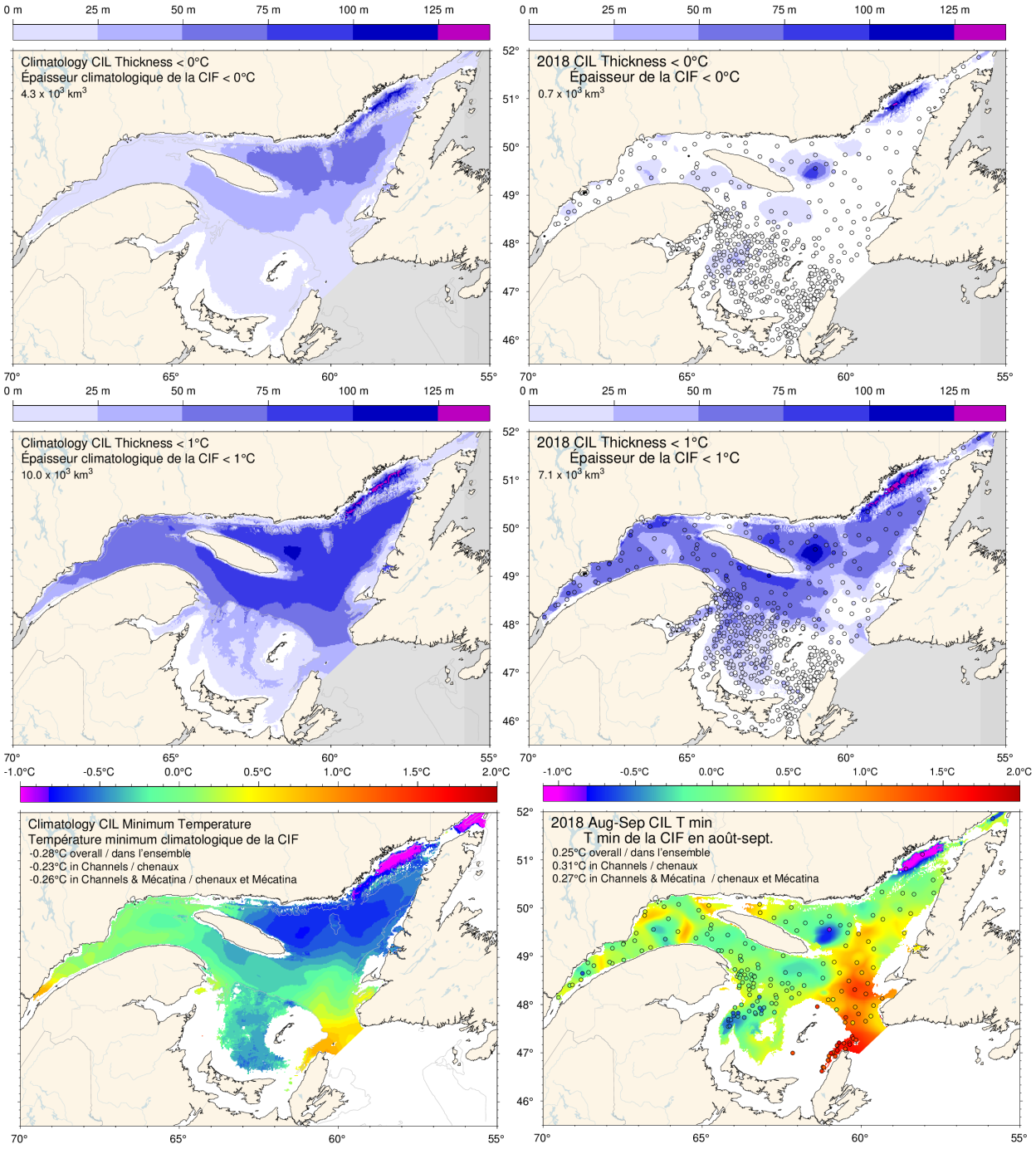


*Fig. 33. Cold intermediate layer thickness (T<0ºC, top panels; T<1ºC, middle panels) and minimum temperature (bottom panels) in August and September 2018 (right) and 1985-2010 climatology (left). Station symbols are colour-coded according to their CIL thickness and minimum temperature. Numbers in the upper and middle panels are integrated CIL volumes and in the lower panels are monthly average temperatures.*

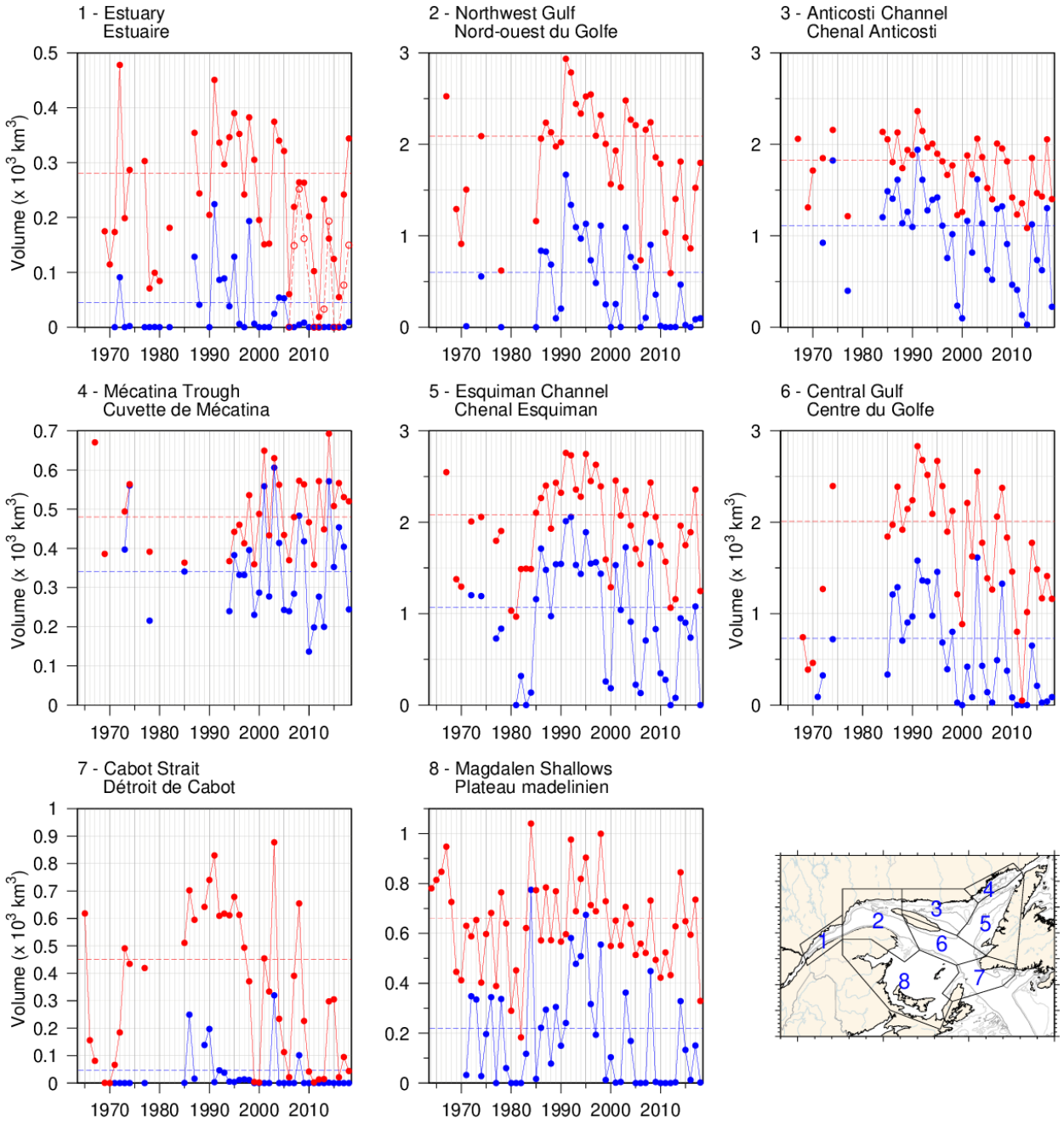


*Fig. 34. Volume of the CIL colder than 0ºC (blue) and colder than 1ºC (red) in August and September (primarily region 8 in September). The volume of the CIL colder than 1ºC in November for available years since 2006 is also shown for the St. Lawrence Estuary (dashed line).*

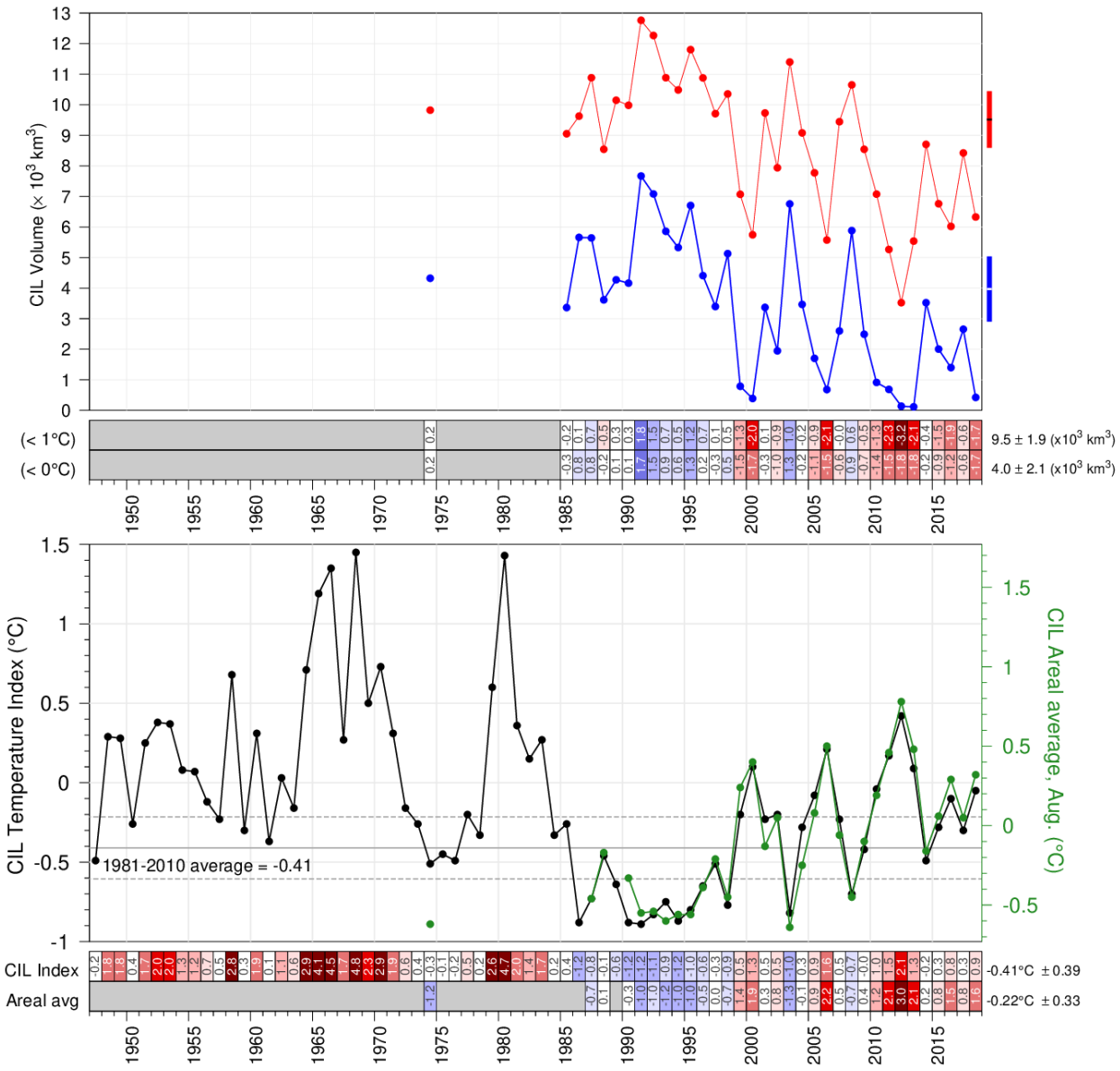


*Fig. 35. CIL volume (top panel) delimited by 0ºC (in blue) and 1ºC (in red), and minimum temperature index (bottom panel) in the Gulf of St. Lawrence. The volumes are integrals of each of the annual interpolated thickness grids such as those shown in the top panels of Fig. 33 excluding Mécatina Trough and the Strait of Belle Isle. Rectangles on right side show mean ± 0.5 SD. In the lower panel, the black line is the updated Gilbert and Pettigrew (1997) index interpolated to 15 July (with dashed lines showing mean ± 0.5 SD) and the green line is the spatial average of each of the annual interpolated grid such as those shown in the two bottom panels of Fig. 33, excluding Mécatina Trough, the Strait of Belle Isle and the Magdalen Shallows. The numbers in the boxes are normalized anomalies relative to 1980-2010 climatologies constructed using all available years.*

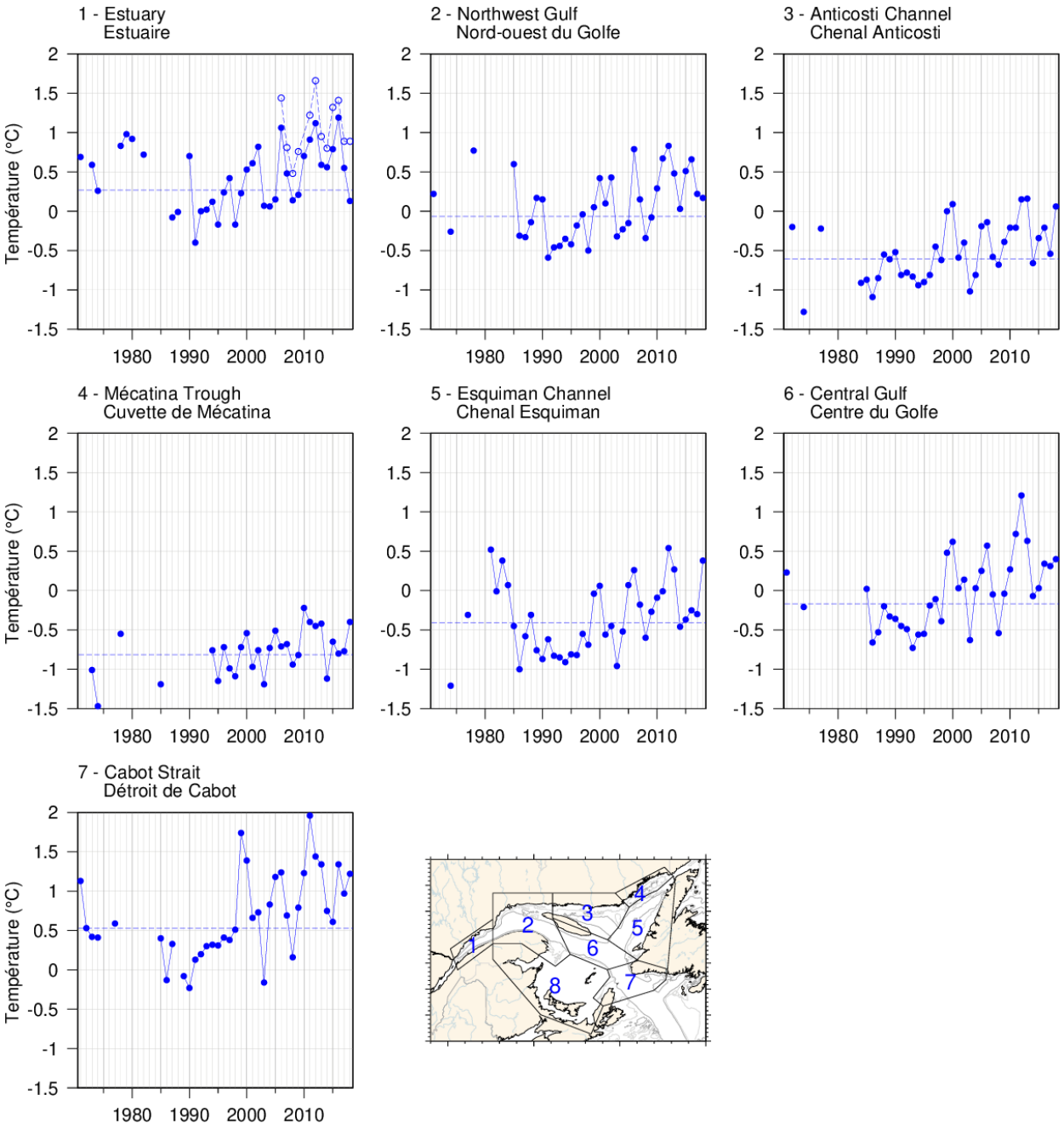


*Fig. 36. Temperature minimum of the CIL spatially averaged for the seven areas where the CIL minimum temperature can be clearly identified. The spatial average of the November CIL temperature minimum for available years since 2006 is also shown for the St. Lawrence Estuary (dashed line).*

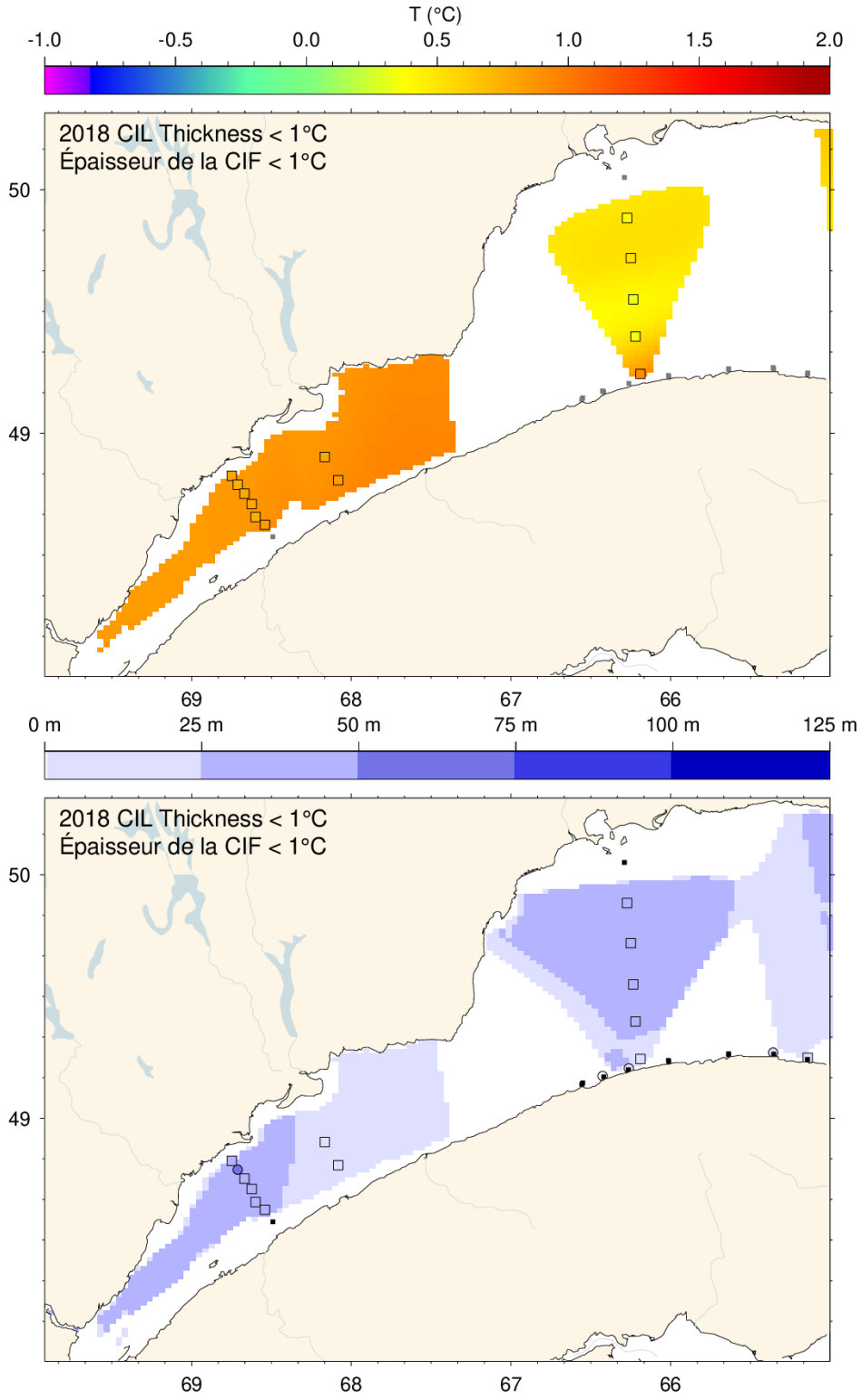


*Fig. 37. Cold intermediate layer minimum temperature and thickness (T<1°C) in November 2018 in the St. Lawrence Estuary. The absence of CIL at the mouth of the estuary is an interpolation artefact caused by the low number of observations from the 2018 fall survey.*

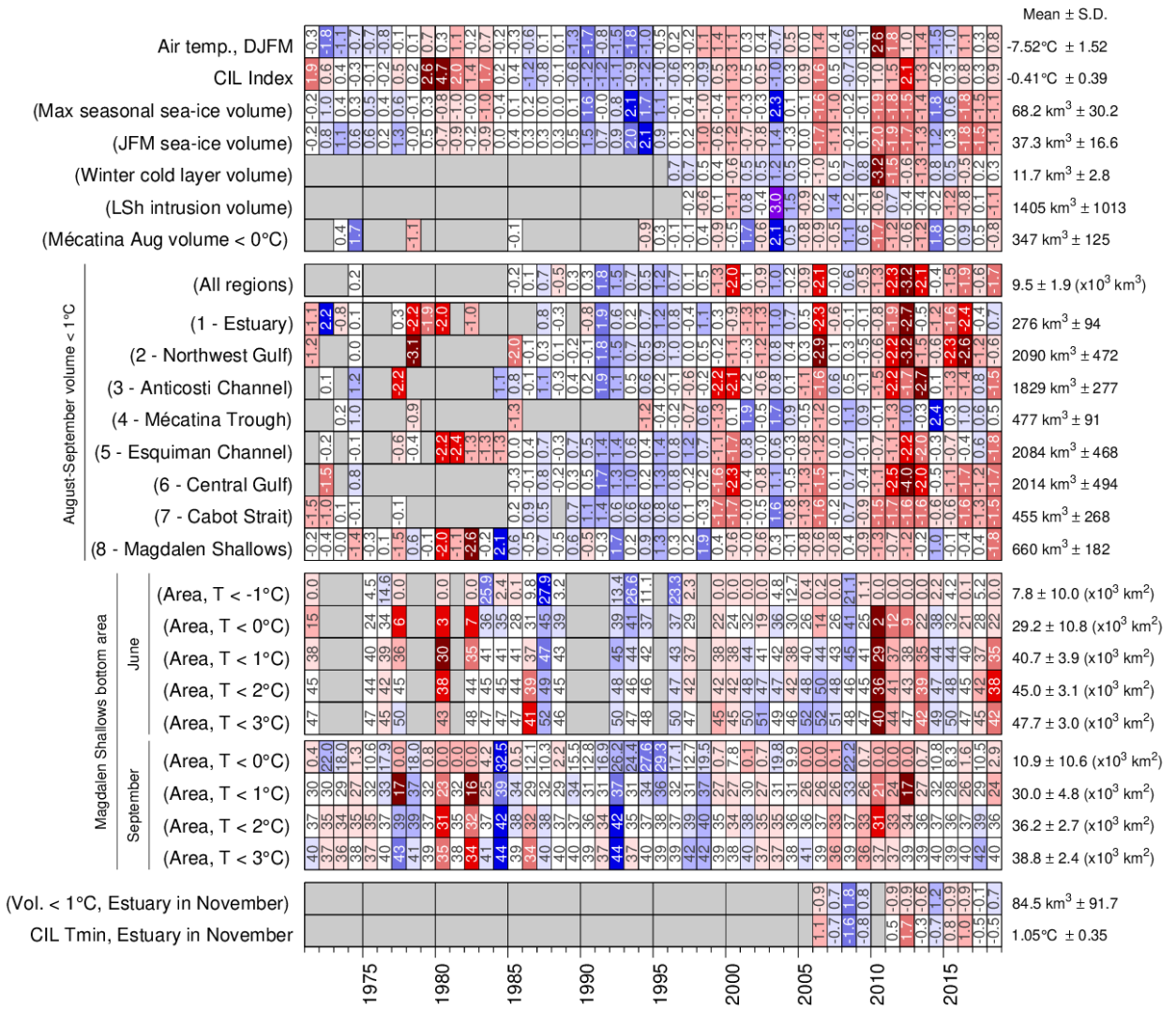


*Fig. 38. Winter and summertime CIL related properties. The top block shows the scorecard time series for Dec-Jan-Feb-March air temperature (Fig. 5), the Gilbert and Pettigrew (1997) CIL index, yearly maximum sea-ice volume (Gulf + Scotian Shelf), Dec-Jan-Feb average sea-ice volume, winter (March) cold-layer (<-1°C) volume, volume of Labrador Shelf Water intrusion into the Gulf observed in March, and the August–September volume of cold water (<0°C) observed in the Mécatina Trough. Labels in parentheses have their colour coding reversed (blue for high values). The second block shows scorecard time series for August–September CIL volumes (<1°C) for all eight regions and for the entire Gulf when available. The third block shows the scorecard time series for the bottom areas of the Magdalen Shallows covered by waters colder than 0, 1, 2, and 3°C during the June and September survey. The last block shows the November survey CIL volume (<1°C) and average CIL minimum temperature in the Estuary. Numbers in cells express anomalies in units of standard deviation, except for bottom areas which are expressed in units of area (×10³ km²) (because of the occurrence of zeros).*

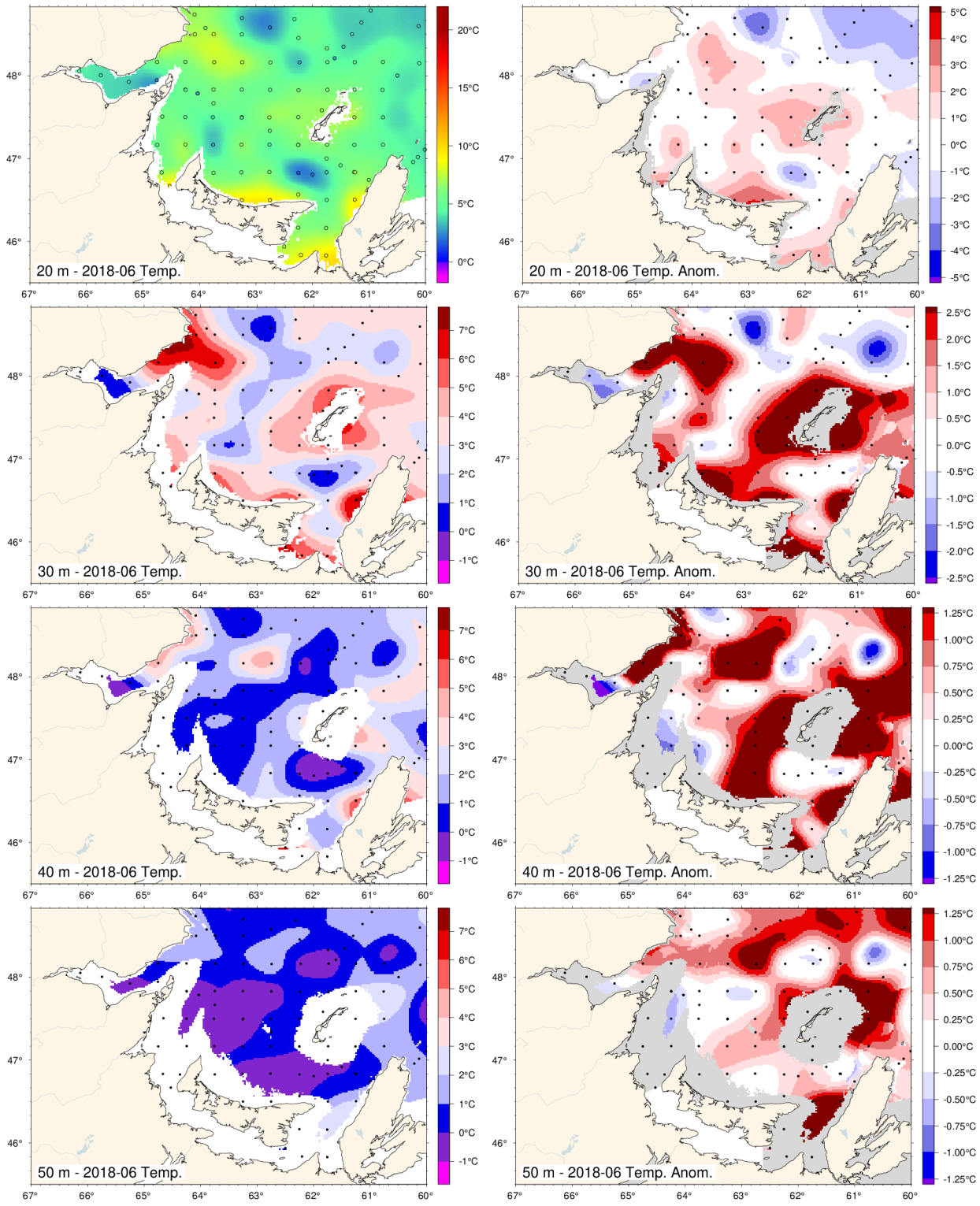


*Fig. 39. June depth-layer temperature and anomaly fields on the Magdalen Shallows at 20, 30, 40 and 50 m. Anomalies are based on 1971-2010 climatologies for all available years (appearing on Fig. 40). Dots are station occupations.*

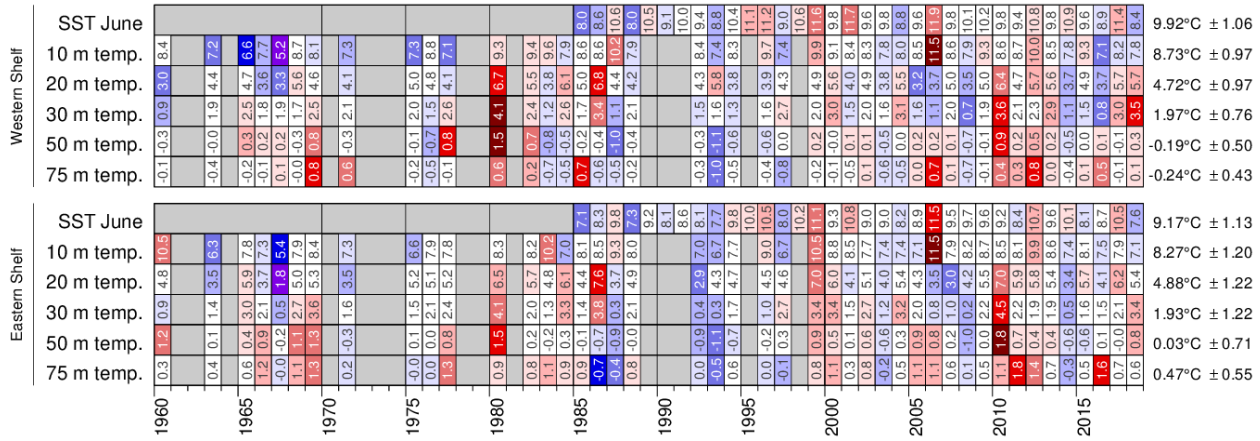


*Fig. 40. Depth-layer average temperature anomalies for western and eastern Magdalen Shallows for the June mackerel survey. The SST data are June averages from NOAA remote sensing repeated from Fig. 19. The SST colour-coding is based on the 1985-2010 climatology and the numbers are mean temperatures in ºC. The colour-coding of the 10 to 75 m lines are according to normalized anomalies based on the 1981-2010 climatologies, but the numbers are mean temperatures in ºC.*

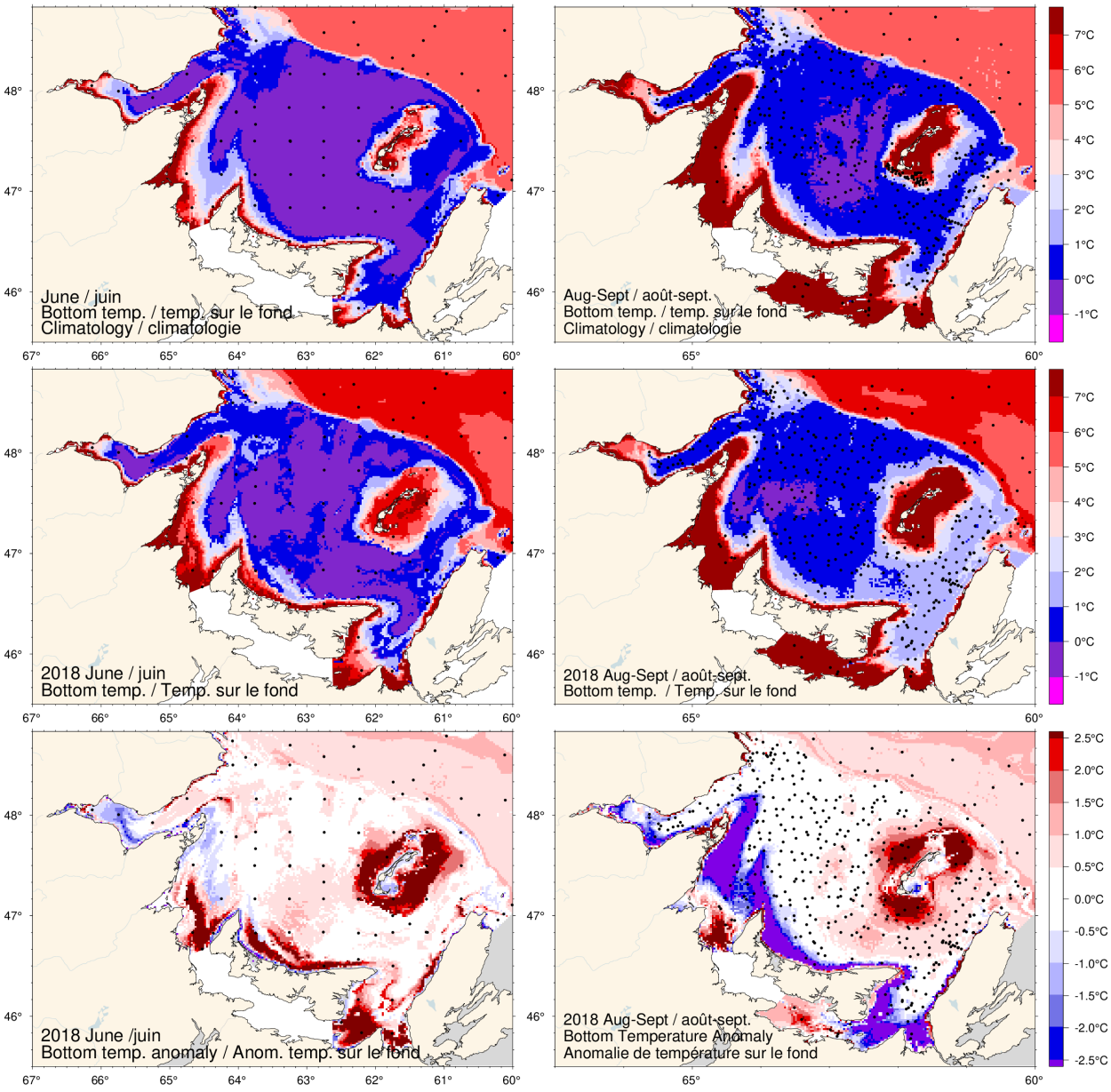


*Fig. 41. June (left) and August-September (right) bottom temperature climatology (top), 2018 observations (middle) and anomaly (bottom).*

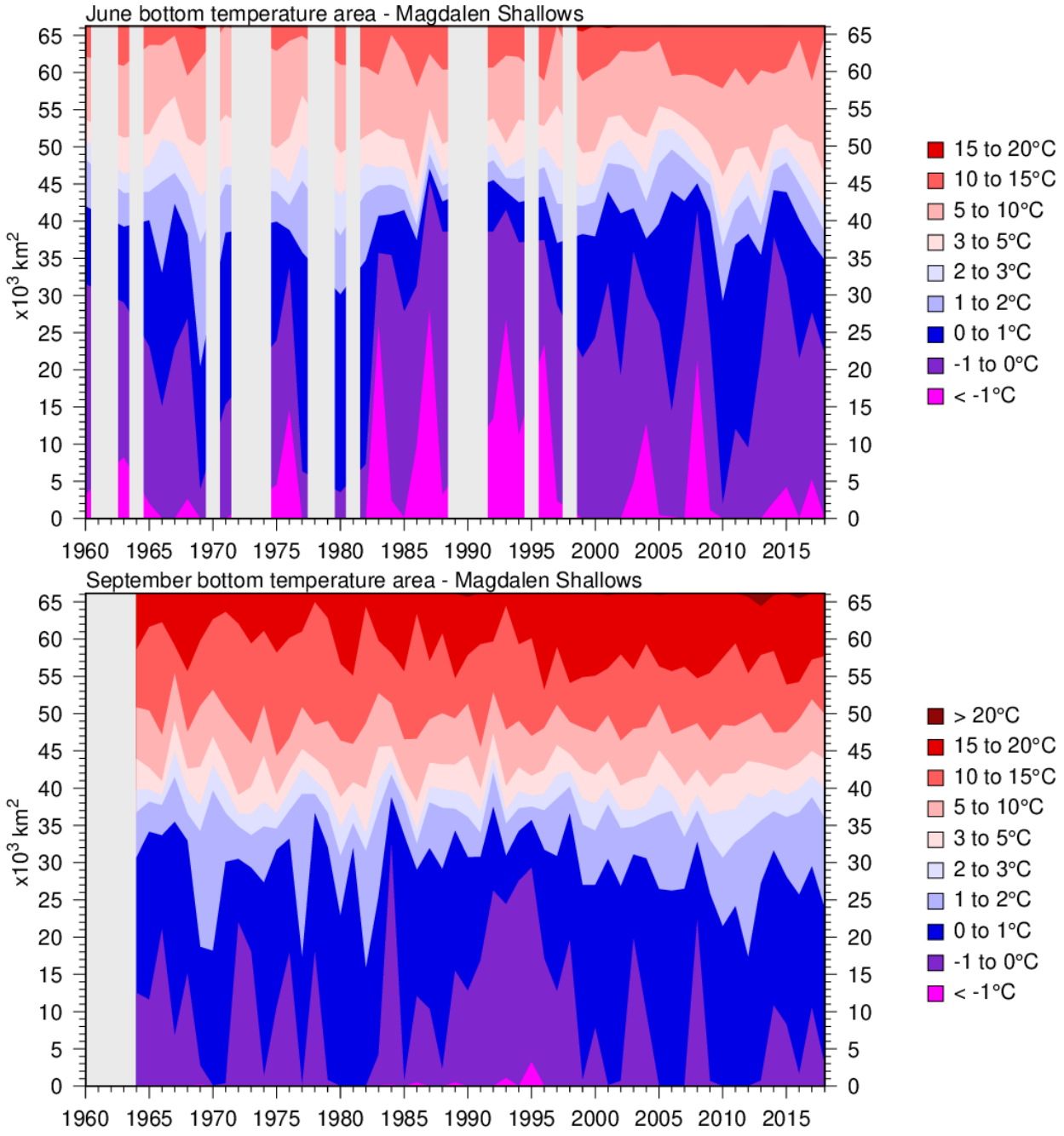


*Fig. 42. Time series of the bottom areas covered by different temperature bins in June (top) and August-September (bottom) for the Magdalen Shallows (region 8). Data are mostly from September for the bottom panel.*

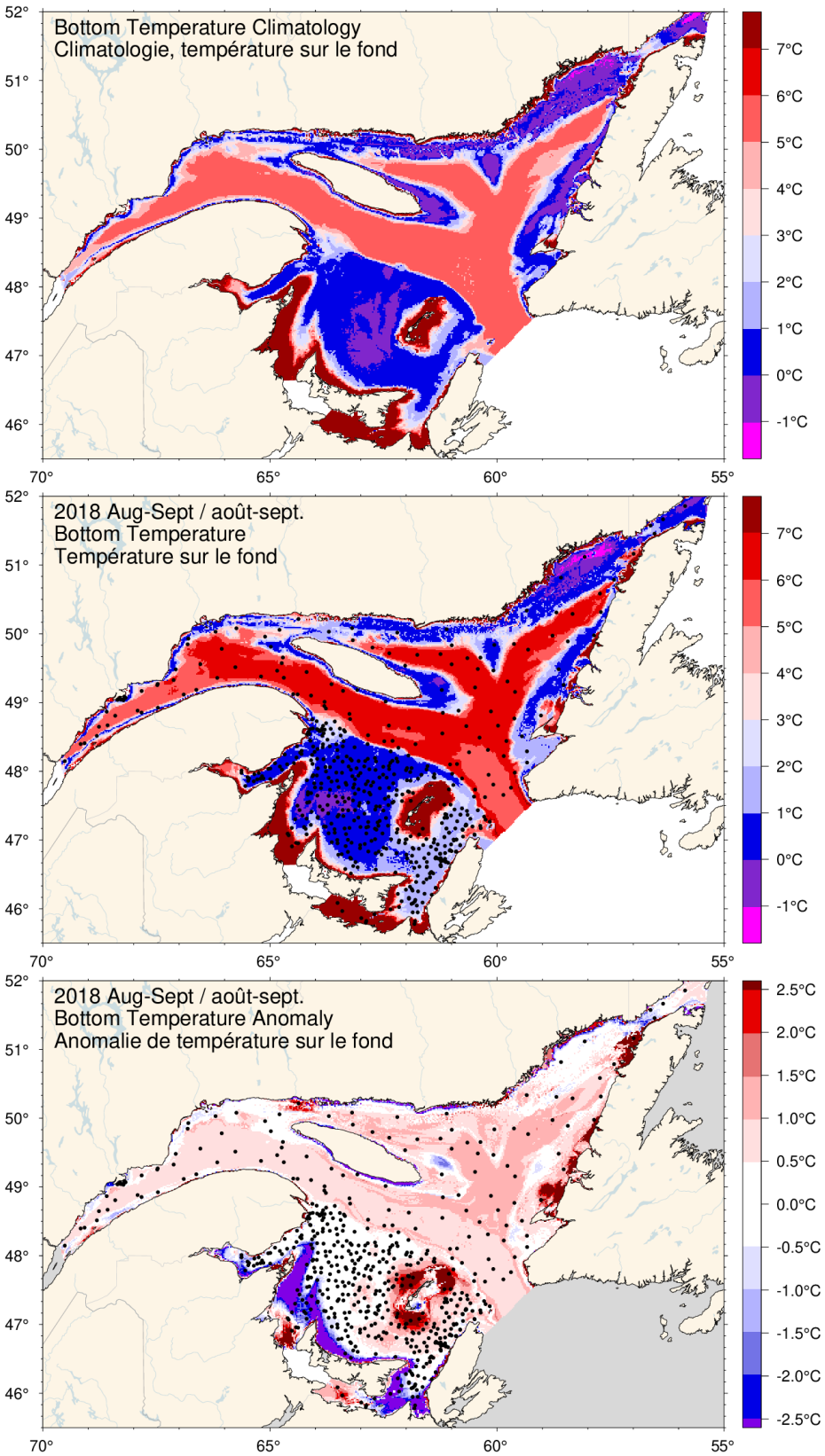


*Fig. 43. August-September bottom temperature climatology (top), 2018 observations (middle) and anomaly (bottom).*

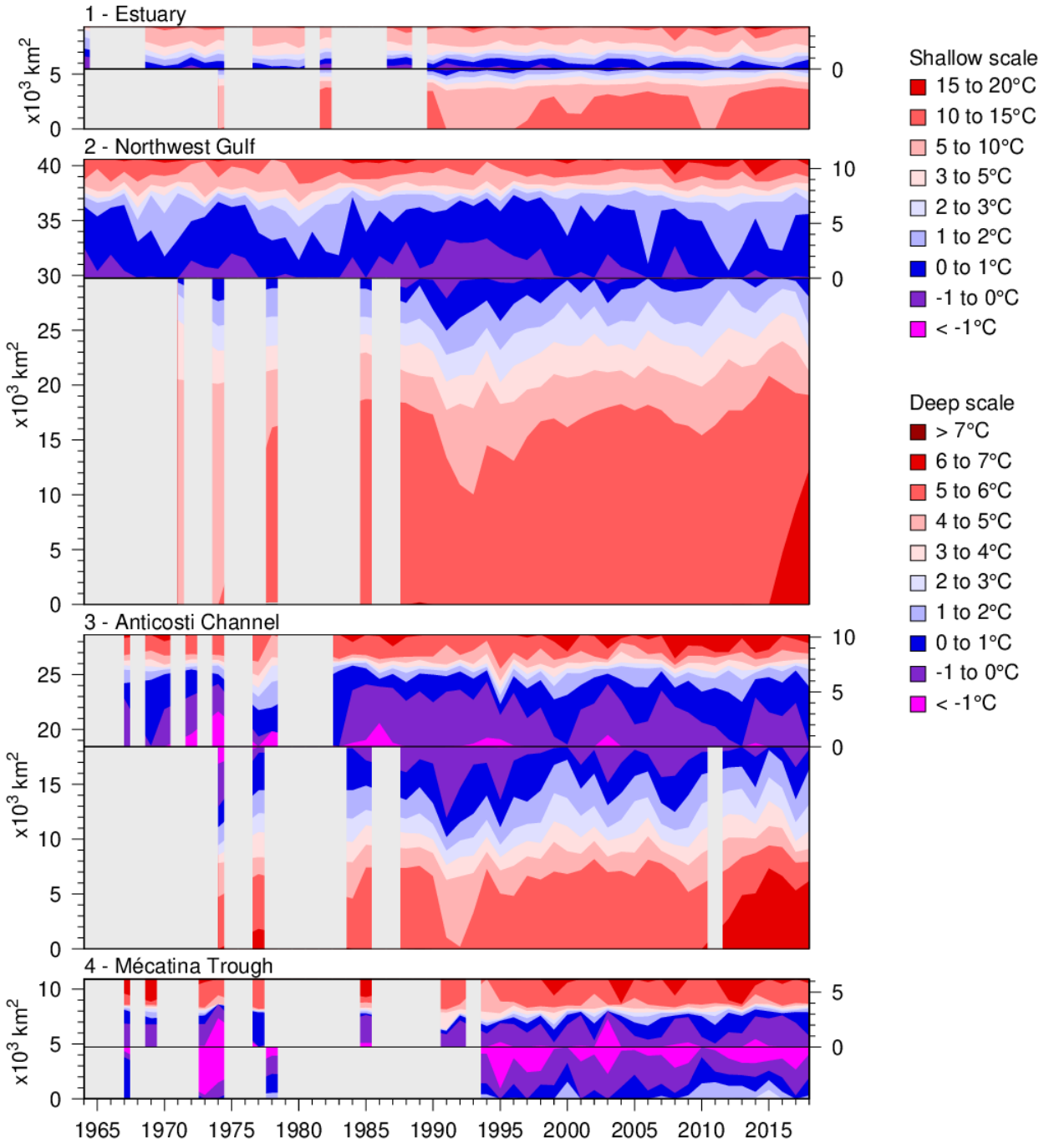


*Fig. 44. Time series of the bottom areas covered by different temperature bins in August and September for regions 1 to 4. The panels are separated by a black horizontal line into shallow (<100m) and deep (>100 m) areas to distinguish between warmer waters above and below the CIL. The shallow areas are shown on top using the area scale on the right-hand side and have warmer waters shown starting from the top end. The deep areas are shown below the horizontal line and have warmer waters starting at the bottom end. The CIL areas above and below 100 m meet near the horizontal line.*

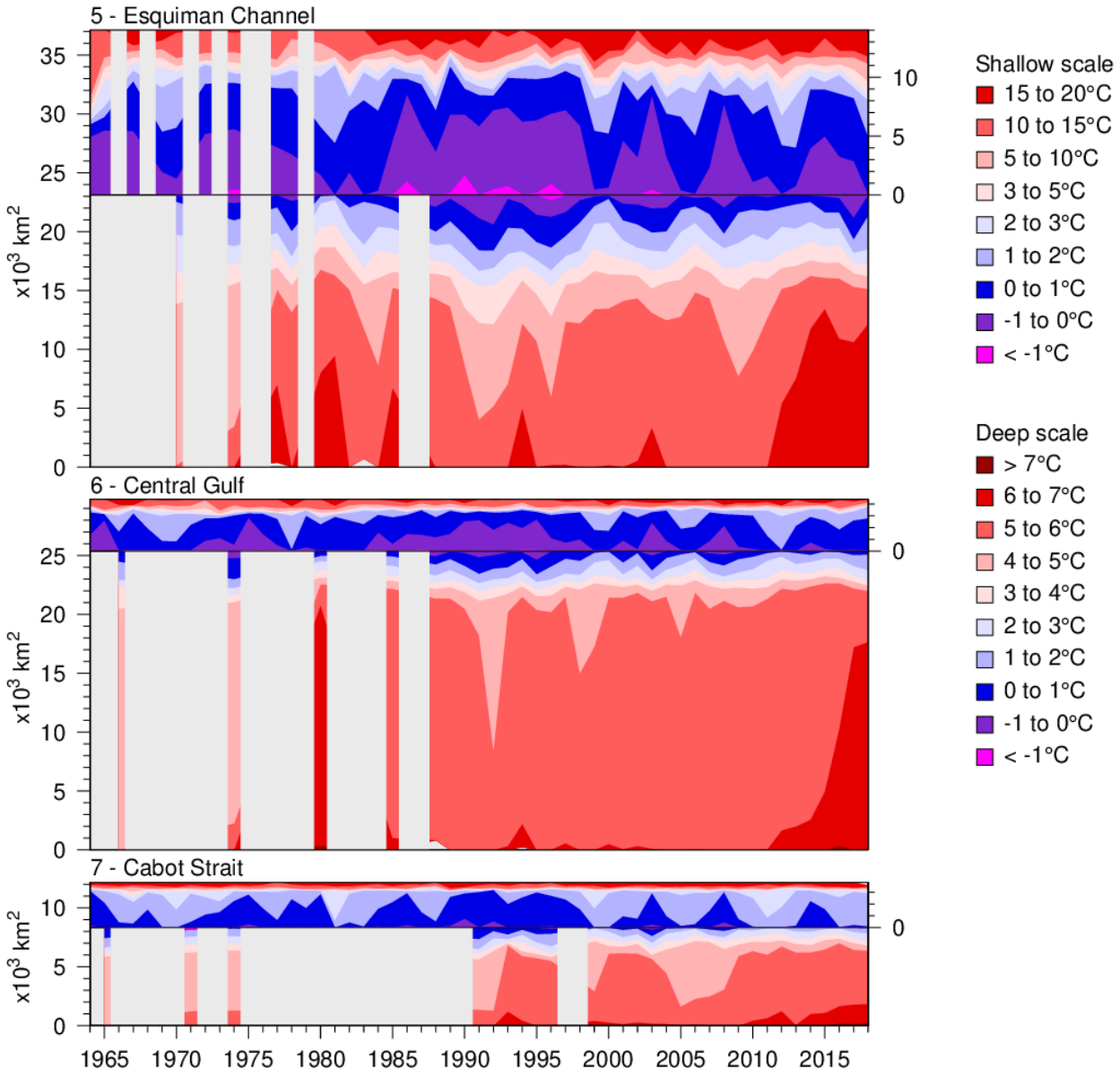


*Fig. 45. Time series of the bottom areas covered by different temperature bins in August and September for regions 5 to 7. The panels are separated into shallow (<100 m) and deep (>100 m) areas to distinguish between warmer waters above and below the CIL See Fig. 44 caption.*

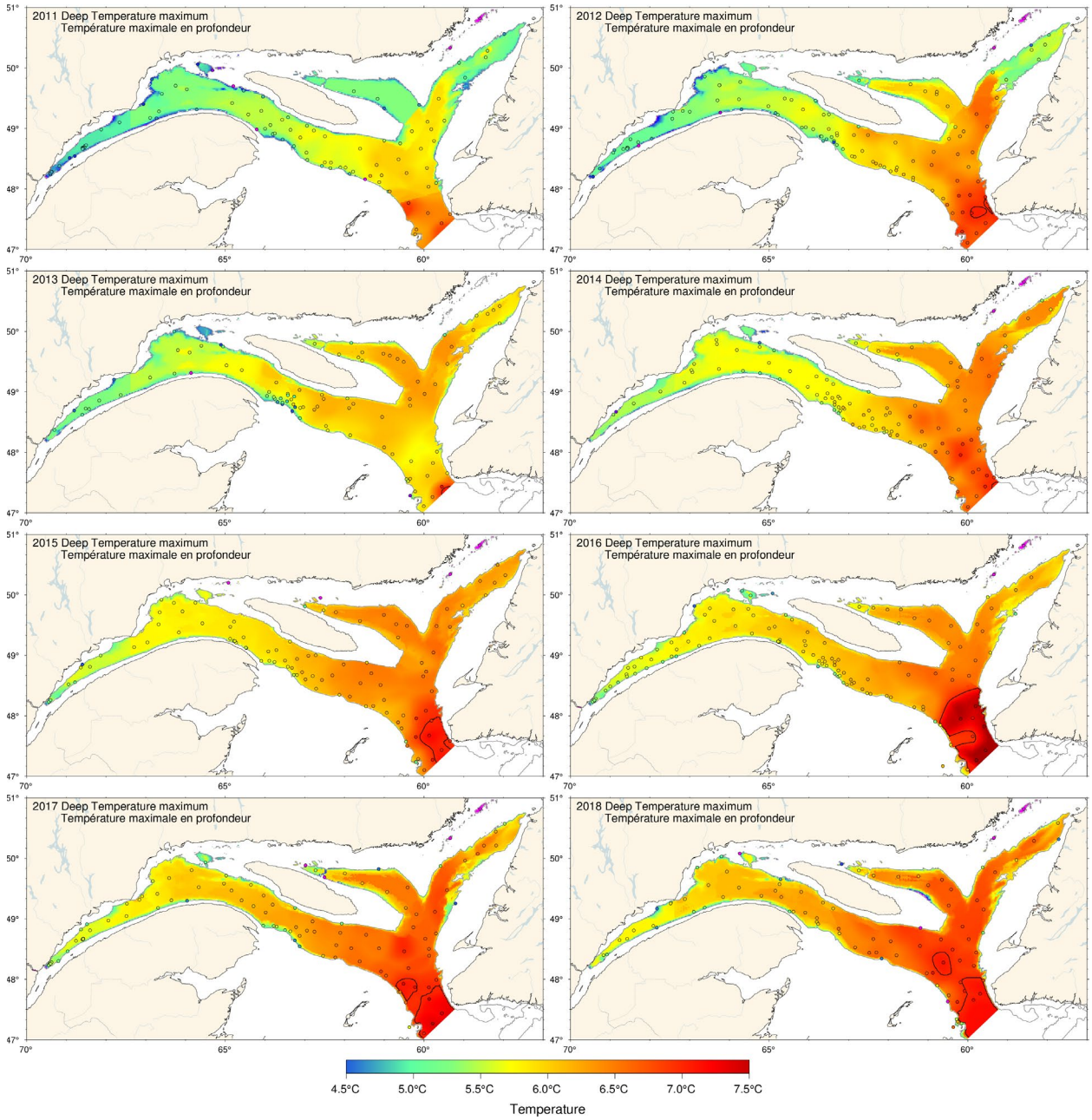


*Fig. 46. Map of the deep temperature maximum found typically between 200 and 300 m, 2011-2018. Maps are interpolated from August-September data available for each year. For 2012, 2013 and 2017, casts made in Cabot Strait during the fall survey were used to fill August sampling gaps.*

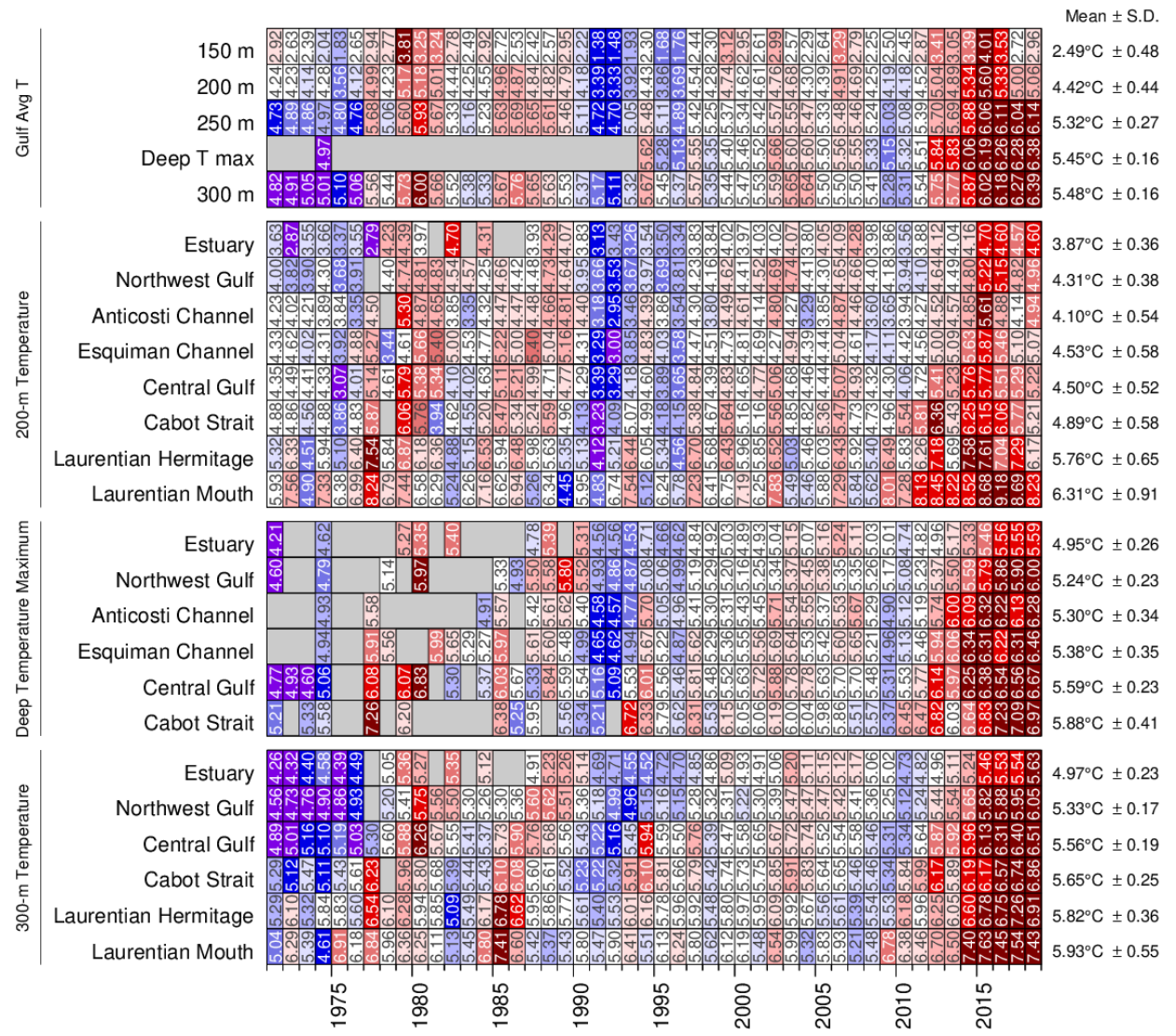


*Fig. 47. Deep layer temperature. Gulf averages for temperature are shown for 150, 200, 250, 300 m, as well as for the deep temperature maximum usually found between 200 and 300 m. Regional averages are shown for 200 and 300m, and deep temperature maximum. The numbers on the right are the 1981–2010 climatological means and standard deviations. The numbers in the boxes are average temperatures. The colour-coding is according to the temperature anomaly relative to the 1981–2010 climatology of each region and depth.*

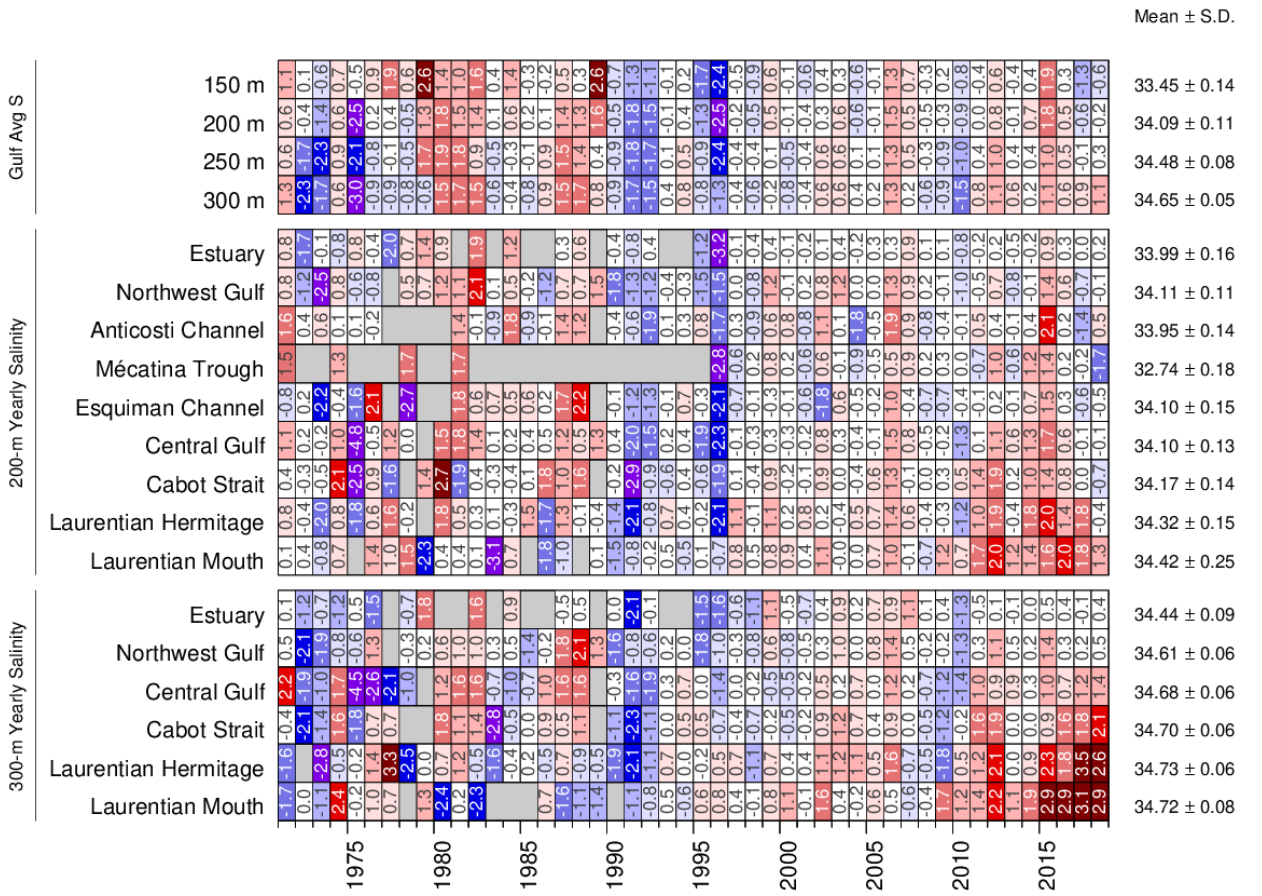


*Fig. 48. Deep layer salinity. Gulf averages for salinity are shown for 150, 200, 250, and 300 m. Regional averages are shown for 200 and 300m. The numbers on the right are the 1981–2010 climatological means and standard deviations. The numbers in the boxes are normalized anomalies.*

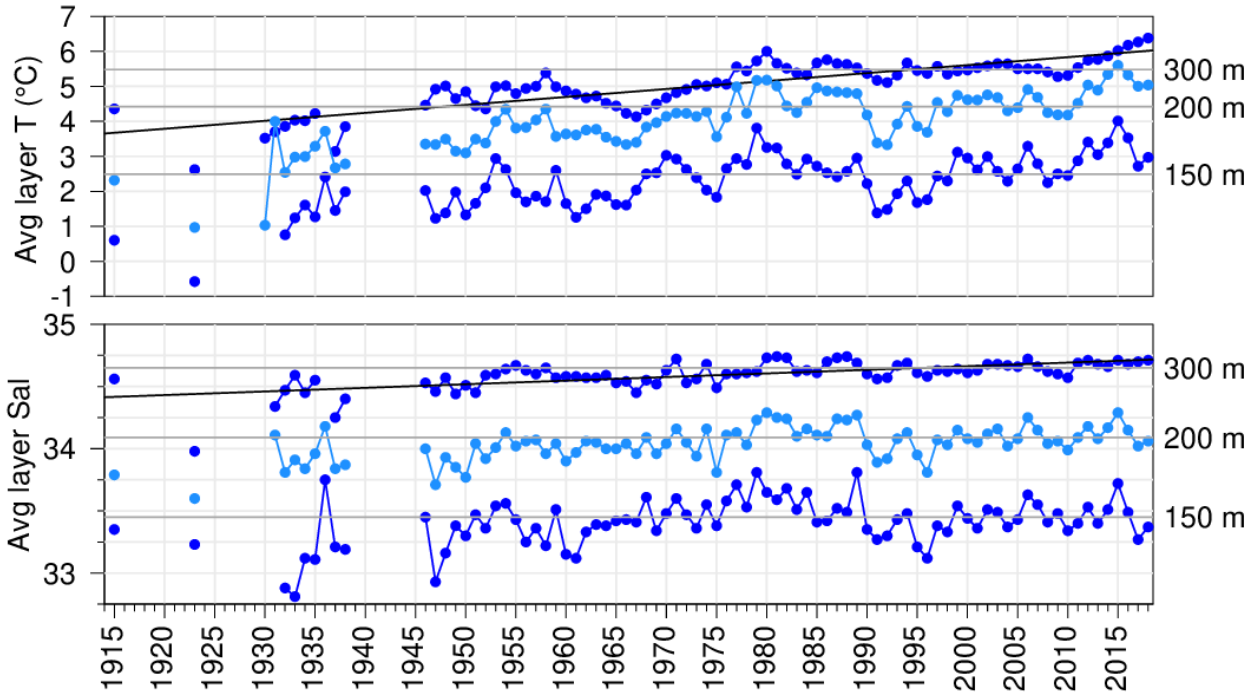


*Fig. 49. Layer-averaged temperature and salinity time series for the Gulf of St. Lawrence. The temperature and salinity panels show the 150 m, 200 m, and 300 m annual averages and the horizontal lines are 1981–2010 means. Sloped lines show linear regressions for temperature and salinity at 300 m of respectively 2.3°C and 0.3 per century.*

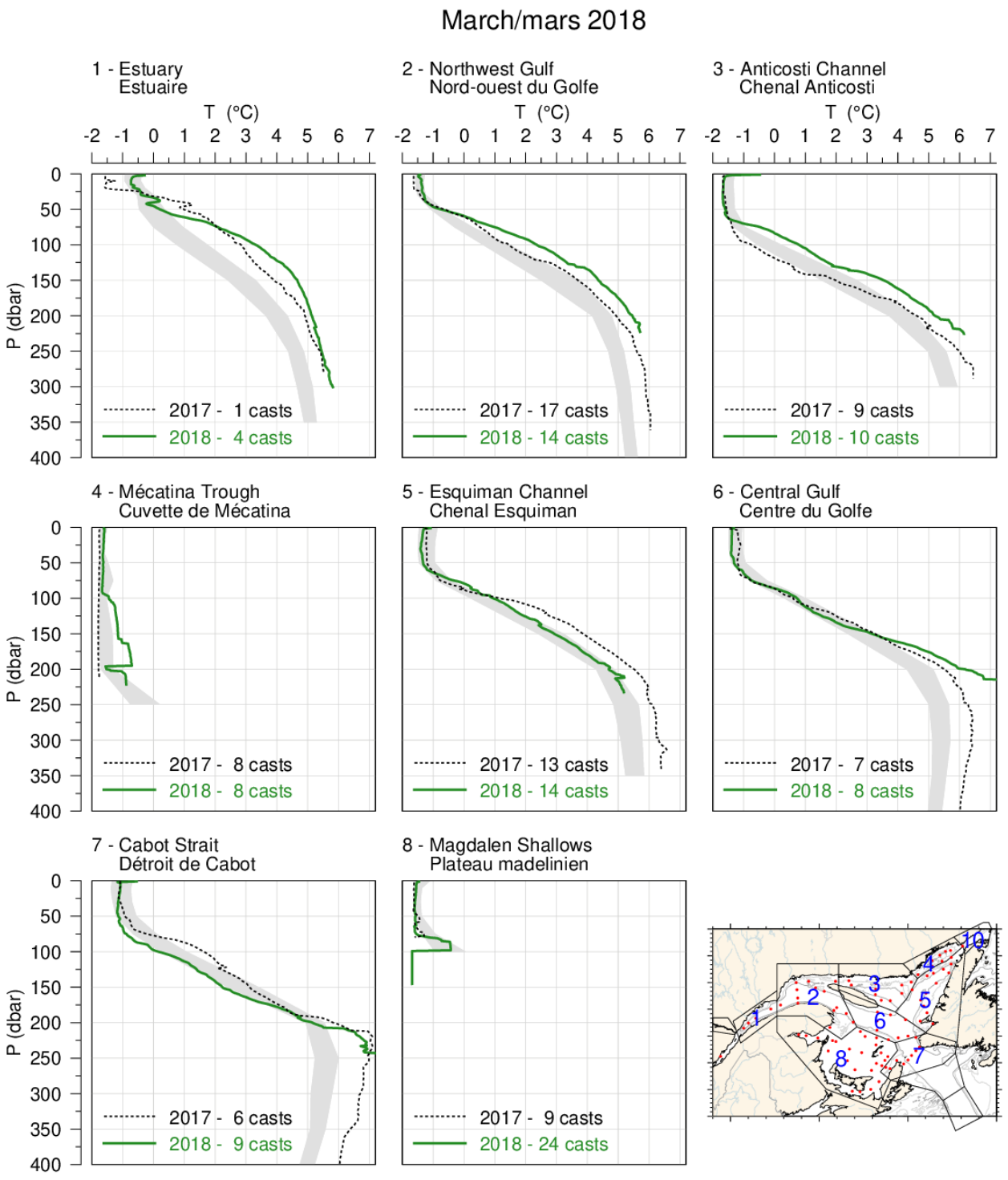


*Fig. 50. Mean temperature profiles observed in each region of the Gulf during the March 2018 survey. The shaded area represents the 1981–2010 (but mostly 1996–2010) climatological monthly mean ± 0.5 SD. Mean profiles for 2017 are also shown for comparison.*

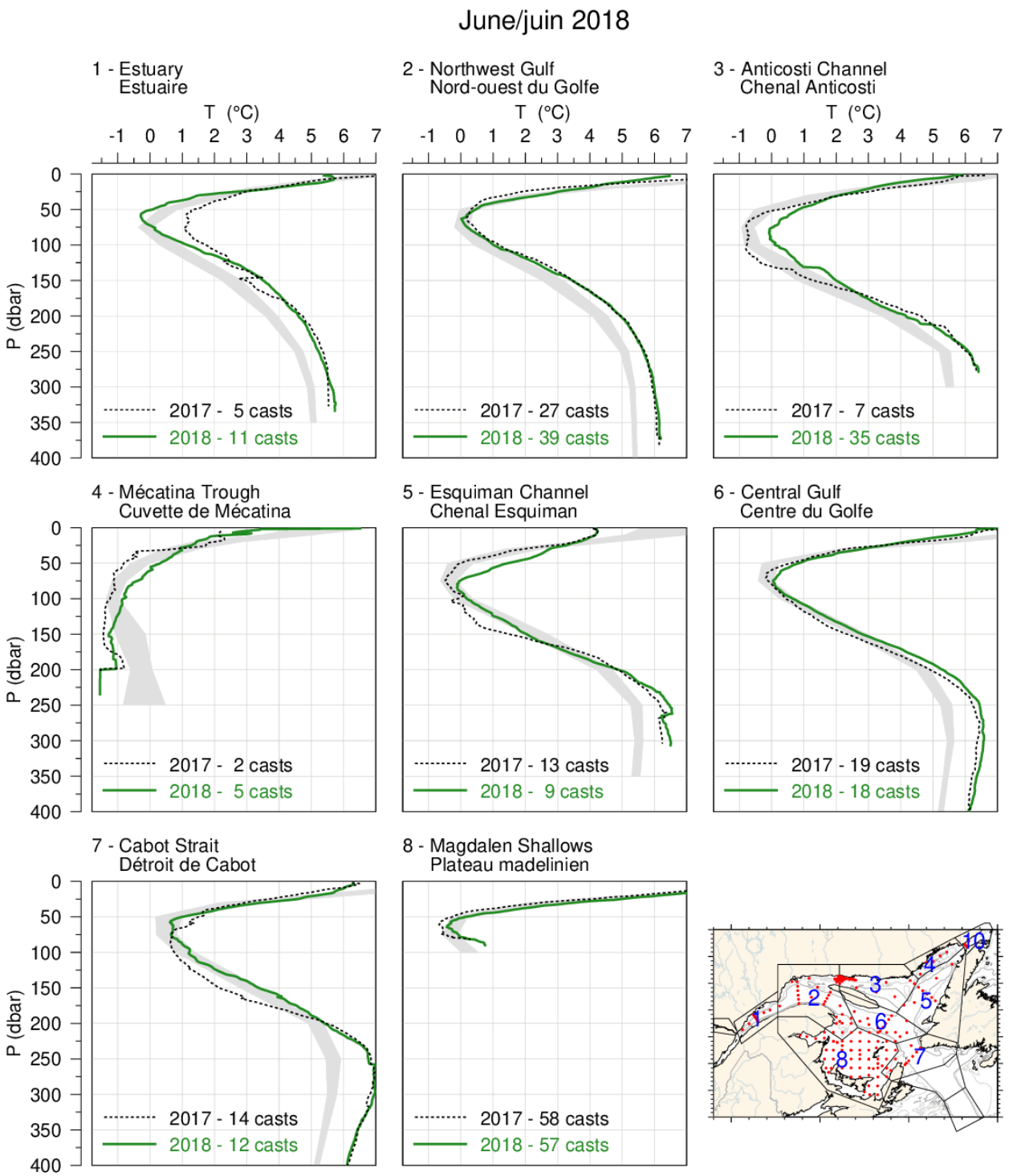


*Fig. 51. Mean temperature profiles observed in each region of the Gulf during June 2018. The shaded area represents the 1981–2010 climatological monthly mean ± 0.5 SD. Mean profiles for 2017 are also shown for comparison.*

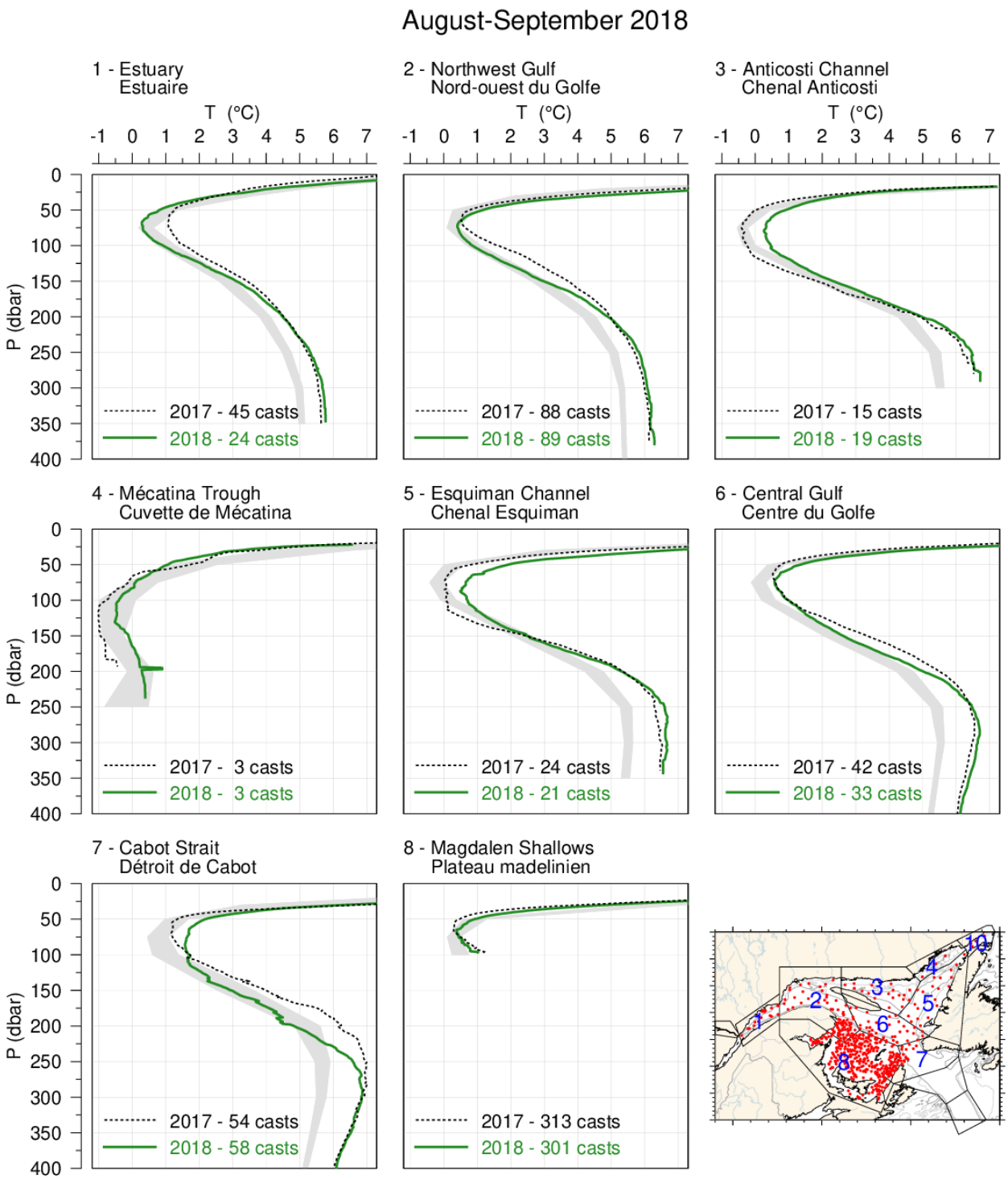


*Fig. 52. Mean temperature profiles observed in each region of the Gulf during August and September 2018. The shaded area represents the 1981–2010 climatological monthly mean ± 0.5 SD for August for regions 1 through 7 and for September for region 8. Mean profiles for 2017 are also shown for comparison.*

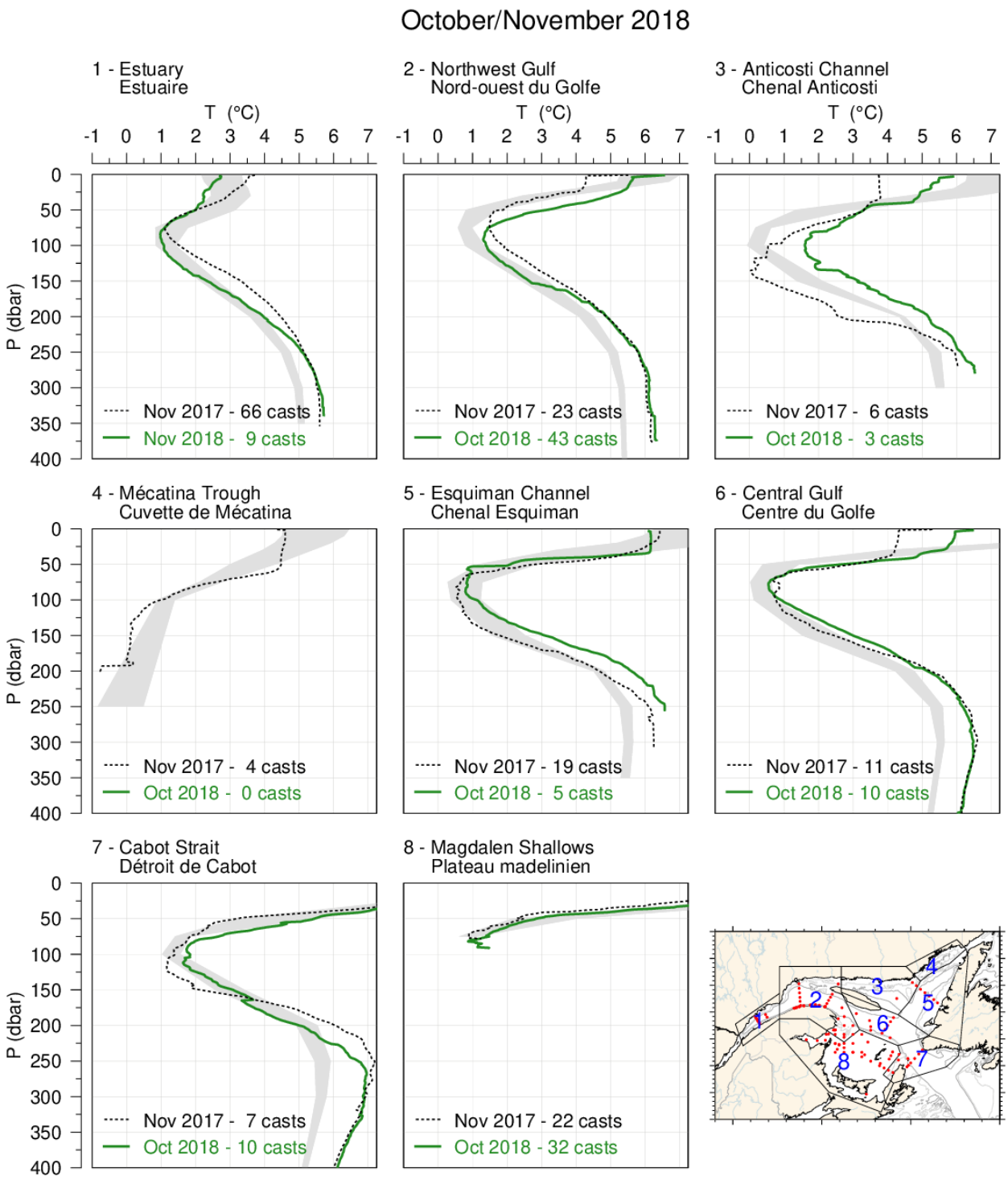


*Fig. 53. Mean temperature profiles observed in each region of the Gulf during the November 2018 AZMP survey. The shaded area represents the 1981–2010 climatological monthly mean ± 0.5 SD. Mean profiles for 2017 are also shown for comparison.*

1 - Estuary / Estuaire

| | 2017 | | | | 2018 | | | |
|---|---|---|---|---|---|---|---|---|
| | Mar | Juin | Août | Nov | Mar | Juin | Août | Nov |
| 0 m | -1.02 | 7.2 | 7.3 | 3.3 | -0.50 | 5.6 | 10.2 | 2.7 |
| 10 m | -1.04 | 5.0 | 5.4 | 3.4 | -0.61 | 5.5 | 6.9 | 2.6 |
| 20 m | -0.85 | 3.7 | 3.5 | 3.2 | -0.52 | 3.8 | 4.1 | 2.4 |
| 30 m | -0.09 | 2.3 | 2.4 | 3.0 | -0.33 | 1.7 | 2.6 | 2.2 |
| 50 m | 0.6 | 1.1 | 0.9 | 2.0 | -0.17 | 0.1 | 0.8 | 2.0 |
| 75 m | 1.5 | 0.8 | 1.1 | 1.1 | 0.7 | 0.1 | 0.3 | 1.1 |
| 100 m | 2.4 | 1.7 | 1.7 | 1.5 | 1.7 | 1.2 | 0.9 | 1.1 |
| 150 m | 3.8 | 3.4 | 3.6 | 3.3 | 4.0 | 3.5 | 3.1 | 2.2 |
| 200 m | 4.84 | 4.51 | 4.61 | 4.46 | 4.91 | 4.54 | 4.50 | 3.97 |
| 250 m | 5.32 | 5.18 | 5.23 | 5.15 | 5.24 | 5.22 | 5.28 | 5.09 |
| 300 m | 5.52 | 5.51 | 5.58 | 5.54 | 5.60 | 5.60 | 5.68 | 5.56 |
| 350 m | | 5.53 | 5.64 | 5.59 | | 5.75 | 5.75 | 5.69 |

2 - Northwest Gulf / Nord-ouest du Golfe

| | 2017 | | | | 2018 | | | |
|---|---|---|---|---|---|---|---|---|
| | Mar | Juin | Août | Nov | Mar | Juin | Août | Oct |
| 0 m | -1.63 | 8.9 | 14.1 | 3.1 | -1.47 | 6.3 | 15.9 | 5.7 |
| 10 m | -1.64 | 6.2 | 11.5 | 3.1 | -1.36 | 5.2 | 13.8 | 5.6 |
| 20 m | -1.63 | 2.8 | 6.7 | 3.0 | -1.33 | 3.8 | 8.0 | 5.5 |
| 30 m | -1.59 | 1.4 | 3.1 | 2.3 | -1.27 | 2.4 | 4.3 | 5.0 |
| 50 m | -0.54 | 0.3 | 0.7 | 1.7 | -0.71 | 0.5 | 1.1 | 3.1 |
| 75 m | 0.6 | 0.4 | 0.6 | 1.5 | 0.9 | 0.2 | 0.4 | 1.4 |
| 100 m | 1.4 | 1.1 | 1.6 | 1.9 | 2.3 | 1.0 | 0.8 | 1.4 |
| 150 m | 3.8 | 3.5 | 3.6 | 3.5 | 4.3 | 3.4 | 2.9 | 2.6 |
| 200 m | 4.96 | 4.92 | 4.99 | 4.88 | 5.34 | 4.95 | 4.88 | 4.79 |
| 250 m | 5.62 | 5.69 | 5.78 | 5.79 | | 5.65 | 5.78 | 5.82 |
| 300 m | 5.89 | 5.93 | 6.04 | 6.04 | | 6.00 | 6.05 | 6.14 |
| 350 m | 5.95 | 6.01 | 6.11 | 6.06 | | 6.11 | 6.17 | 6.16 |
| 400 m | | 6.15 | 6.14 | 6.19 | | | 6.29 | 6.33 |

3 - Anticosti Channel / Chenal Anticosti

| | 2017 | | | | 2018 | | | |
|---|---|---|---|---|---|---|---|---|
| | Mar | Juin | Août | Nov | Mar | Juin | Août | Oct |
| 0 m | -1.66 | 5.8 | 13.0 | 3.8 | -1.58 | 5.6 | 15.2 | 5.5 |
| 10 m | -1.67 | 5.4 | 11.8 | 3.8 | -1.65 | 4.3 | 13.5 | 5.5 |
| 20 m | -1.67 | 3.6 | 4.8 | 3.8 | -1.66 | 3.0 | 5.3 | 5.2 |
| 30 m | -1.63 | 2.1 | 2.0 | 3.8 | -1.67 | 2.1 | 2.6 | 4.9 |
| 50 m | -1.56 | 0.2 | 0.0 | 3.3 | -1.59 | 0.9 | 0.9 | 3.3 |
| 75 m | -1.38 | -0.8 | -0.4 | 1.7 | -0.50 | 0.1 | 0.3 | 2.4 |
| 100 m | -0.74 | -0.8 | -0.2 | 0.9 | 0.8 | 0.1 | 0.5 | 1.6 |
| 150 m | 1.4 | 1.3 | 1.9 | 0.5 | 3.5 | 2.0 | 2.3 | 3.1 |
| 200 m | 4.61 | 4.63 | 4.68 | 2.63 | 5.20 | 4.17 | 4.98 | 5.18 |
| 250 m | 6.00 | 6.04 | 6.19 | 5.93 | | 6.10 | 6.41 | 6.14 |

4 - Mécatina Trough / Cuvette de Mécatina

| | 2017 | | | | 2018 | | |
|---|---|---|---|---|---|---|---|
| | Mar | Juin | Août | Nov | Mar | Juin | Août |
| 0 m | -1.75 | 2.2 | 14.2 | 4.7 | -1.59 | 4.2 | 14.7 |
| 10 m | -1.76 | 2.1 | 13.4 | 4.7 | -1.60 | 2.5 | 14.4 |
| 20 m | -1.76 | 2.0 | 6.8 | 4.7 | -1.61 | 1.4 | 10.4 |
| 30 m | -1.75 | 0.7 | 3.7 | 4.6 | -1.62 | 0.9 | 3.2 |
| 50 m | -1.74 | -0.8 | 1.7 | 4.5 | -1.63 | 0.3 | 1.1 |
| 75 m | -1.76 | -1.1 | -0.1 | 2.5 | -1.65 | -0.4 | 0.1 |
| 100 m | -1.78 | -1.2 | -0.8 | 1.0 | -1.44 | -0.8 | -0.4 |
| 150 m | -1.79 | -1.4 | -0.9 | 0.1 | -1.16 | -1.3 | -0.1 |
| 200 m | -1.78 | -0.80 | -0.46 | 0.15 | -0.68 | -1.04 | 0.24 |

5 - Esquiman Channel / Chenal Esquiman

| | 2017 | | | | 2018 | | | |
|---|---|---|---|---|---|---|---|---|
| | Mar | Juin | Août | Nov | Mar | Juin | Août | Oct |
| 0 m | -1.20 | 4.3 | 16.1 | 5.8 | -1.28 | 4.2 | 17.5 | 6.2 |
| 10 m | -1.21 | 4.2 | 15.5 | 5.8 | -1.34 | 4.2 | 16.9 | 6.2 |
| 20 m | -1.22 | 3.5 | 10.0 | 5.7 | -1.37 | 3.6 | 11.2 | 6.2 |
| 30 m | -1.22 | 1.9 | 4.7 | 5.5 | -1.41 | 2.8 | 6.6 | 6.2 |
| 50 m | -1.20 | -0.0 | 0.8 | 2.9 | -1.32 | 1.4 | 1.9 | 2.1 |
| 75 m | -0.76 | -0.5 | 0.0 | 0.7 | -0.34 | -0.0 | 0.7 | 0.8 |
| 100 m | 1.2 | -0.1 | 0.1 | 0.6 | 0.7 | 0.2 | 0.7 | 1.1 |
| 150 m | 3.9 | 1.5 | 2.3 | 1.8 | 2.9 | 2.0 | 2.6 | 3.1 |
| 200 m | 5.51 | 4.85 | 5.35 | 4.68 | 4.47 | 4.89 | 5.31 | 5.61 |
| 250 m | 6.03 | 6.14 | 6.34 | 6.11 | | 6.47 | 6.51 | 6.57 |
| 300 m | 6.22 | 6.24 | 6.47 | 6.25 | | 6.50 | 6.66 | |

6 - Central Gulf / Centre du Golfe

| | 2017 | | | | 2018 | | | |
|---|---|---|---|---|---|---|---|---|
| | Mar | Juin | Août | Nov | Mar | Juin | Août | Oct |
| 0 m | -1.19 | 6.6 | 16.9 | 4.3 | -1.38 | 6.3 | 16.8 | 6.0 |
| 10 m | -1.19 | 6.2 | 15.2 | 4.3 | -1.38 | 5.8 | 16.0 | 5.9 |
| 20 m | -1.13 | 4.5 | 7.2 | 4.3 | -1.39 | 4.1 | 9.2 | 5.8 |
| 30 m | -1.14 | 2.3 | 3.3 | 4.2 | -1.40 | 2.8 | 4.2 | 5.5 |
| 50 m | -1.20 | 0.6 | 0.8 | 3.0 | -1.31 | 0.8 | 1.5 | 2.6 |
| 75 m | -0.77 | -0.1 | 0.5 | 0.8 | -0.74 | 0.0 | 0.7 | 0.6 |
| 100 m | 0.6 | 0.4 | 1.0 | 0.8 | 0.7 | 0.7 | 1.0 | 0.9 |
| 150 m | 3.3 | 2.3 | 3.3 | 2.5 | 3.1 | 2.8 | 2.5 | 3.0 |
| 200 m | 5.52 | 4.91 | 5.50 | 5.26 | 5.97 | 5.30 | 4.98 | 4.98 |
| 250 m | 6.17 | 6.24 | 6.45 | 6.28 | | 6.44 | 6.59 | 6.18 |
| 300 m | 6.38 | 6.37 | 6.53 | 6.54 | | 6.56 | 6.71 | 6.43 |
| 350 m | 6.16 | 6.24 | 6.28 | 6.30 | | 6.37 | 6.41 | 6.33 |
| 400 m | 6.04 | 6.06 | 6.04 | 6.13 | | 6.21 | 6.16 | 6.19 |
| 450 m | 5.98 | 6.00 | 5.97 | 5.91 | | 5.99 | 6.01 | |

7 - Cabot Strait / Détroit de Cabot

| | 2017 | | | | 2018 | | | |
|---|---|---|---|---|---|---|---|---|
| | Mar | Juin | Août | Nov | Mar | Juin | Août | Oct |
| 0 m | -1.08 | 6.5 | 19.3 | 7.9 | -1.07 | 6.3 | 21.9 | 9.4 |
| 10 m | -1.09 | 5.7 | 19.1 | 7.9 | -1.08 | 6.0 | 21.3 | 9.4 |
| 20 m | -1.14 | 4.3 | 15.0 | 7.6 | -1.11 | 5.1 | 12.0 | 9.0 |
| 30 m | -1.08 | 2.9 | 5.8 | 7.3 | -1.15 | 3.5 | 5.2 | 8.0 |
| 50 m | -0.92 | 1.5 | 1.3 | 3.2 | -1.14 | 1.0 | 1.7 | 5.4 |
| 75 m | -0.21 | 0.7 | 1.1 | 2.0 | -0.92 | 0.7 | 1.5 | 2.6 |
| 100 m | 1.7 | 0.8 | 1.5 | 1.4 | 0.1 | 1.2 | 1.6 | 1.8 |
| 150 m | 3.1 | 2.2 | 3.6 | 2.2 | 2.2 | 3.4 | 2.6 | 3.1 |
| 200 m | 5.99 | 5.47 | 6.07 | 6.05 | 5.02 | 5.41 | 5.00 | 5.03 |
| 250 m | 6.99 | 6.84 | 6.82 | 7.18 | 6.86 | 6.77 | 6.76 | 6.72 |
| 300 m | 6.68 | 6.82 | 6.92 | 6.92 | | 6.95 | 6.95 | 6.86 |
| 350 m | 6.39 | 6.44 | 6.45 | 6.46 | | 6.43 | 6.52 | 6.56 |
| 400 m | 6.03 | 6.12 | 6.08 | 6.01 | | 6.11 | 6.08 | 6.11 |
| 450 m | 5.93 | 5.94 | 5.93 | 5.88 | | 5.95 | 5.94 | 5.91 |
| 500 m | 5.93 | 5.92 | 5.88 | | | 5.91 | 5.88 | |

8 - Magdalen Shallows / Plateau madelinien

| | 2017 | | | | 2018 | | | |
|---|---|---|---|---|---|---|---|---|
| | Mar | Juin | Sep | Nov | Mar | Juin | Sep | Oct |
| 0 m | -1.62 | 9.7 | 16.3 | 5.9 | -1.52 | 9.1 | 17.0 | 8.8 |
| 10 m | -1.63 | 8.1 | 16.1 | 5.9 | -1.55 | 8.4 | 16.8 | 8.7 |
| 20 m | -1.62 | 5.7 | 11.0 | 5.9 | -1.56 | 6.2 | 12.9 | 8.3 |
| 30 m | -1.62 | 2.8 | 4.6 | 5.2 | -1.59 | 3.8 | 6.0 | 7.5 |
| 50 m | -1.48 | -0.3 | 0.8 | 2.3 | -1.58 | 0.3 | 1.6 | 2.9 |
| 75 m | -1.41 | -0.5 | 0.5 | 1.3 | -1.54 | -0.1 | 0.7 | 1.3 |
| 100 m | | | 1.1 | | -0.43 | 0.8 | | 1.1 |

*Fig. 54. Depth-layer monthly average temperature summary for months during which the eight Gulf-wide oceanographic surveys took place in 2017 and 2018. The colour-coding is according to the temperature anomaly relative to the monthly 1981–2010 climatology of each region.*

1 - Estuary / Estuaire

| | 2017 | | | | 2018 | | | |
|---|---|---|---|---|---|---|---|---|
| | Mar | Juin | Août | Nov | Mar | Juin | Août | Nov |
| Strat. | 3.12 | 5.4 | 3.5 | 3.8 | 2.64 | 4.3 | 4.3 | 2.9 |
| 0 m | 27.3 | 24.8 | 28.2 | 27.0 | 28.2 | 26.3 | 27.4 | 27.4 |
| 10 m | 28.0 | 26.6 | 29.1 | 28.0 | 29.0 | 26.6 | 28.3 | 28.0 |
| 20 m | 29.2 | 27.7 | 30.1 | 29.3 | 29.5 | 27.7 | 29.5 | 28.8 |
| 30 m | 30.3 | 29.1 | 30.8 | 30.5 | 30.2 | 29.4 | 30.5 | 29.6 |
| 50 m | 31.2 | 31.0 | 31.9 | 31.6 | 31.4 | 31.2 | 31.5 | 31.0 |
| 75 m | 32.5 | 32.1 | 32.3 | 32.2 | 32.4 | 32.2 | 32.1 | 32.0 |
| 100 m | 33.0 | 32.7 | 32.8 | 32.6 | 32.9 | 32.7 | 32.5 | 32.3 |
| 150 m | 33.7 | 33.5 | 33.6 | 33.4 | 33.8 | 33.6 | 33.4 | 33.0 |
| 200 m | 34.10 | 33.96 | 34.01 | 33.94 | 34.15 | 34.00 | 33.98 | 33.77 |
| 250 m | 34.32 | 34.27 | 34.28 | 34.25 | 34.28 | 34.29 | 34.30 | 34.23 |
| 300 m | 34.41 | 34.42 | 34.45 | 34.43 | 34.45 | 34.46 | 34.49 | 34.43 |
| 350 m | | 34.44 | 34.47 | 34.46 | | 34.53 | 34.52 | 34.48 |

2 - Northwest Gulf / Nord-ouest du Golfe

| | 2017 | | | | 2018 | | | |
|---|---|---|---|---|---|---|---|---|
| | Mar | Juin | Août | Nov | Mar | Juin | Août | Oct |
| Strat. | 0.55 | 4.8 | 4.7 | 1.2 | 0.84 | 2.9 | 4.5 | 1.7 |
| 0 m | 31.0 | 26.6 | 27.9 | 30.2 | 31.0 | 28.6 | 28.4 | 29.4 |
| 10 m | 31.0 | 28.2 | 28.5 | 30.4 | 31.4 | 29.6 | 28.8 | 29.6 |
| 20 m | 31.1 | 29.8 | 29.8 | 30.7 | 31.6 | 30.4 | 29.9 | 30.0 |
| 30 m | 31.2 | 30.7 | 30.7 | 31.1 | 31.7 | 30.9 | 30.6 | 30.4 |
| 50 m | 31.7 | 31.6 | 31.7 | 31.6 | 32.1 | 31.6 | 31.5 | 31.2 |
| 75 m | 32.2 | 32.2 | 32.3 | 32.1 | 32.6 | 32.2 | 32.0 | 32.0 |
| 100 m | 32.6 | 32.6 | 32.8 | 32.7 | 33.1 | 32.6 | 32.4 | 32.4 |
| 150 m | 33.6 | 33.5 | 33.6 | 33.5 | 33.9 | 33.5 | 33.4 | 33.1 |
| 200 m | 34.09 | 34.09 | 34.09 | 34.06 | 34.27 | 34.10 | 34.06 | 34.03 |
| 250 m | 34.43 | 34.45 | 34.46 | 34.47 | | 34.42 | 34.47 | 34.47 |
| 300 m | 34.61 | 34.63 | 34.65 | 34.66 | | 34.62 | 34.66 | 34.69 |
| 350 m | 34.66 | 34.73 | 34.78 | 34.73 | | 34.72 | 34.74 | 34.74 |
| 400 m | | 34.82 | 34.83 | 34.84 | | | 34.81 | 34.88 |

3 - Anticosti Channel / Chenal Anticosti

| | 2017 | | | | 2018 | | | |
|---|---|---|---|---|---|---|---|---|
| | Mar | Juin | Août | Nov | Mar | Juin | Août | Oct |
| Strat. | 0.01 | 1.4 | 2.9 | 0.2 | 0.09 | 2.4 | 2.8 | 0.5 |
| 0 m | 31.9 | 30.5 | 30.3 | 31.2 | 31.7 | 29.1 | 30.6 | 31.0 |
| 10 m | 31.9 | 30.7 | 30.5 | 31.2 | 31.7 | 30.4 | 30.7 | 31.1 |
| 20 m | 31.9 | 31.2 | 31.3 | 31.2 | 31.7 | 31.0 | 31.3 | 31.1 |
| 30 m | 31.9 | 31.5 | 31.6 | 31.2 | 31.8 | 31.4 | 31.5 | 31.2 |
| 50 m | 31.9 | 31.8 | 32.0 | 31.4 | 31.8 | 31.7 | 31.7 | 31.4 |
| 75 m | 32.0 | 32.2 | 32.3 | 31.9 | 32.2 | 31.9 | 32.0 | 31.6 |
| 100 m | 32.2 | 32.4 | 32.5 | 32.1 | 32.6 | 32.3 | 32.3 | 31.9 |
| 150 m | 32.8 | 33.0 | 33.1 | 32.8 | 33.6 | 33.1 | 33.2 | 33.4 |
| 200 m | 33.85 | 33.90 | 33.94 | 33.35 | 34.13 | 33.75 | 34.02 | 34.10 |
| 250 m | 34.37 | 34.45 | 34.52 | 34.41 | | 34.45 | 34.57 | 34.48 |

4 - Mécatina Trough / Cuvette de Mécatina

| | 2017 | | | | 2018 | | |
|---|---|---|---|---|---|---|---|
| | Mar | Juin | Août | Nov | Mar | Juin | Août |
| Strat. | 0.18 | 0.9 | 3.0 | 0.1 | 0.15 | 1.3 | 2.9 |
| 0 m | 32.2 | 31.0 | 30.1 | 31.1 | 31.6 | 30.3 | 30.4 |
| 10 m | 32.3 | 31.0 | 30.5 | 31.1 | 31.7 | 30.9 | 30.5 |
| 20 m | 32.3 | 31.1 | 31.2 | 31.1 | 31.7 | 31.3 | 30.8 |
| 30 m | 32.3 | 31.5 | 31.4 | 31.1 | 31.7 | 31.4 | 31.4 |
| 50 m | 32.4 | 32.0 | 31.7 | 31.1 | 31.8 | 31.6 | 31.7 |
| 75 m | 32.6 | 32.2 | 32.1 | 31.7 | 31.9 | 31.8 | 31.9 |
| 100 m | 32.7 | 32.4 | 32.3 | 32.1 | 32.0 | 32.0 | 32.0 |
| 150 m | 32.7 | 32.7 | 32.6 | 32.4 | 32.2 | 32.2 | 32.4 |
| 200 m | 32.66 | 32.80 | 32.77 | 32.62 | 32.43 | 32.35 | 32.52 |

5 - Esquiman Channel / Chenal Esquiman

| | 2017 | | | | 2018 | | | |
|---|---|---|---|---|---|---|---|---|
| | Mar | Juin | Août | Nov | Mar | Juin | Août | Oct |
| Strat. | 0.03 | 0.8 | 3.4 | 0.9 | 0.13 | 0.4 | 3.4 | 0.8 |
| 0 m | 31.8 | 31.3 | 30.3 | 30.8 | 31.5 | 31.4 | 30.3 | 31.1 |
| 10 m | 31.8 | 31.4 | 30.4 | 30.8 | 31.5 | 31.4 | 30.4 | 31.1 |
| 20 m | 31.8 | 31.5 | 30.9 | 30.9 | 31.5 | 31.4 | 31.0 | 31.1 |
| 30 m | 31.8 | 31.6 | 31.4 | 31.0 | 31.6 | 31.5 | 31.3 | 31.1 |
| 50 m | 31.8 | 31.9 | 31.8 | 31.6 | 31.7 | 31.6 | 31.6 | 31.6 |
| 75 m | 32.1 | 32.2 | 32.2 | 32.2 | 31.9 | 31.8 | 31.9 | 32.0 |
| 100 m | 32.7 | 32.5 | 32.5 | 32.5 | 32.5 | 32.2 | 32.3 | 32.4 |
| 150 m | 33.5 | 33.1 | 33.2 | 33.0 | 33.4 | 33.1 | 33.2 | 33.4 |
| 200 m | 34.13 | 33.93 | 34.11 | 33.89 | 33.84 | 33.96 | 34.11 | 34.23 |
| 250 m | 34.39 | 34.48 | 34.53 | 34.45 | | 34.55 | 34.56 | 34.62 |
| 300 m | 34.54 | 34.54 | 34.65 | 34.52 | | 34.56 | 34.75 | |

6 - Central Gulf / Centre du Golfe

| | 2017 | | | | 2018 | | | |
|---|---|---|---|---|---|---|---|---|
| | Mar | Juin | Août | Nov | Mar | Juin | Août | Oct |
| Strat. | 0.08 | 1.3 | 4.6 | 0.6 | 0.06 | 1.1 | 3.6 | 0.9 |
| 0 m | 31.6 | 30.6 | 28.9 | 30.8 | 31.6 | 30.7 | 30.0 | 30.7 |
| 10 m | 31.6 | 30.8 | 29.4 | 30.8 | 31.6 | 30.8 | 30.1 | 30.7 |
| 20 m | 31.7 | 31.1 | 30.7 | 30.9 | 31.6 | 31.1 | 30.7 | 30.7 |
| 30 m | 31.7 | 31.3 | 31.3 | 31.0 | 31.6 | 31.3 | 31.3 | 30.8 |
| 50 m | 31.7 | 31.6 | 31.8 | 31.4 | 31.7 | 31.6 | 31.6 | 31.4 |
| 75 m | 31.9 | 32.0 | 32.2 | 32.3 | 31.9 | 31.8 | 31.9 | 32.0 |
| 100 m | 32.3 | 32.3 | 32.5 | 32.6 | 32.6 | 32.4 | 32.3 | 32.5 |
| 150 m | 33.3 | 33.1 | 33.4 | 33.2 | 33.5 | 33.3 | 33.2 | 33.4 |
| 200 m | 34.14 | 33.94 | 34.16 | 34.07 | 34.30 | 34.11 | 34.02 | 34.03 |
| 250 m | 34.51 | 34.48 | 34.59 | 34.53 | | 34.55 | 34.60 | 34.52 |
| 300 m | 34.73 | 34.72 | 34.79 | 34.77 | | 34.75 | 34.82 | 34.75 |
| 350 m | 34.82 | 34.84 | 34.88 | 34.89 | | 34.87 | 34.92 | 34.92 |
| 400 m | 34.87 | 34.90 | 34.93 | 34.92 | | 34.91 | 34.96 | 34.94 |
| 450 m | 34.92 | 34.93 | 34.94 | 34.97 | | 34.97 | 34.97 | |

7 - Cabot Strait / Détroit de Cabot

| | 2017 | | | | 2018 | | | |
|---|---|---|---|---|---|---|---|---|
| | Mar | Juin | Août | Nov | Mar | Juin | Août | Oct |
| Strat. | 0.28 | 1.4 | 5.9 | 2.1 | 0.29 | 1.1 | 6.2 | 1.5 |
| 0 m | 31.1 | 30.4 | 27.8 | 29.5 | 31.4 | 30.6 | 28.2 | 30.0 |
| 10 m | 31.1 | 30.7 | 28.0 | 29.5 | 31.4 | 30.7 | 28.3 | 30.0 |
| 20 m | 31.1 | 31.0 | 28.7 | 29.9 | 31.4 | 30.9 | 29.4 | 30.2 |
| 30 m | 31.2 | 31.2 | 30.7 | 30.2 | 31.5 | 31.1 | 30.6 | 30.4 |
| 50 m | 31.4 | 31.6 | 31.7 | 31.5 | 31.7 | 31.4 | 31.6 | 31.2 |
| 75 m | 31.8 | 32.0 | 32.2 | 32.2 | 31.8 | 31.9 | 32.1 | 31.9 |
| 100 m | 32.6 | 32.3 | 32.6 | 32.6 | 32.2 | 32.4 | 32.5 | 32.4 |
| 150 m | 33.3 | 32.9 | 33.5 | 33.1 | 33.1 | 33.5 | 33.2 | 33.3 |
| 200 m | 34.24 | 34.07 | 34.27 | 34.20 | 34.08 | 34.14 | 34.01 | 33.97 |
| 250 m | 34.70 | 34.61 | 34.64 | 34.70 | 34.59 | 34.60 | 34.60 | 34.56 |
| 300 m | 34.79 | 34.79 | 34.84 | 34.88 | | 34.84 | 34.85 | 34.79 |
| 350 m | 34.88 | 34.87 | 34.91 | 34.94 | | 34.93 | 34.95 | 34.89 |
| 400 m | 34.91 | 34.93 | 34.94 | 34.95 | | 34.97 | 34.97 | 34.97 |
| 450 m | 34.93 | 34.95 | 34.95 | 34.98 | | 34.98 | 34.98 | 34.98 |
| 500 m | 34.93 | 34.95 | 34.97 | | | 34.98 | 34.98 | |

8 - Magdalen Shallows / Plateau madelinien

| | 2017 | | | | 2018 | | | |
|---|---|---|---|---|---|---|---|---|
| | Mar | Juin | Sep | Nov | Mar | Juin | Sep | Oct |
| Strat. | 0.12 | 3.4 | 5.1 | 1.8 | 0.37 | 2.8 | 4.4 | 1.8 |
| 0 m | 30.7 | 28.1 | 27.8 | 29.2 | 30.8 | 28.7 | 28.6 | 29.6 |
| 10 m | 30.7 | 28.6 | 27.9 | 29.3 | 30.8 | 29.0 | 28.7 | 29.6 |
| 20 m | 30.7 | 29.4 | 28.9 | 29.5 | 30.8 | 29.8 | 29.3 | 29.7 |
| 30 m | 30.8 | 30.3 | 30.2 | 29.9 | 31.0 | 30.5 | 30.3 | 30.0 |
| 50 m | 30.9 | 31.1 | 31.5 | 31.0 | 31.2 | 31.1 | 31.3 | 31.1 |
| 75 m | 31.0 | 31.6 | 32.0 | 31.8 | 31.4 | 31.7 | 31.7 | 31.7 |
| 100 m | | | 32.4 | | 32.0 | 32.2 | | 31.9 |

*Fig. 55. Depth-layer monthly average stratification and salinity summary for months during which the eight Gulf-wide oceanographic surveys took place in 2017 and 2018. Stratification is defined as the density difference between 50 m and the surface and its colour-coding is reversed (blue for positive anomaly).*

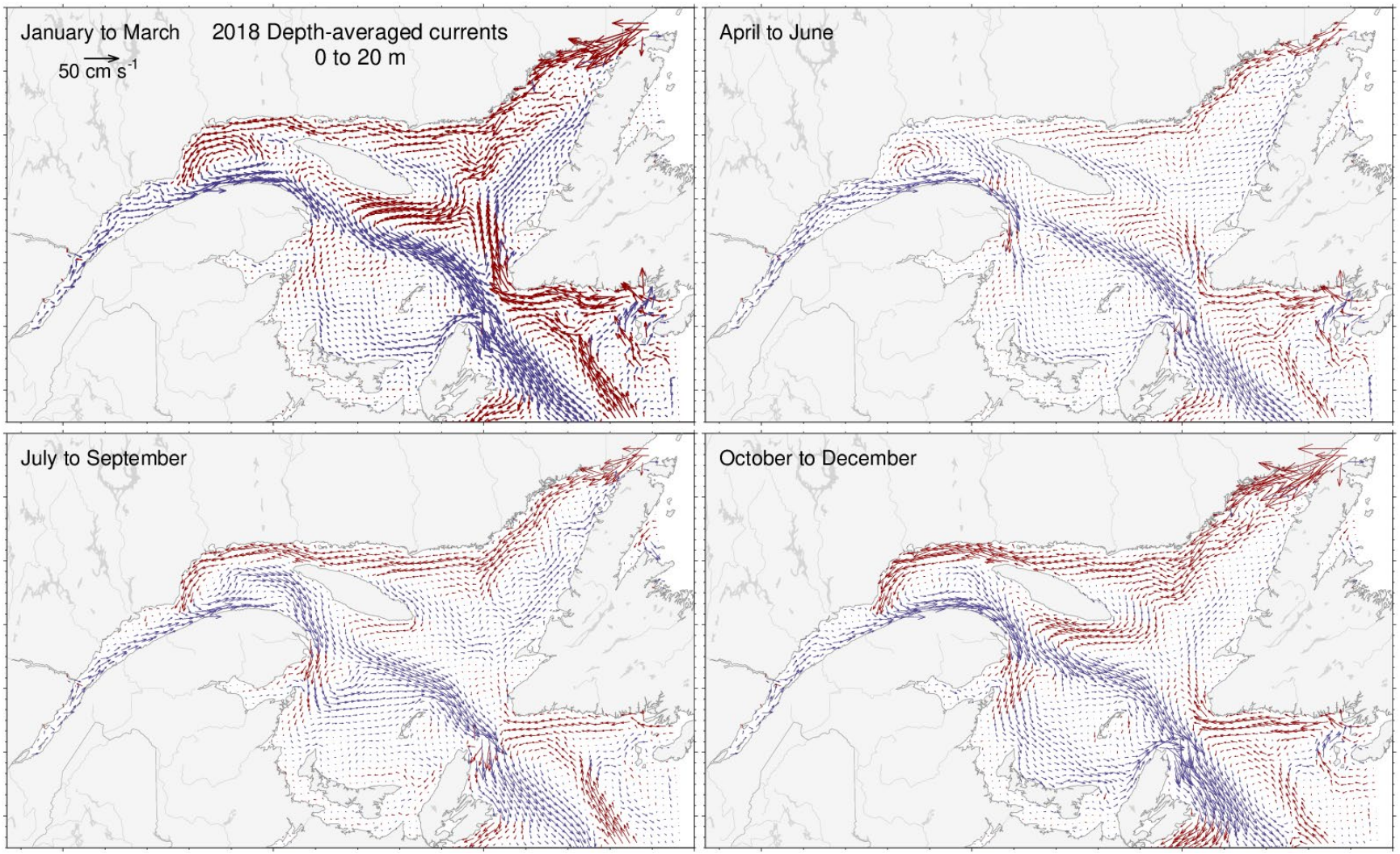


*Fig. 56. Depth-averaged currents from 0 to 20 m for each three-month period of 2018. Vectors drawn in blue are towards the East and those drawn in red are towards the West.*

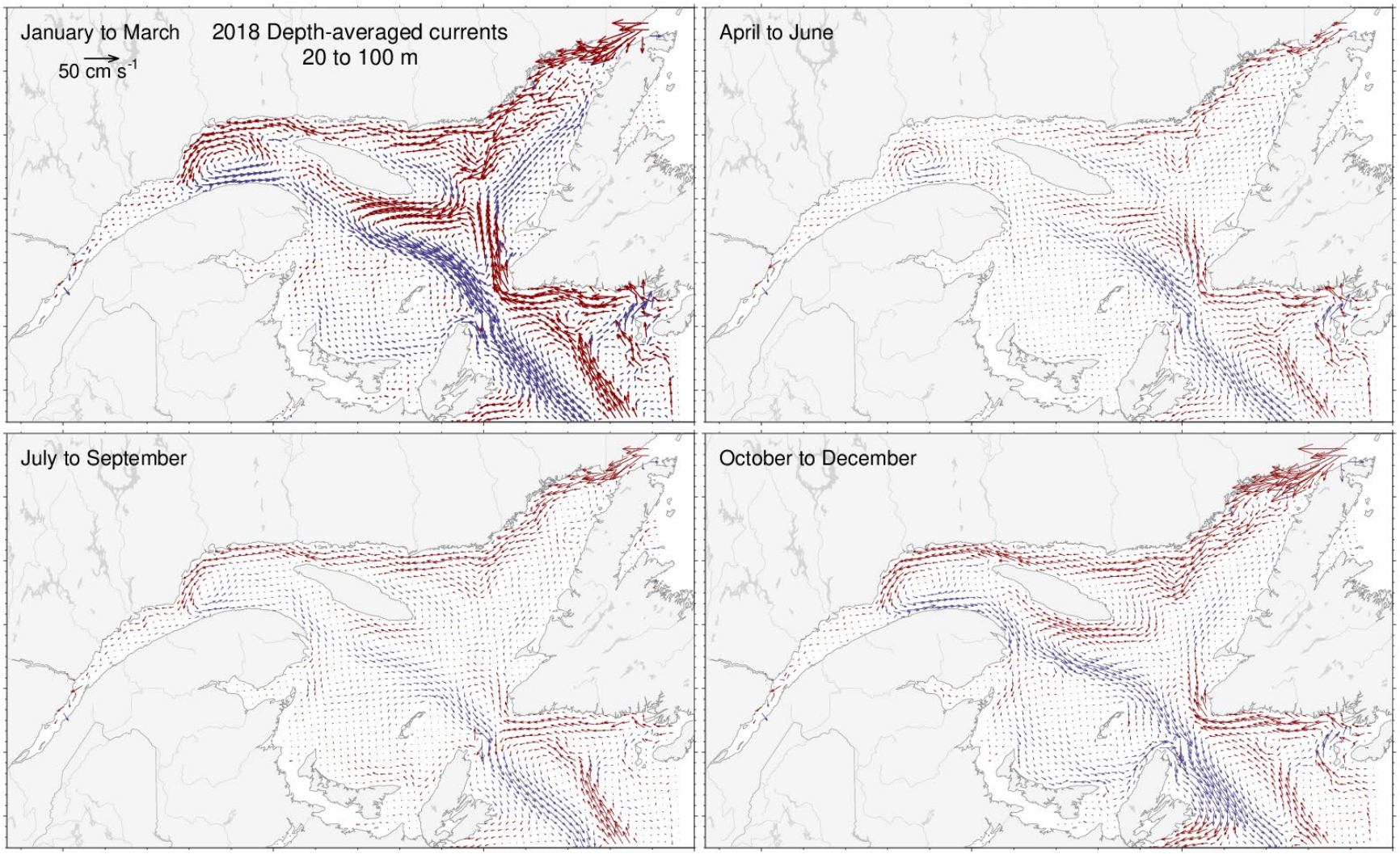


*Fig. 57. Depth-averaged currents from 20 to 100 m for each three-month period of 2018. Vectors drawn in blue are towards the East and those drawn in red are towards the West.*

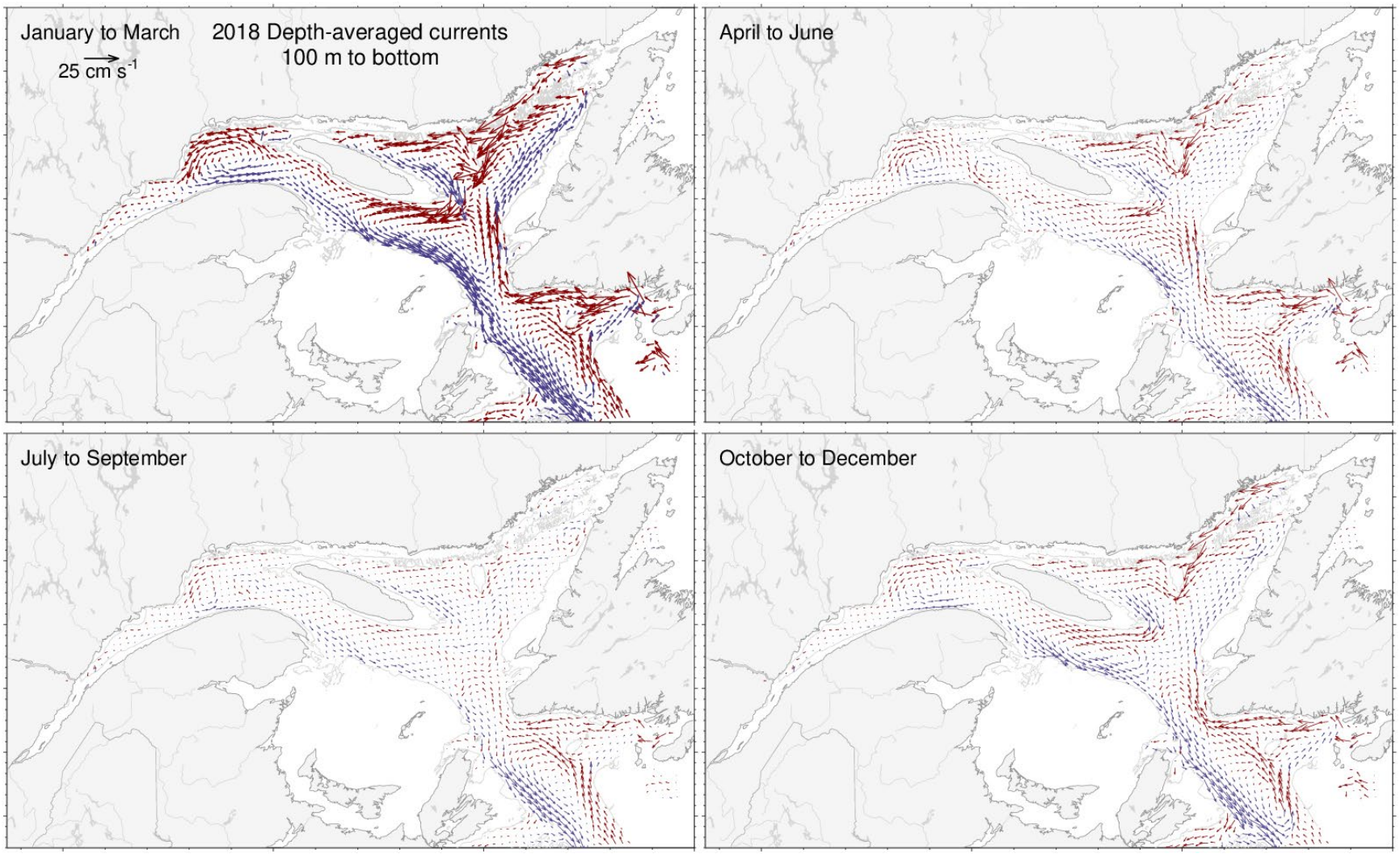


*Fig. 58. Depth-averaged currents from 100 m to the bottom for each three-month period of 2018. Vectors drawn in blue are towards the East and those drawn in red are towards the West.*

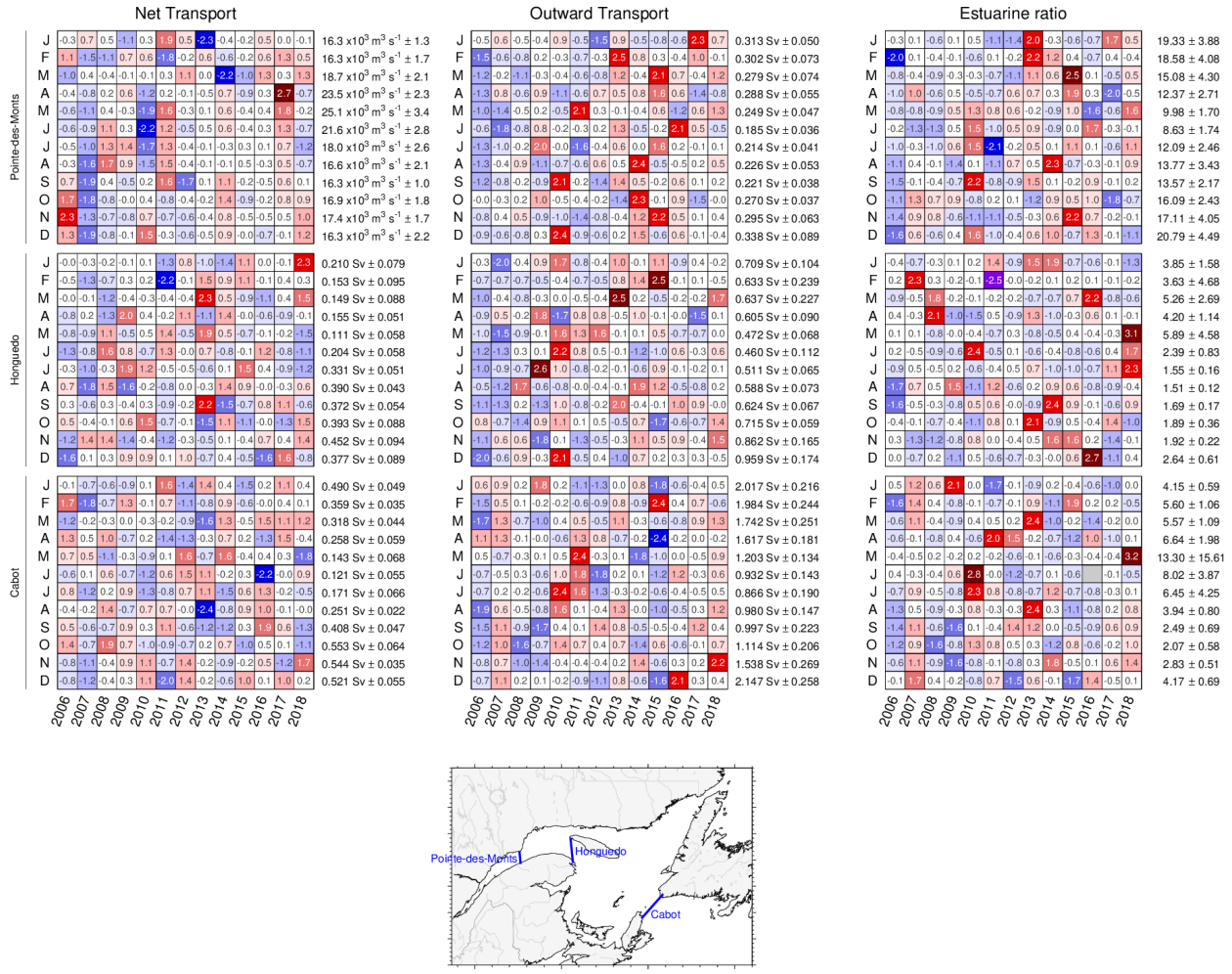





*Fig. 59. Monthly averaged modelled transports and estuarine ratio across sections of the Gulf of St. Lawrence since 2006. The numbers on the right are the 2006–2018 means and standard deviations. The numbers in the boxes are normalized anomalies. Colours indicate the magnitude of the anomaly. Sv (Sverdrup) are units of transport equal to $10^6$ $m^3s^{-1}$.*

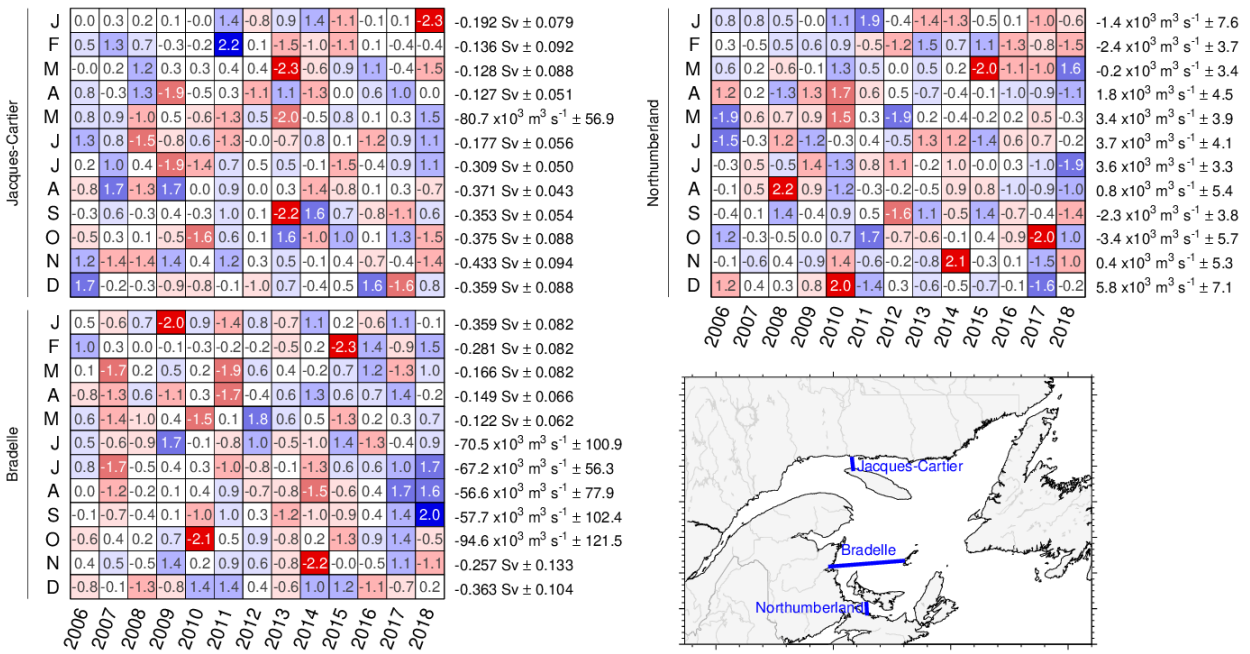


*Fig. 60. Monthly averaged modelled transports across sections of the Gulf of St. Lawrence since 2006. The numbers on the right are the 2006–2018 means and standard deviations, with positive values toward east and north. The numbers in the boxes are normalized anomalies. Colours indicate the magnitude of the anomaly (e.g., negative anomalies are still shown in red when the mean transport is negative across the section).*

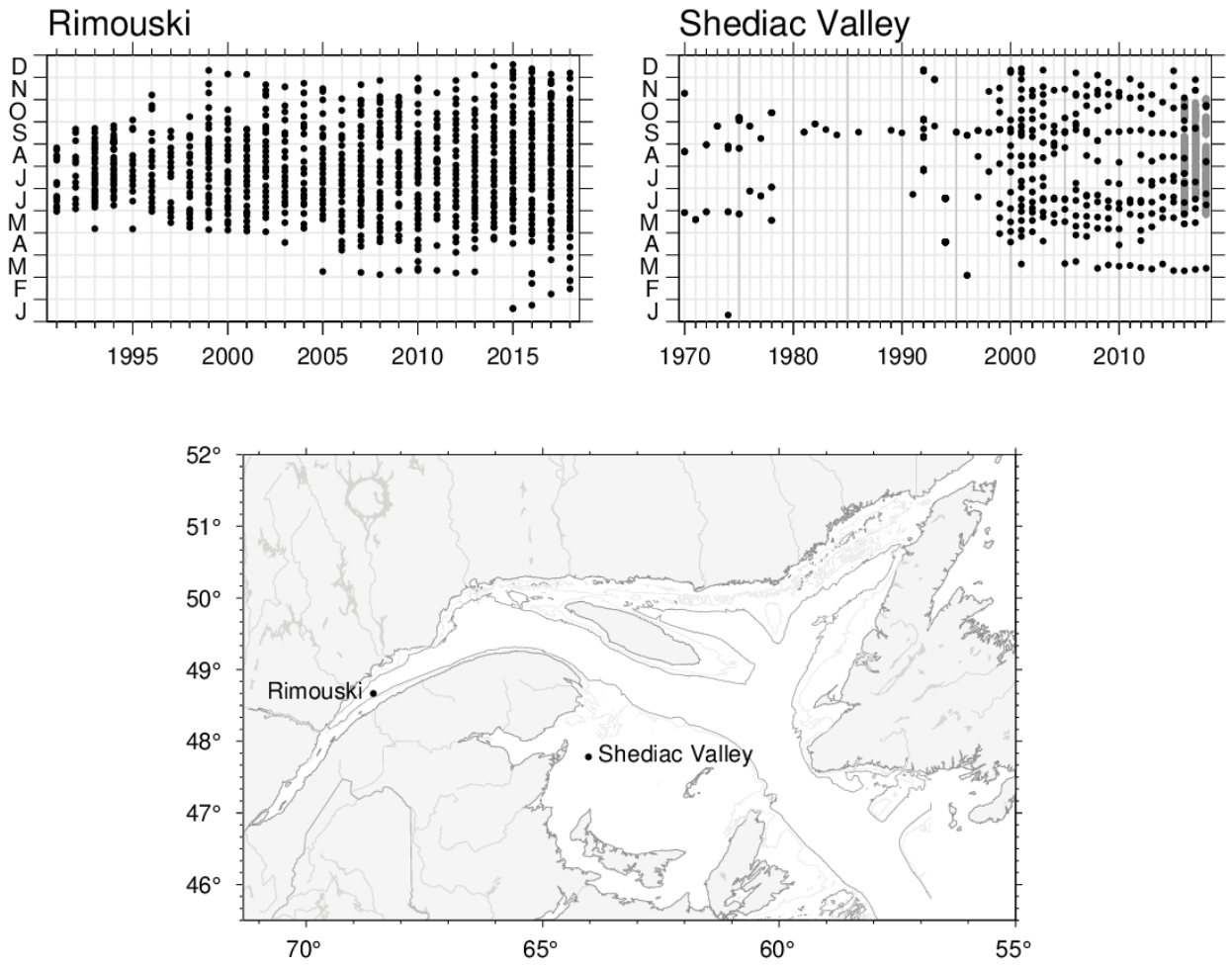


*Fig. 61. Sampling frequency and positions of the AZMP stations Rimouski and Shediac Valley. Gray overlay in 2018 at Shediac Valley shows span of 327 temperature and salinity profiles made by the PMZA-VAS automatic oceanographic buoy.*

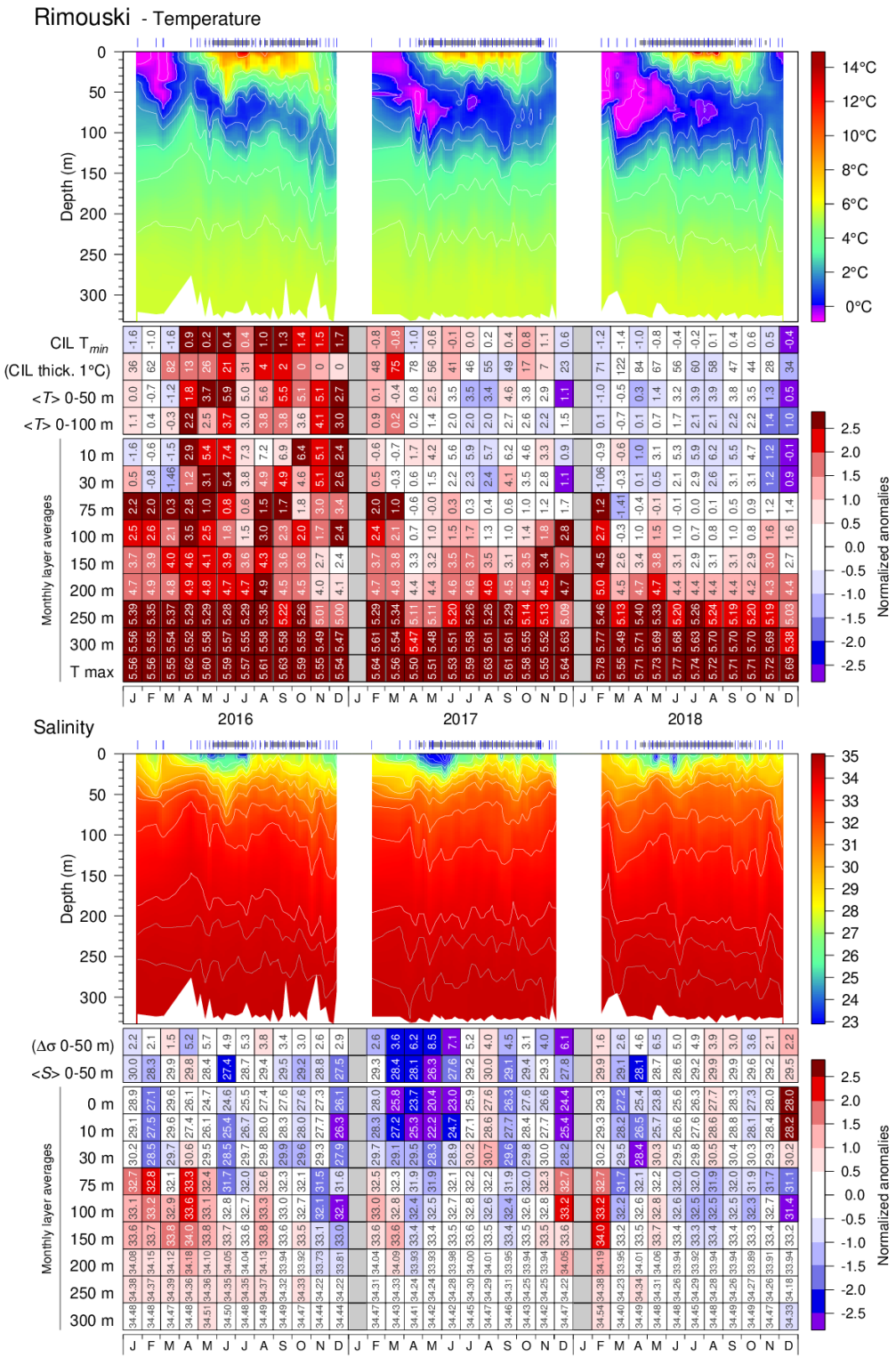


*Fig. 62. Isotherm (top) and isohaline (bottom) time series at the Rimouski station; tick marks above indicate sample dates and shaded area indicates casts made by a Viking automatic buoy. The scorecard tables are monthly layer averages colour-coded according to the anomaly relative to the 1991–2010 monthly climatology for the station (yearly climatology for 250 m and deeper). Thickness of the CIL and stratification have reversed colour codes where red indicates thinner CIL (warmer water) and less stratification (higher surface salinity).*

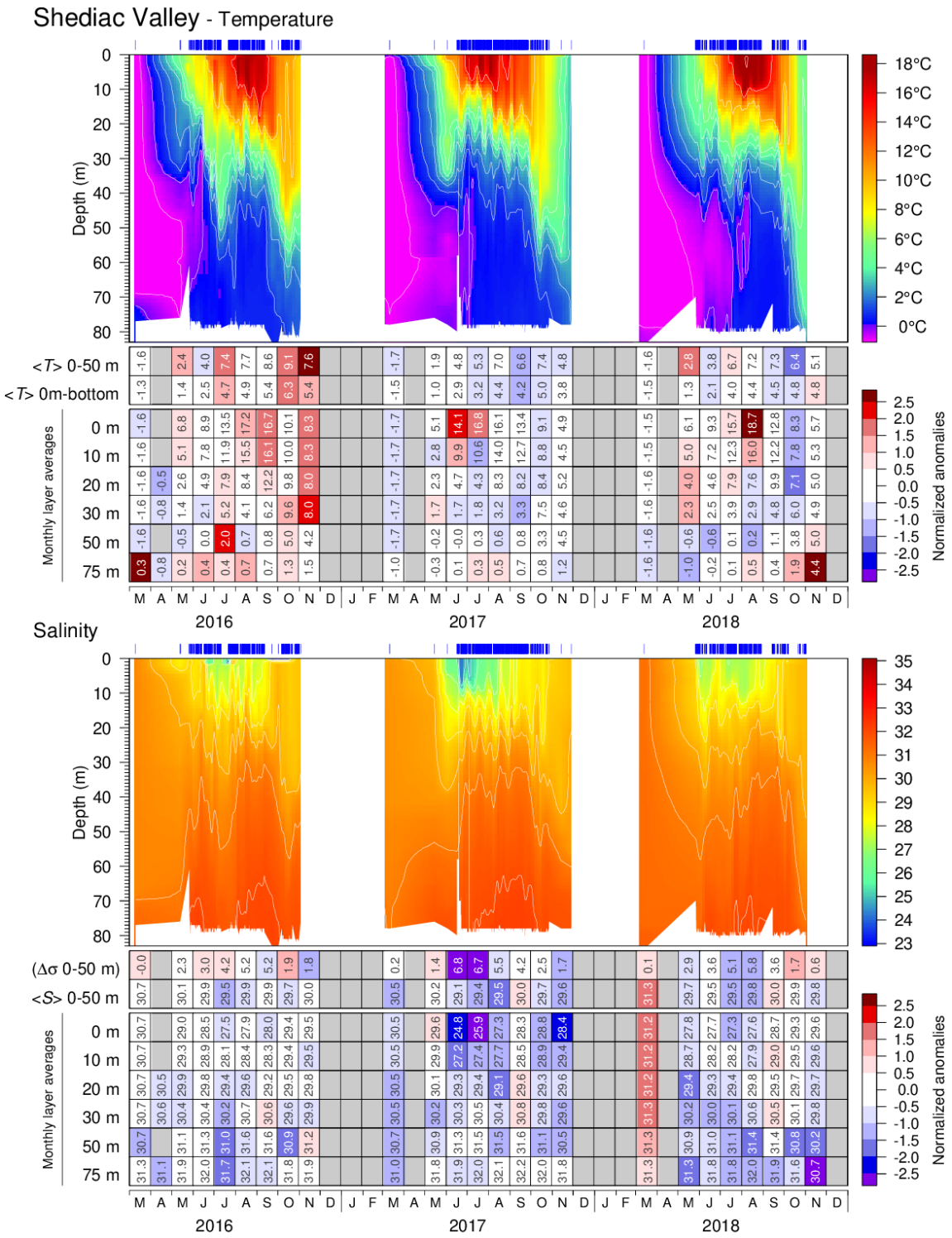


*Fig. 63. Isotherm (top) and isohaline (bottom) time series at the Shediac Valley station; tick marks above indicate sample dates (including from automatic buoy starting in 2016). Scorecard tables are monthly layer averages colour-coded according to the anomaly relative to the 1981–2017 monthly climatology for the station (input to climatology is sparse prior to 1999). The 10, 20, 30 and 75 m monthly layer averages for June–September 2015 are from mooring data. Internal tide oscillations are smoothed out.*

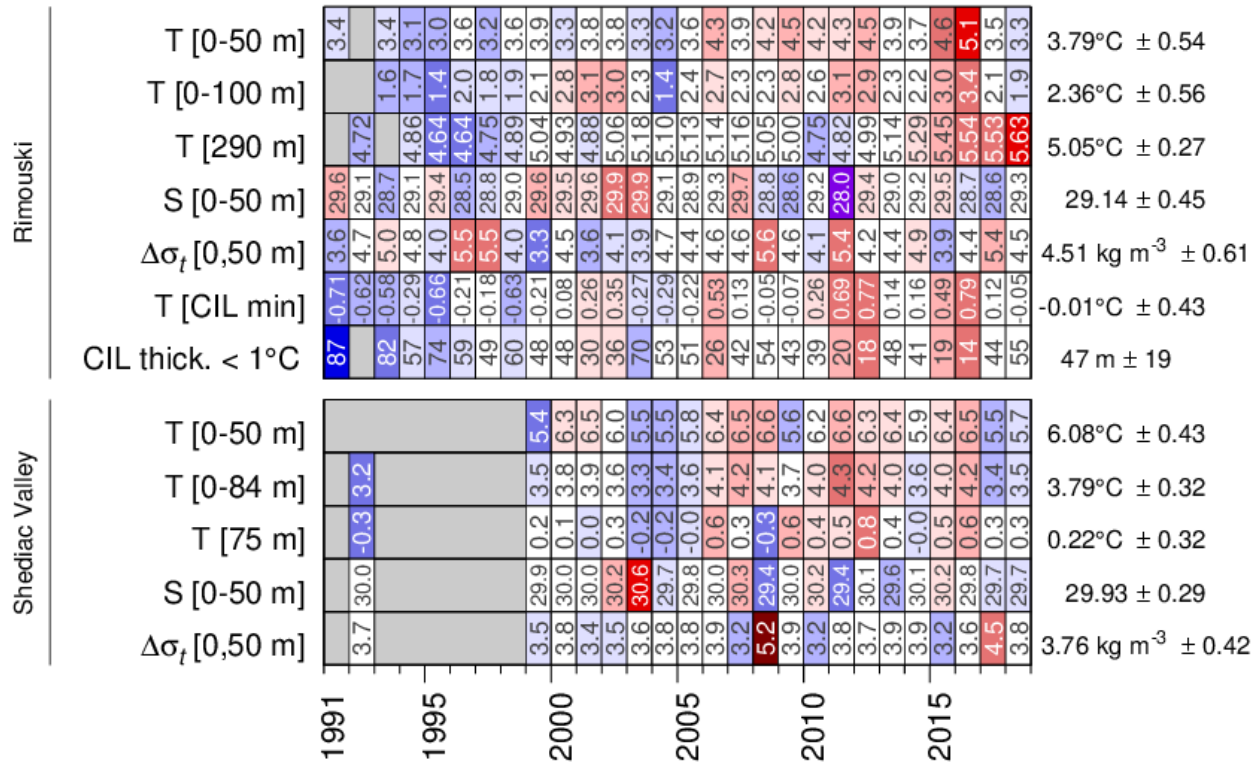


*Fig. 64. May to October temperature and salinity layer averages, stratification (expressed as the density difference between 0 and 50 m), and CIL temperature minimum and thickness (T<1°C) for high frequency monitoring stations. Numbers in panels are monthly average values colour-coded according to the anomaly relative to the 1991–2018 time series. Three months of anomaly data, between May and October, are required to show an average anomaly for any given year, except for deep water temperature at Rimouski station. Temperatures at 290 m and 75 m at Rimouski station and Shediac Valley station are considered to represent near-bottom temperatures.*

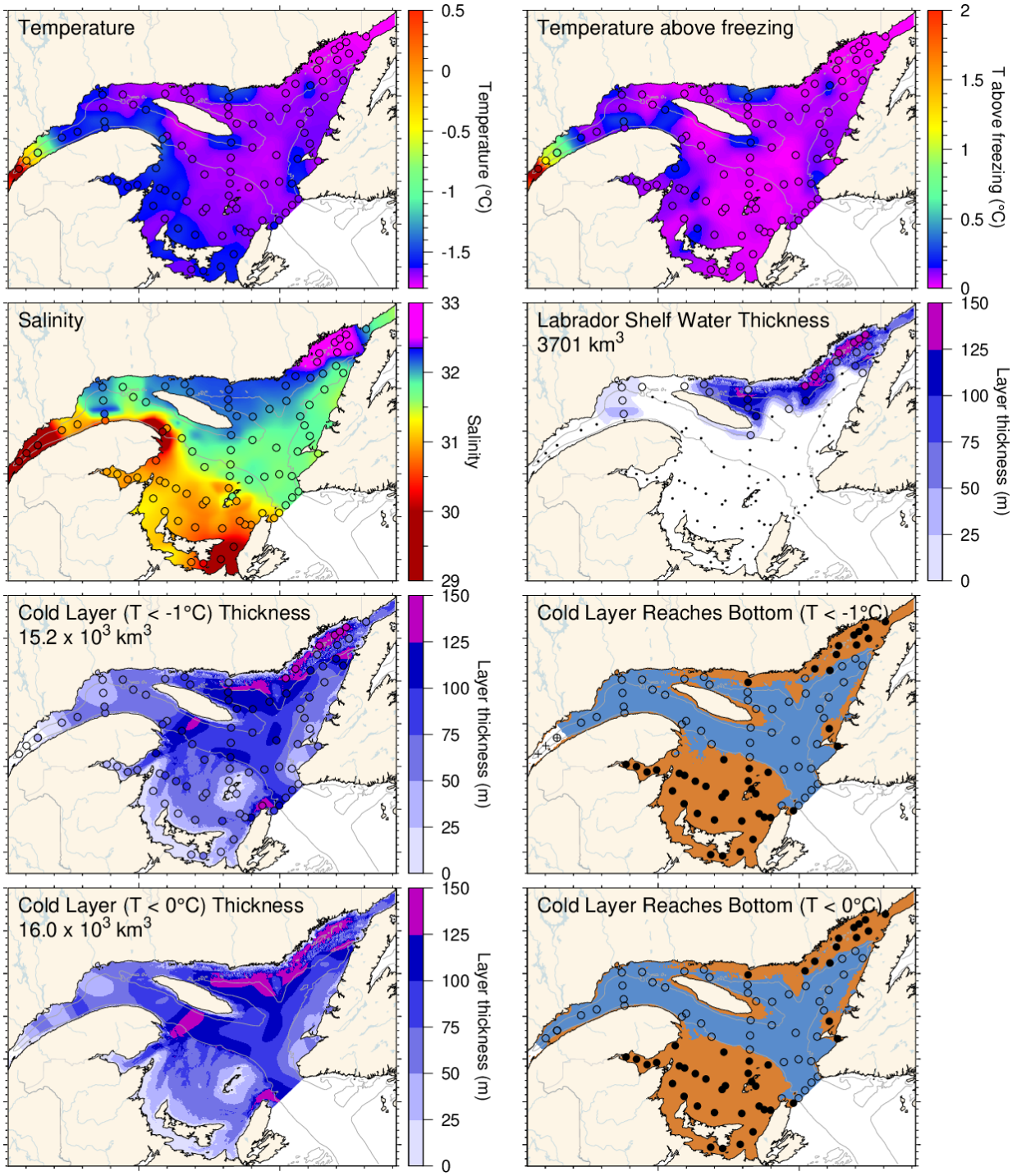


*Fig. 65. March 2019 surface cold layer characteristics: surface water temperature (upper left), temperature difference with the freezing point (upper right), salinity (second row left), estimate of the thickness of the Labrador Shelf water intrusion (second row right), and cold layer (T<-1°C and <0°C) thicknesses and where they reach bottom. The symbols are coloured according to the value observed at the station, using the same colour palette as the interpolated image. A good match is seen between the interpolation and the station observations where the station colours blend into the background.*

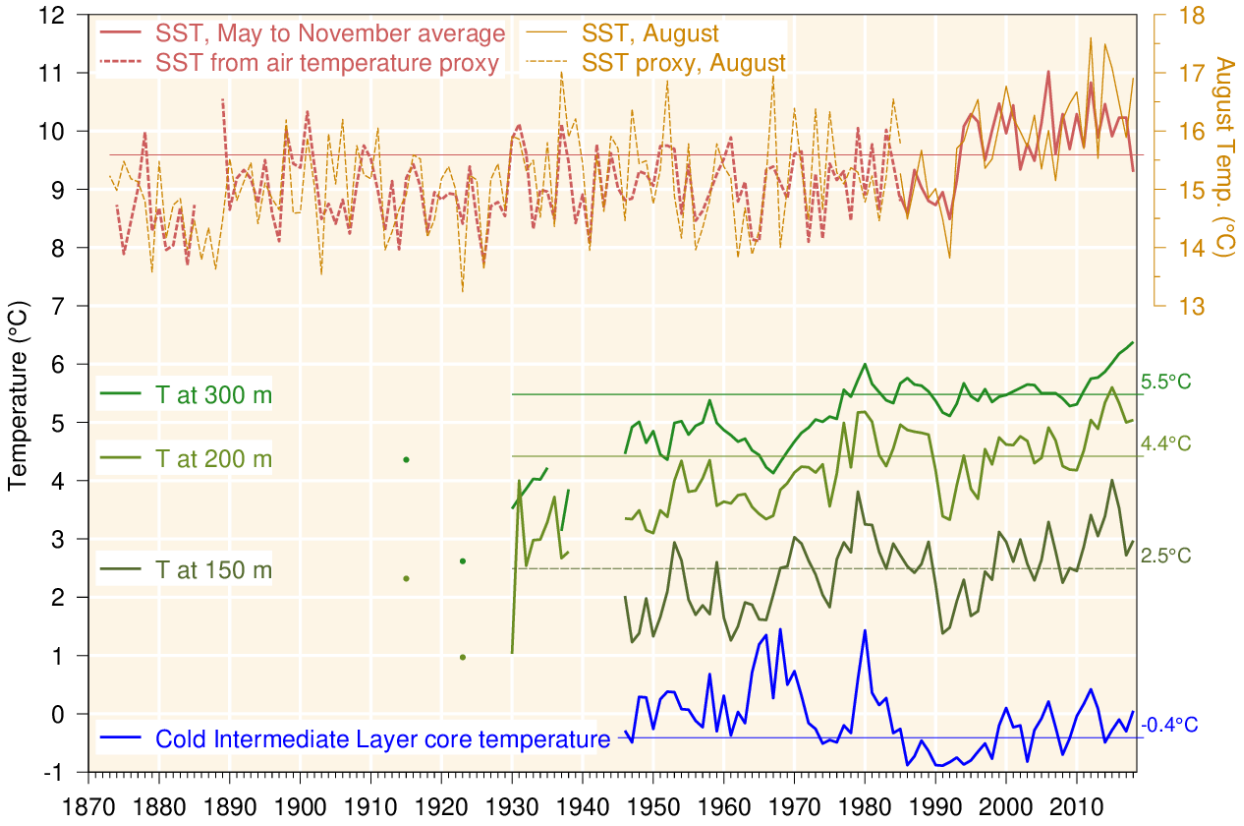


*Fig. 66. Water temperatures in the Gulf of St. Lawrence. May–November SST averaged over the Gulf excluding the Estuary (1985–2018, red line), completed by a proxy based on April–November air temperature (1873–1984, red dashed line; average of all AHCCD stations in Fig. 4 but excluding Estuary stations at Baie Comeau and Mont-Joli). August SST is shown using temperature scale offset by 6°C; its proxy is based on the average air temperature in July and August. Layer-averaged temperature for the Gulf of St. Lawrence at 150, 200 and 300 m (green lines). Cold intermediate layer minimum temperature index in the Gulf of St. Lawrence (blueline). SST air temperature proxy is similar to that of Galbraith et al. (2012). Climatological averages based on the 1981-2010 period are indicated by thin lines labeled on the right side. Figure adapted from Benoît et al. (2012).*

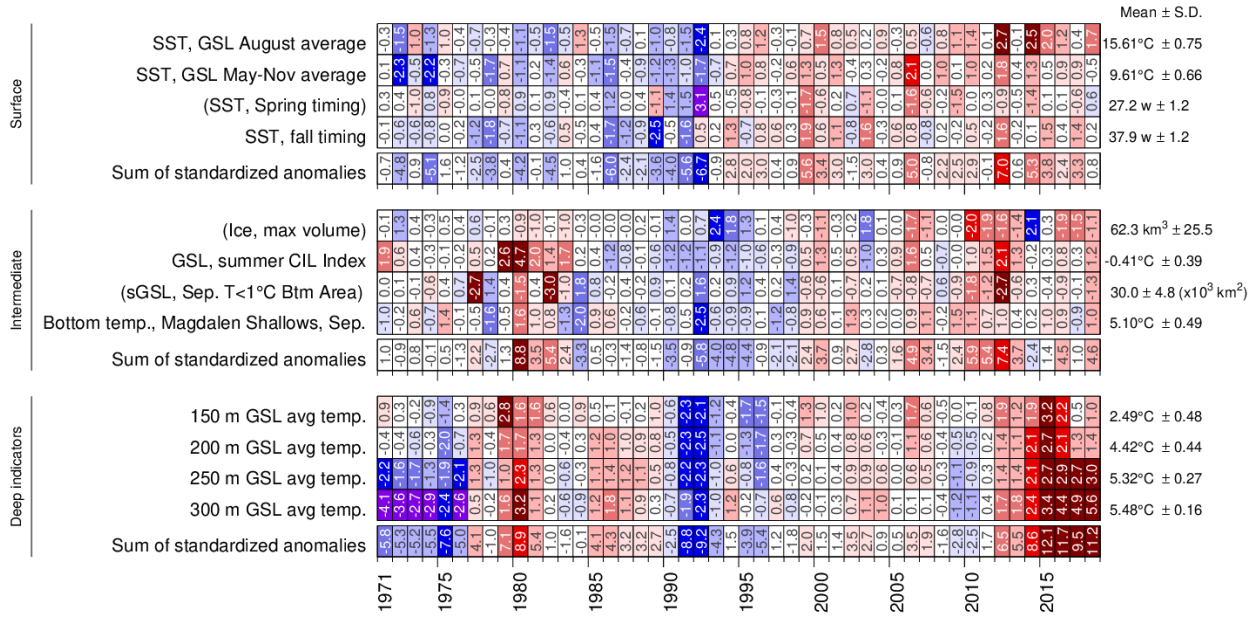


*Fig. 67. Surface, intermediate (and sea-ice) and deep indicators used in the composite climate index (Fig. 68). The SST spring and fall timing are for 12°C.*

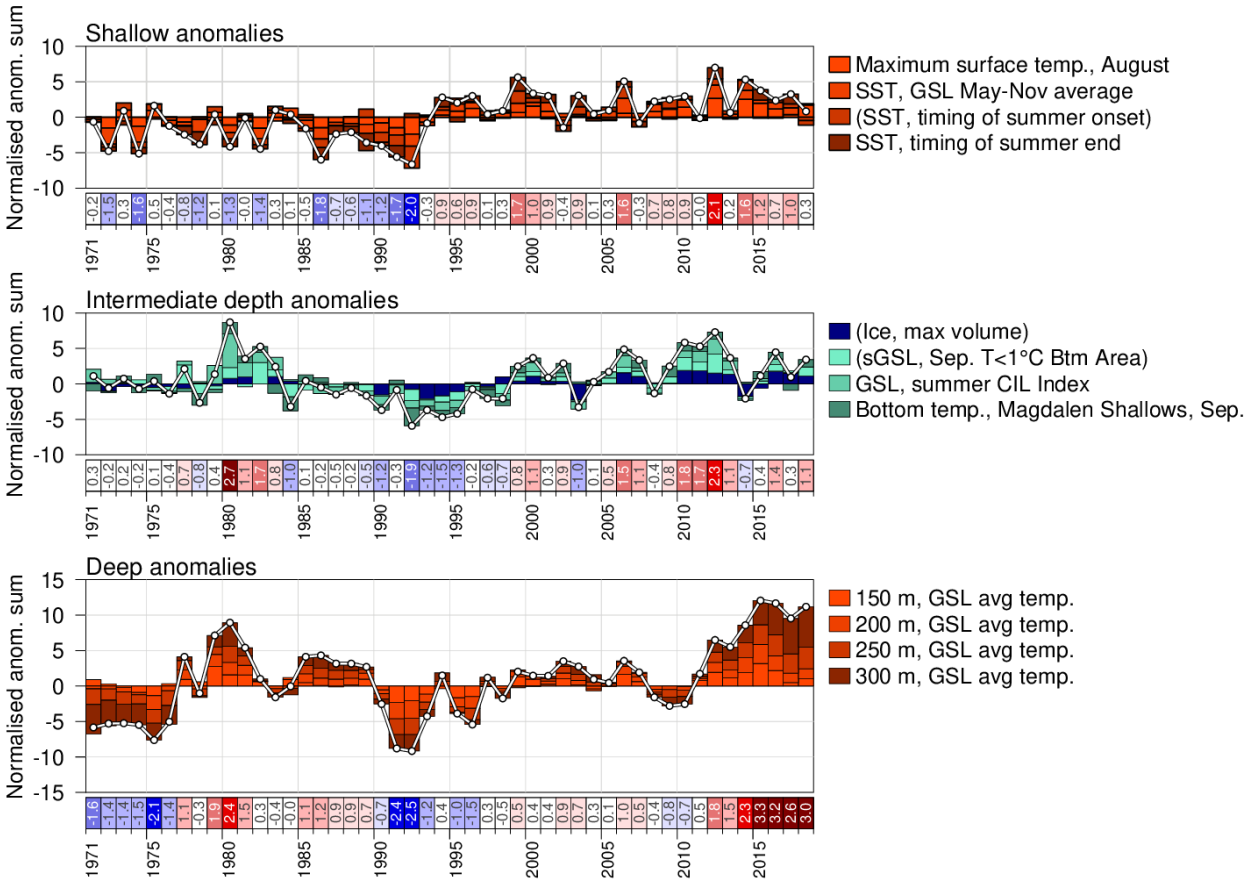


*Fig. 68. Composite climate indices (white lines and dots) derived by summing various normalized anomalies from different parts of the environment (colored boxes stacked above the abscissa are positive anomalies, and below are negative). Top panel sums anomalies representing shallow temperature anomalies, middle panel sums intermediate depth temperature anomalies and sea-ice (all related to winter formation), and bottom panel sums deep temperature anomalies.*